Alt, J.C., Kinoshita, H., Stokking, L.B., and Michael, P.J. (Eds.), 1996
Proceedings of the Ocean Drilling Program, Scientific Results, Vol. 148

10. ALTERATION OF UPPER OCEAN CRUST IN A RIDGE-FLANK HYDROTHERMAL UPFLOW ZONE: MINERAL, CHEMICAL, AND ISOTOPIC CONSTRAINTS FROM HOLE 896A[1]

Damon A.H. Teagle,[2] Jeffrey C. Alt,[2] Wolfgang Bach,[3,4] Alex N. Halliday,[2] and Jörg Erzinger[3]

ABSTRACT

Hole 896A penetrates into the upper volcanic section of a ridge-flank hydrothermal upflow zone. Analyses of the secondary mineralogy and chemistry, whole-rock geochemistry, and oxygen, carbon, and strontium isotope ratios of whole rocks and secondary minerals were conducted to constrain the chemical and thermal evolution of hydrothermal alteration and its effects on the upper crust at Site 896.

Celadonite ± Fe-oxyhydroxides are the earliest secondary minerals and formed at low temperatures. The crust was open to free circulation of seawater, but solutions derived from deeper in the crust may have provided some of the Fe, Si, and alkalies required for celadonite formation. Whole-rock chemical changes involved increased alkalies, and slight increases in H_2O, $Fe^{3+}/Fe^{(Total)}$, $\delta^{18}O$, and $^{87}Sr/^{86}Sr$.

Subsequently, Fe-oxyhydroxides formed reddish alteration halos in the rocks in relatively young crust, where open circulation of large volumes of seawater maintained oxidizing conditions and low temperatures. Whole-rock chemical changes are characterized mainly by oxidation, but include increased H_2O, alkalies, U, P, $\delta^{18}O$, and $^{87}Sr/^{86}Sr$; local losses of S and possibly Tl; and possible minor losses of Ca and Mg.

The next alteration stage was characterized by the pervasive formation of saponite in slightly older crust, where circulation of seawater was more restricted, conditions were less oxidizing, and temperatures were probably higher though less than 100°–150°C. Whole-rock chemical changes include increased Mg, H_2O, $\delta^{18}O$, and $^{87}Sr/^{86}Sr$; slight alkali increases; and local gains of S and Tl. Significant uptake of Mg by the upper crust occurred through the formation of saponite in veins and breccias. Four saponites have $^{87}Sr/^{86}Sr = 0.70842–0.70875$ indicating that fluids were partly evolved seawater, but one fibrous saponite has $^{87}Sr/^{86}Sr = 0.704363$, requiring localized, rock-dominated fluid compositions.

Calcium carbonates and zeolites were the last secondary phases to form. An early, lower temperature (26°–35°C) generation of carbonates, has low Mg, Fe, and Mn concentrations and high Sr contents. These carbonates formed from partly reacted seawater that had decreased Mg/Ca ratios and contained 2.5%–10% basaltic Sr (carbonate $^{87}Sr/^{86}Sr = 0.708775 \pm 0.000066$ [2σ], $N = 11$). A second generation of carbonates formed at higher temperatures (47°–67°C), from seawater-derived fluids with lowered Mg/Ca and Sr/Ca ratios and elevated Fe, and Mn concentrations. Trace-element chemistry of the high-temperature carbonates in general, and the lower $^{87}Sr/^{86}Sr$ of rare high-temperature aragonites (0.7079–0.7084) suggest more restricted circulation of seawater and reducing conditions. The higher temperature carbonates formed at temperatures consistent with the present-day thermal regime at Site 896; a ridge-flank hydrothermal upflow zone with basement temperatures greater than 50°C.

All rocks from Hole 896A have interacted with seawater at low temperatures, and samples commonly record the integrated legacy of superimposed alteration processes. The most intense chemical changes have occurred within hyaloclastite and fragmentation breccias that comprise at least 5% of the uppermost oceanic crust at Site 896.

The sequence of alteration processes present in Hole 896A is broadly similar to that recorded in the upper crust (above ≈300 m sub-basement) of Hole 504B, which is located approximately 1 km to the northwest, in a zone of average regional heat flow. The main differences between the material from Holes 896A and 504B is the greater abundance of carbonates, and hyaloclastite and fragmentation breccias, and the common occurrence of thick (≈1 cm) saponite veins in the new hole.

INTRODUCTION

Following the suspension of drilling in Hole 504B on Ocean Drilling Program (ODP) Leg 148, operations were moved to Site 896, approximately 1 km to the southeast (Alt, Kinoshita, Stokking, et al., 1993). This site was previously occupied during Leg 111 (Site 678; Becker, Sakai et al., 1988). Hole 896A is located in the eastern equatorial Pacific in 5.9-m.y.-old crust, approximately 202 km south of the intermediate spreading rate (3.4 cm/yr half-rate) Costa Rica Rift (Fig. 1). This second hole was drilled in such close proximity to the ocean crust reference hole at Site 504 to examine the local variation in basement lithostratigraphy and geochemistry, to evaluate the spatial heterogeneity of magmatic and hydrothermal processes, and to provide a potential site for future paired borehole seismic and electrical resistivity experiments.

Hole 896A is situated on a bathymetric high that coincides with the topographic high point of a tilted basement fault block and a local heat flow maximum (Fig. 2; Langseth et al., 1988). Regional seismic and heat-flow studies in the vicinity of Sites 504 and 896 (Langseth et al., 1988) have documented the presence of seafloor heat-flow anomalies, elongate east-west, subparallel to the trend of the Costa Rica Rift. There is a positive correlation between areas of high heat flow and both elevated bathymetry and basement topography with basement troughs being zones of lower heat flow. Sediment pore water profiles show that basement fluids well up at high heat-flow sites (e.g., Site 678/896) and that bottom seawater is being drawn into the crust through the sediment blanket in zones of low heat flow (Fig. 2, Site 677; Mottl, 1989). Hydrologic modeling of the heat-flow anomalies indicates that there is significant convection of low-temperature hydrothermal fluids in the upper few hundred meters of the basaltic

[1]Alt, J.C., Kinoshita, H., Stokking, L.B., and Michael, P.J. (Eds.), 1996. *Proc. ODP, Sci. Results,* 148: College Station, TX (Ocean Drilling Program).

[2]Department of Geological Sciences, 2534 C.C. Little Building, The University of Michigan, Ann Arbor, MI 48109-1063, U.S.A. Teagle: teagle@umich.edu; Alt: jalt@umich.edu; Halliday: anh@umich.edu

[3]GeoForschungsZentrum Potsdam, Projektbereich 4.2, Telegrafenberg A50, D-14473 Potsdam, Federal Republic of Germany. Bach: wbach@gfz-potsdam.de; Erzinger: erz@gfz-potsdam.de

[4]Present address: Universität Potsdam, Institut für Geowissenschaften, Postfach 601553, D-14415 Potsdam, Federal Republic of Germany.

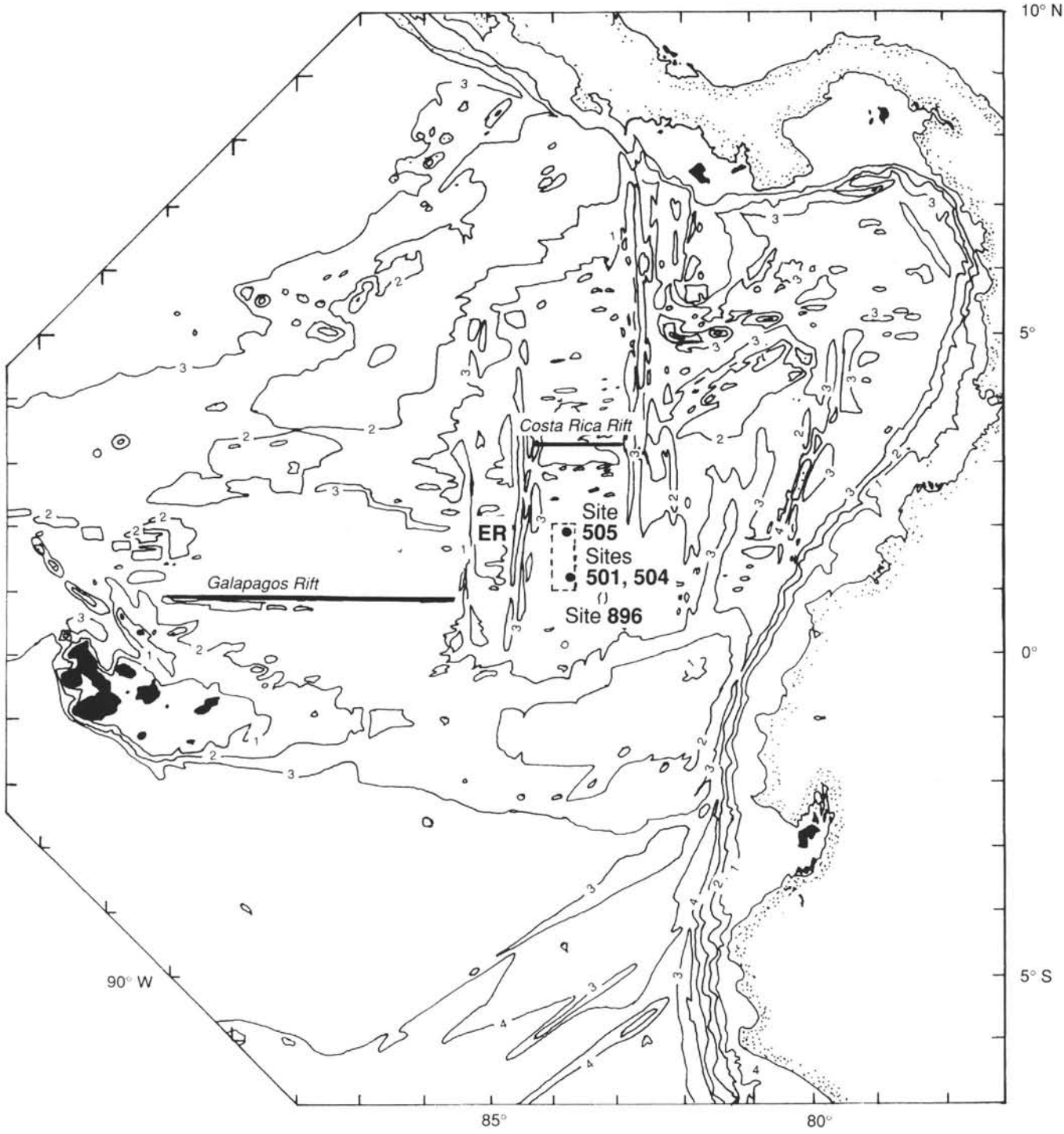

Figure 1. Location of DSDP Sites 501 and 505, DSDP/ODP Site 504, and ODP Site 896 south of the Costa Rica Rift in the eastern equatorial Pacific (after Hobart et al., 1985).

basement in this area (Fisher et al., 1990, 1994). This modeling also reveals that basement topography and sediment thickness control convection patterns in the basement. The position of Hole 896A at a basement and heat-flow high in a zone of present-day fluid upwelling provides a unique opportunity to contrast the styles of ridge-flank alteration and secondary mineral growth with the well-characterized upper volcanic section of Hole 504B, which is sited in a zone of ambient heat flow.

This paper documents the distribution of secondary minerals, styles of alteration, and geochemical changes resulting from interactions between seawater and basalt in Hole 896A. Descriptions, compositions, and isotopic ($\delta^{18}O$, $\delta^{13}C$, $^{87}Sr/^{86}Sr$) data for the secondary minerals encountered in Hole 896A are presented, as well as whole-rock geochemical and isotopic ($\delta^{18}O$, $^{87}Sr/^{86}Sr$) analyses. From this extensive chemical and isotopic database the chemical and physical conditions and bulk chemical changes associated with processes oc-

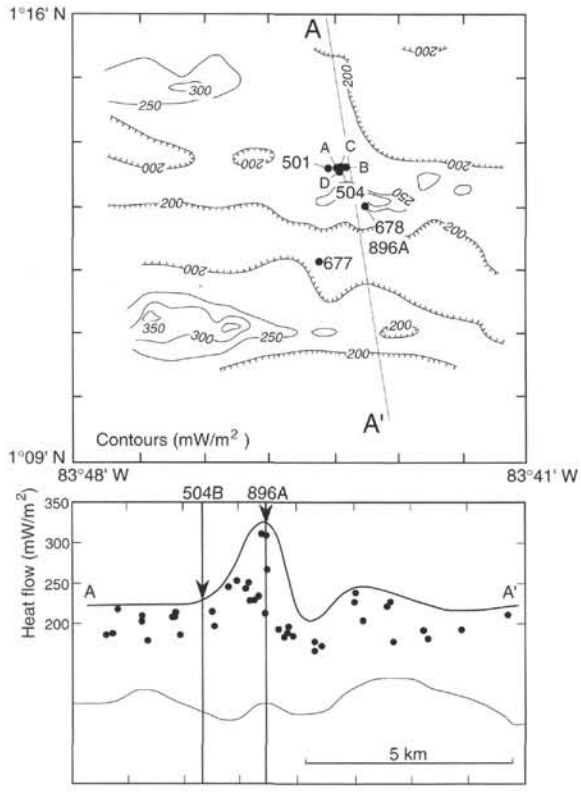

Figure 2. Location of Hole 896A, showing its position relative to Hole 504B and other ODP sites, on a map of heat-flow contours. The lower diagram shows cross section A–A′ of the heat-flow data and the relative basement topography as defined by a single-channel seismic section (adapted from Langseth et al., 1988).

curring in the upper few hundred meters of ocean basement are assessed.

SITE 896

Hole 896A penetrated to 469 m below seafloor (mbsf), through 179 m of sediment and 290 m of basement, with an average basement recovery of 27.7%. The basaltic basement sampled comprises interlayered pillow lavas (57%), massive flows (38%), breccias (5%), and two subvertical dikes (Fig. 3; Alt, Kinoshita, Stokking, et al., 1993). Breccias were classified aboard the *JOIDES Resolution* into three main types: hyaloclastite, pillow-margin breccias, and fragmentation breccias (see Alt, Kinoshita, Stokking, et al., 1993; Harper et al., this volume). Breccias comprise 5% of the core recovered from Hole 896A however, interpretation of Formation MicroScanner (FMS) and geochemical logging tool (GLT) data recovered on Leg 148 (Brewer et al., 1994) suggests that breccias may make up almost 50% of the volcanic stratigraphy penetrated by Hole 896A.

The basalts are predominantly cryptocrystalline to fine-grained, sparsely to highly phyric plagioclase-olivine tholeiitic basalts. The volcanic section has been divided into two sections, an upper region of mainly plagioclase-olivine phyric pillow basalts (<390 mbsf) and a lower section in which olivine is the dominant phenocryst phase over plagioclase and where massive flows are more common (Alt, Kinoshita, Stokking, et al., 1993). Variations in plagioclase and olivine phenocryst abundances indicate possible magmatic cyclicity with depth and an overall downward trend of increasing phenocryst abundance (Alt, Kinoshita, Stokking, et al., 1993).

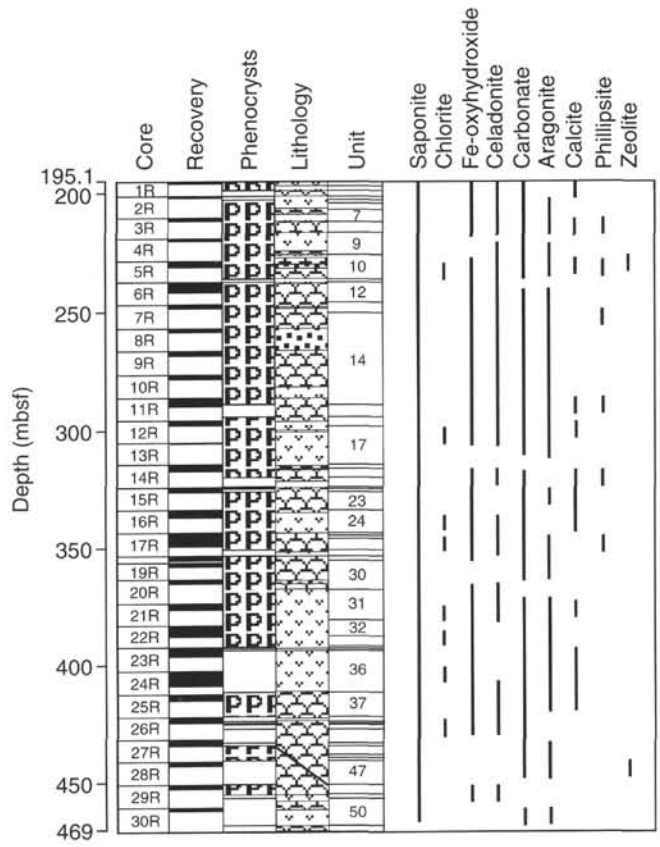

Figure 3. Lithostratigraphy of Hole 896A showing the relative proportions of pillow lavas, massive flows, and breccias and the distribution of secondary minerals with depth. The lavas above 390 mbsf are dominantly plagioclase-olivine phyric. Below this level olivine is the dominant phenocryst. Secondary mineral occurrences are based on thin section, XRD, and electron microprobe studies. Phenocrysts: P-pattern = plagioclase dominant, otherwise olivine dominant. Lithology: convex upward = pillows; v = massive units; squares = breccias; diagonal solid line = a mixture of pillow basalts and breccias.

The chemical compositions of the basalts are strongly depleted, moderately evolved mid-ocean ridge basalts (MORB) (Alt, Kinoshita, Stokking, et al., 1993). Immobile incompatible elements (e.g., TiO_2, Zr, Y) show a slight increase with depth to approximately 340 mbsf, then a step to higher concentrations followed by a gradual decrease with depth. Two models have been proposed for the depleted nature of the Costa Rica Rift basalts. The basalts have been interpreted as either very primitive (Natland et al., 1983; Emmermann, 1985) or the result of multistage melting of a normal MORB mantle source followed by a moderate extent of crystal fractionation (Autio and Rhodes, 1983; Kempton et al., 1985; Autio et al., 1989). Preliminary shipboard data from Hole 896A support the latter suggestion to some extent, but the intercalation of highly depleted and less depleted lavas in the lower part of the hole cannot be explained solely by multistage melting (see Brewer et al., this volume; Fisk et al., this volume).

METHODS

The samples studied are representative of the various types of material recovered from Hole 896A during Leg 148, and include least-altered rocks as well as more intensely altered basalts and breccias.

Secondary minerals were studied in transmitted and reflected light, and identifications were aided by energy-dispersive X-ray analyses and X-ray diffraction (XRD). Chemical compositions of secondary minerals were determined by electron microprobe (Cameca CAMEBAX MBX-microbeam with four wavelength-dispersive spectrometers, University of Michigan) using a 10-nA beam current and 15-kV accelerating potential rastered over a 6×6 µm area. Natural and synthetic mineral standards were used for calibration.

A selection of whole-rock samples, representative of the different alteration types present in Hole 896A, were analyzed for their chemical (major and trace elements) and isotopic compositions ($\delta^{18}O$, $^{87}Sr/^{86}Sr$). Zones of more intense alteration were separated from the less altered gray host rock by sawing, where possible. Whole-rock samples were either ground in tungsten-carbide (University of Michigan) or agate (Giessen). Major element oxides were analyzed at the Universität Giessen by X-ray fluorescence (XRF) on sample disks fused with lithium metaborate with a sample to flux ratio of 1:4. A Philips PW 1400 computerized XRF spectrometer calibrated against international reference standards and the Philips "alphas program" were used to calculate concentrations. Measurements of Cr, Ni, Cu, Zn, Ga, Sr, Y, and Zr were conducted by XRF analysis of pressed-powder pellets, using the rhodium Compton peak of the X-ray tube for matrix corrections. Analytical reproducibility and detection limits for major element oxides and trace elements are detailed in Bach et al. (this volume). Ferrous iron concentrations were determined by manganometric titration.

Rare earth elements (REE), Li, Sc, Rb, Nb, Cs, Hf, Tl, Th, and U were measured in selected samples by inductively coupled plasma mass spectrometry (ICP-MS) using a VG Plasmaquad PQ2+ at GFZ-Potsdam. Sample dissolution and instrumental conditions followed a technique modified from that described by Garbe-Schönberg (1993) (cf. Zuleger et al., this volume). Instrumental sensitivity and precision were checked against external standard solutions (Bach et al., this volume).

H_2O contents were determined by coulometric Karl Fischer titration after thermal decomposition of the samples at 1200°C. Repeat analyses indicate a reproducibility of better than 5%. Measurements of CO_2 and sulfur content were performed on a LECO CS 225 CHS-analyzer. Replicates suggest an analytical precision of better than 10%, but CO_2 contents less than 0.3 wt% should be treated as qualitative only.

Stable isotope measurements were made in the Stable Isotope Laboratory at the University of Michigan. Oxygen was extracted from whole-rock powders and from minerals separated from veins by reaction with ClF_3 and converted to CO_2 gas using the techniques of Clayton and Mayeda (1963). Oxygen isotope ratios were then analyzed on a Finnigan Delta-S mass spectrometer. Results are reported as δ notation relative to standard mean ocean water (SMOW; Craig, 1961), where $\delta^{18}O(‰) = 10^3 \times \{[(^{18}O/^{16}O)_{sample} - (^{18}O/^{16}O)_{SMOW}]/(^{18}O/^{16}O)_{SMOW}\}$.

Repeated extractions and measurements of samples and standards were reproducible within ±0.2‰. CO_2 from secondary carbonates in veins was liberated by dissolution in phosphoric acid, and carbon and oxygen isotopic ratios were then measured on a Finnigan Delta-E mass spectrometer. Data are reported as δ notation relative to SMOW and PeeDee Belemnite (PDB) for oxygen and carbon, respectively.

Strontium isotopic compositions and isotope-dilution rubidium and strontium concentrations were determined by thermal ionization mass spectrometry (TIMS) in the Radiogenic Isotope Geochemistry Laboratory (RIGL) at the University of Michigan. Approximately 30 mg of powdered whole-rock sample underwent a standard HF-HNO_3 dissolution before splitting into two aliquots for separate isotopic composition (IC) measurement and Rb-Sr content determinations by TIMS-isotope dilution (ID). The ID aliquot was spiked with an isotopically enriched Rb-Sr solution. Samples were evaporated to incipient dryness, then taken up in 0.2 mL of 3M HNO_3 before loading on fresh, cleaned Sr-Spec columns with a resin bed volume of ≈0.07 mL. Major elements were eluted with 1 mL of 3M HNO_3 before collecting Sr in 1 mL of H_2O. Spiked solutions were treated in a similar fashion though eluted with a lesser volume of 3M HNO_3 (≈0.6 mL) in order to retain some Rb in the Sr cut for TIMS-ID analysis. The acid wash was saved for each sample and Rb separated by conventional cation exchange resin techniques when necessary.

Strontium isotopic compositions ($^{87}Sr/^{86}Sr$) were determined by loading on single Re filaments with a $TaCl_5$ solution and 5% phosphoric acid. Samples were analyzed on a V.G. Sector multiple collector mass spectrometer ("Big Norm"), using a $2.0 \pm 0.2 \times 10^{-11}$ A ion beam with at least 200 ratios collected in a multidynamic mode and normalized to $^{86}Sr/^{88}Sr = 0.1194$. NIST SRM 987 yielded $^{87}Sr/^{86}Sr = 0.710246 \pm 0.000018$ (2σ; $N = 70$) over the period of analysis (July 1993–August 1994).

Rubidium and strontium concentrations were determined by TIMS-ID using single Re filaments and a similar loading technique, with Rb analyzed at a low current (≈1 A) preceding the Sr determination. Duplicates of Rb concentration were performed using conventional cation exchange resin and run on Ta-Re triple filaments. Results were in close agreement with the values using the Sr-Spec method and single filament analysis. Full analytical procedural blanks were < 50 pg for both Rb and Sr.

$^{87}Sr/^{86}Sr$ and trace-element concentrations were measured for a subset of the calcium carbonate samples for which O and C stable isotopic data are available. Carbonate samples analyzed for $^{87}Sr/^{86}Sr$ were ground in an agate mortar and pestle, sieved, and the fine sand fraction picked by hand to yield 1–30 mg carbonate separates, estimated visually to be better than 99% pure. These separates were then leached in 10% acetic acid for >24 hr and any residue was separated by centrifugation. The leachate was evaporated to incipient dryness, and redissolved in HCl before being split 50:50 into aliquots for the separate measurement of strontium isotopic compositions by the method described above and for the determination of trace-element concentrations by inductively coupled plasma-atomic emission spectrometry (ICP-AES). Concentrations of Ca, Mg, Sr, Fe, and Mn were determined simultaneously by ICP-AES using a Leeman Labs Plasma-Spec III at the University of Michigan, following procedures described by Carpenter et al. (1991).

Sample 148-896A-14R-2, 55–62 cm (Piece 7), comprises a mixture of cloudy and clear, glassy, low-$\delta^{18}O$ calcite. Subsamples of the two calcite habits were hand picked and analyzed along with a sample of the undisturbed mixture for $^{87}Sr/^{86}Sr$ and trace-element contents. The carbonate from Sample 148-896A-22R-1, 53–54 cm (Piece 6), is intimately intergrown with saponite fibers that were not possible to separate mechanically. This sample was leached in 10% acetic acid for 24 hr, centrifuged, and the leachate analyzed for $^{87}Sr/^{86}Sr$ and trace-element concentrations. The dark green residue of saponite fibers was rinsed twice with deionized water, to remove any trace of acid and dissolved carbonate, before it was subjected to the standard procedure for silicate dissolution and $^{87}Sr/^{86}Sr$ determination.

Saponite samples were hand picked to avoid contamination by calcium carbonate and glass fragments, and then lightly ground in an agate mortar and pestle. To remove trace carbonate before the leachate was removed by centrifugation, 10–30 mg of the sample was leached for >24 hr in 10% acetic acid. The residue was rinsed with deionized water and centrifuged twice, before soaking for 24 hr in ≈3 mL of 1M NH_4Cl, to remove any adsorbed cations. This leachate was then removed after centrifugation and the residue rinsed twice. The sample residue then underwent the standard HF-HNO_3 dissolution procedure and column chemistry for $^{87}Sr/^{86}Sr$ and Rb-Sr determinations.

ALTERATION PETROGRAPHY

All rocks recovered from Hole 896A, except for small volumes of pristine volcanic glass, display some degree of alteration. This alteration is manifested by three main phenomena: the replacement of ig-

neous minerals, the filling of primary vugs and interstices by secondary phases, and the presence of crosscutting veins and breccia cements. The following sections describe and classify the types of bulk rock alteration as well as the veins and breccias present in the Hole 896A core.

Alteration of the Bulk Rock

Alteration types and abundances were logged and described in detail aboard ship, using the terms "oxidative" or "nonoxidative" to denote the presence or absence, respectively, of a reddish color imparted by secondary iron-oxyhydroxides ($Fe[O,OH]_x$) (see Alt, Kinoshita, Stokking, et al., 1993). This division of alteration types is not supported by the whole-rock geochemistry (see later) or secondary mineralogy, and a new classification system based on the secondary mineral assemblages is given below.

1. Saponite is the essential secondary mineral in the dark gray rocks, which are the most abundant alteration type and occur throughout the core in both the pillow lavas and massive flows. Olivine is partially to totally replaced by saponite ± calcium carbonate; these secondary minerals also fill primary pore space. Plagioclase is partly replaced by saponite. Secondary pyrite is locally disseminated in the groundmass or occurs with saponite filling vugs or after olivine. This type of alteration is sometimes referred to as the "background alteration."

2. Saponite + $Fe(O,OH)_x$ characterize the second most abundant alteration type. The presence of $Fe(O,OH)_x$ in these rocks imparts reddish, yellow, or brown tints to the core. Different colored zones occur in millimeter- to centimeter-wide halos along veins and fractures, particularly within the massive units, though narrow brown discolorations can be present at the boundary between cryptocrystalline pillow interiors and glassy rims. Uncommonly, small pillow fragments are pervasively altered by saponite + $Fe(O,OH)_x$. Iron-oxyhydroxides occur disseminated in the groundmass, within primary pore space and in small veinlets. Olivine is partly to totally replaced, and pore spaces are filled by saponite and mixtures of saponite + $Fe(O,OH)_x$ (the "iddingsite" of Alt, Kinoshita, Stokking, et al., 1993).

3. Celadonite + saponite + $Fe(O,OH)_x$ define the third alteration type. These rocks are identical to the saponite + $Fe(O,OH)_x$ zones except for the presence of celadonite. Celadonite replaces olivine and fills pore space in millimeter- to centimeter-sized patches or bands within the reddish colored rocks. Celadonite occurs either alone or intergrown with Fe-oxyhydroxides. This type of alteration is generally formed in the central portions of large red saponite + $Fe(O,OH)_x$ halos, and the rocks are red-black in hand specimen.

4. Celadonite + saponite characterize the fourth, least common, alteration type. This type develops in millimeter- to centimeter-sized patches or bands, generally within pillow lavas. These rocks are similar to the dark gray saponite-bearing background zones, but they also contain celadonite replacing olivine and filling vugs. Celadonite commonly lines the walls of vesicles and vugs, with saponite filling the center. This alteration correlates with the three occurrences of "black halos" recorded on Leg 148 (Alt, Kinoshita, Stokking, et al., 1993). The celadonite + saponite-bearing zones appear to have formed as halos around fractures or veins.

Veins

Veins are extremely common throughout Hole 896A. The most abundant vein types, in order of decreasing abundance, are green smectite, green smectite + carbonate, smectite + $Fe(O,OH)_x$, smectite + $Fe(O,OH)_x$ + carbonate, and carbonate alone (Alt, Kinoshita, Stokking, et al., 1993). The XRD and electron probe analyses indicate that all smectite veins are saponite. Vein widths vary from 0.1 to 2 mm (mean ≈ 1 mm), though spectacular, thick (up to 8 mm) green saponite ± carbonate veins are commonly observed within the pillow lavas. The saponite within these veins has either a vermicular/spherulitic or fibrous texture. Some saponite veins are colored brown or reddish, owing to the presence of Fe-oxyhydroxides. Centimeter-wide $Fe(O,OH)_x$-rich halos are common around saponite + $Fe(O,OH)_x$ veins and in many examples, these halos are distinctly cuspate.

Carbonate veins are abundant in the upper part of the hole, from 179 to 300 mbsf, and between 390 and 415 mbsf (Fig. 3). These veins comprise either calcite or aragonite, though a mixed carbonate mineralogy is commonly present. The veins range from submillimeter to 4 mm in width and both calcite and aragonite may exhibit fibrous, prismatic, or blocky habits. Carbonates can occur alone, at the middle of saponite veins, or intergrown with saponite, and rarely with pyrite. Fibrous or prismatic carbonate commonly occurs with fibrous saponite in veins; otherwise, the carbonate appears to postdate saponite in many cases. Rarely, the middle of a fibrous saponite vein is partially filled by carbonate. In these areas, single fibers or clusters of fibers have carbonate cores but saponite tips at the vein margins. Where veins cut across reddish alteration halos, the vein composition appears influenced by the type of the bulk-rock alteration: veins that propagate from zones of saponite only to saponite + $Fe(O,OH)_x$ alteration are commonly filled with carbonate in the saponitic area and saponite + $Fe(O,OH)_x$ in the Fe-oxyhydroxide-rich region.

Fine (<0.5 mm) phillipsite veins are common. These appear to be relatively late stage, and cut across or occur at the center of saponite veins. Celadonite is uncommonly present in veins that are generally extremely fine (≈0.1 mm). In two examples, celadonite lines the walls of saponite veins, while in another occurrence it forms a band that postdates saponite lining the walls of the vein and, in turn predates saponite filling the center of the vein.

Breccias

The cements of pillow-margin and fragmentation breccias are most commonly composed of green saponite and highly comminuted fragments of host rock, though subordinate $Fe(O,OH)_x$ and/or carbonate may be present. Clasts of host rock can contain Type 1, 2, or 3 alteration assemblages, but clasts within two fragmentation breccias (Samples 148-896A-23R-1, 24–28 cm, Piece 3, and 28R-1, 97–100 cm, Piece 18) also contain minor secondary potassic feldspar replacing plagioclase phenocrysts. Hyaloclastite breccias consist of clasts of cryptocrystalline or glassy basalt cemented by saponite, calcium carbonate, local celadonite, phillipsite, and minor other zeolites (analcite and natrolite). Volcanic glass is partly to totally altered to saponitic smectite plus local phillipsite, celadonite and, natrolite.

SECONDARY MINERALOGY

Figure 3 is a compilation of shipboard and new shore-based data based on thin section, hand specimen, and XRD studies and shows the distribution of secondary minerals with depth in Hole 896A. A lithologic section summarizing the igneous rock types is also presented in Figure 3. There is minimal variation in the occurrence and abundance of secondary minerals with depth and all four alteration types are distributed throughout the core. Whether the host rocks are pillow lavas or massive flows appears to have greater control on the occurrence of alteration minerals than the primary chemistry of the magmas or the type and abundance of phenocrysts present (Fig. 3). Brightly colored, $Fe(O,OH)_x$-rich red halos are more commonly developed in the massive flows and carbonates and smectite are more abundant in the pillow lavas and associated hyaloclastic and pillow margin breccias (see fig. 34, p. 144, Alt, Kinoshita, Stokking, et al., 1993).

As logged aboard ship, "green smectite" is the most abundant secondary mineral in Hole 896A and is ubiquitously present in veins and filling vugs, and as a breccia cement throughout the core. This mineral appears a pale brown color in thin section and has been identified by XRD and electron microprobe analyses to be saponite, a trioctahedral Mg-smectite (Table 1; Figs. 4, 5). The saponite in Hole 896A

Table 1. Representative electron microprobe analyses of saponite from Hole 896A.

Core, section:	2R-122	2R-122	2R-122	3R-117	3R-117	4R-11	4R-11	11R-17	11R-17	17R-34	27R-11	27R-11	29R-1
Interval (cm):	101–108	101–108	101–108	135–139	135–139	5–8	5–8	64–71	64–71	45–47	4–12	4–12	10–14
Piece no.:	22	22	22	17	17	1	1	7	7	4	1	1	2
Spot:	1:1	1:3	3:1	4:1	4:2	1:2	1:3	1:1	3:2	4:2	1:2	2:3	5:1
Occurrence:	Vein	Vein	After olivine	Vein	Vein	Vein	Vein	Fibrous vein	Vug	Vug	Breccia vug	Breccia vug	Vug
SiO_2	46.97	42.81	43.26	47.07	45.73	46.42	44.40	45.53	45.23	47.27	43.85	42.31	44.96
TiO_2	0.05	0.02	0.02	0.01	0.02	0.03	0.01	0.03	0.02	0.00	0.01	0.02	0.12
Al_2O_3	5.10	6.53	6.34	5.25	5.30	6.77	5.14	6.13	5.26	4.64	7.76	7.62	6.57
FeO	8.39	9.67	10.39	8.19	8.98	10.20	11.14	10.93	10.47	10.14	8.17	8.57	10.04
MnO	0.13	0.10	0.22	0.17	0.19	0.09	0.19	0.18	0.16	0.04	0.12	0.05	0.06
MgO	23.87	22.62	22.30	23.54	23.42	24.60	21.45	22.42	21.90	23.24	23.43	22.09	21.47
CaO	1.38	1.37	1.10	1.02	1.08	1.78	1.53	1.99	0.71	0.77	2.07	2.37	1.51
Na_2O	0.09	0.10	0.13	0.15	0.18	0.07	0.04	0.08	0.07	0.19	0.12	0.09	0.12
K_2O	0.12	0.05	0.17	0.20	0.24	0.05	0.09	0.08	0.11	0.15	0.07	0.09	0.08
Total	86.09	83.26	83.93	85.61	85.14	90.01	83.98	87.37	83.93	86.44	85.60	83.20	84.93
Cations													
Tetrahedral													
Si^{4+}	3.506	3.348	3.368	3.525	3.471	3.356	3.462	3.409	3.498	3.537	3.311	3.303	3.436
Al^{3+} (IV)	0.448	0.602	0.582	0.463	0.474	0.577	0.472	0.541	0.480	0.409	0.689	0.697	0.564
Fe^{3+}													
Sum (IV)	3.954	3.950	3.950	3.988	3.945	3.933	3.934	3.950	3.978	3.946	4.000	4.000	4.000
Octahedral													
Ti^{4+}	0.003	0.001	0.001	0.001	0.001	0.002	0.001	0.002	0.001	0.000	0.001	0.001	0.007
Al^{3+} (VI)											0.001	0.003	0.027
Fe^{2+}	0.524	0.632	0.676	0.513	0.570	0.617	0.727	0.684	0.677	0.635	0.516	0.560	0.642
Mn^{2+}	0.008	0.007	0.014	0.011	0.012	0.005	0.012	0.011	0.010	0.002	0.008	0.003	0.004
Mg^{2+}	2.656	2.636	2.588	2.627	2.650	2.652	2.493	2.503	2.525	2.593	2.638	2.570	2.446
Sum (VI)	3.190	3.277	3.280	3.152	3.233	3.275	3.232	3.200	3.213	3.230	3.163	3.137	3.125
Interlayer													
Ca^{2+}	0.111	0.114	0.092	0.082	0.088	0.138	0.128	0.159	0.059	0.061	0.168	0.198	0.123
Na^{+}	0.013	0.015	0.020	0.022	0.026	0.010	0.006	0.012	0.010	0.027	0.017	0.014	0.018
K^{+}	0.011	0.005	0.017	0.019	0.023	0.005	0.009	0.008	0.011	0.014	0.007	0.009	0.008
Interlayer total	0.135	0.134	0.129	0.123	0.137	0.153	0.142	0.179	0.080	0.103	0.192	0.220	0.149
$Fe^{2+}/(Fe^{2+} + Mg)$	0.165	0.194	0.207	0.163	0.177	0.189	0.226	0.215	0.211	0.197	0.164	0.179	0.208

Note: Structural formulas calculated on the basis of $O_{10}(OH)_2$. Iron assumed to be Fe^{2+} in all analyses.

is magnesium-rich with Fe/(Fe + Mg) = 0.13–0.24 (Fig. 4). There are no apparent chemical differences in saponites from different modes of occurrence or crystal habits (e.g., fibrous or vermicular), and analyses from each sample tend to plot in tight clusters. Al contents are low (<0.6 atoms per formula $O_{10}[OH]_2$), and higher values associated with pillow margin breccias may indicate the presence of partially saponitized glass. Ca is the dominant interlayer cation, though K can also be significant in samples that also contain celadonite. All the saponites analyzed have high octahedral totals (2.9–3.3), which may result from the presence of Mg in interlayer positions. Talc may also be present, but in abundances too minor to be detected by microprobe or routine XRD analysis.

Celadonite in Hole 896A is generally green in thin section, though it can display red-brownish tints in $Fe(O,OH)_x$-rich samples. Analyses are consistent within each sample but a range of compositions is exhibited from near end-member celadonite, with high K and low tetrahedral Al, to glauconite, which has higher Al, and to mixed layers or mixtures of celadonite or glauconite with smectite (Table 2; Fig. 5). The celadonites are iron rich (Fe/[Fe + Mg] = 0.61–0.76) and exhibit trends to higher Mg contents within increasing octahedral cations and decreasing K (Fig. 4), which indicates that the mixed compositions are combinations of celadonite and saponite (trioctahedral Mg-smectite), rather than celadonite-nontronite (dioctahedral ferric-smectite) mixtures. The trend between K and Fe/(Fe + Mg) also indicates that the mixed layers are not merely the result of the addition of Fe-oxyhydroxide to celadonite, although this process does occur to a lesser extent in some occurrences. Octahedral cation totals in celadonite increase from 2 up to 2.4, which indicates a significant proportion of divalent cations in this site. Whether these intermediate compositions are mixed layers or physical mixtures of superimposed celadonite and saponite in submicroscopic intergrowths is presently unconstrained, and further detailed XRD and probably transmission electron microscopy (TEM) work is required to resolve this issue.

Chlorite, exhibiting bluish-green pleochroism and anomalous interference tints, occurs in some of the coarser grained portions of some massive units (Fig. 3) and its presence has been confirmed by XRD (Dilek et al., this volume). Chlorite fills primary pore space and replaces interstitial material, and although chemical compositions are unavailable, it is identical in mode of occurrence and optical properties to chlorite identified in massive basalts from Deep Sea Drilling Project (DSDP) Site 417 (Alt and Honnorez, 1984). In rocks in which saponite or celadonite are also present, chlorite is the earliest secondary phase to have formed, probably during the initial cooling of massive flows soon after eruption (Alt and Honnorez, 1984).

When observed in hand specimen and thin section, occurrences of calcium carbonate were not recorded as aragonite or calcite unless identified by XRD (Fig. 3). Both aragonite and calcite can occur in fibrous, blocky, or prismatic habits, and either aragonite, calcite, or mixtures of these minerals can be present as veins and breccia cements. Chemical and isotopic compositions of carbonates from Hole 896A are discussed later in this chapter.

Phillipsite is present both as veins and replacing volcanic glass, commonly as fine veinlets between zones of vitreous and saponitized glass. Fe-oxyhydroxides, natrolite, and analcite were identified in hand specimen and optically in thin section, but microprobe analyses of these phases were not conducted. One spectacular zeolite-filled vug was recovered in Sample 148-896A-27R-3, 10–16 cm (Piece 2). This vug, approximately 5 cm in diameter, comprises euhedral analcite icositetrahedra and fibroradial natrolite (see fig. 36, p. 146, Alt, Kinoshita, Stokking, et al., 1993). The $^{87}Sr/^{86}Sr$ of these phases are presented in a following section. K-feldspar was identified optically and confirmed by energy dispersive (EDS) microprobe analysis in two breccia samples (at 393 and 444 mbsf), where it partly replaces plagioclase phenocrysts.

WHOLE-ROCK GEOCHEMISTRY

The assessment of the changes in bulk-rock compositions that result from interactions between seawater and basalt is important for

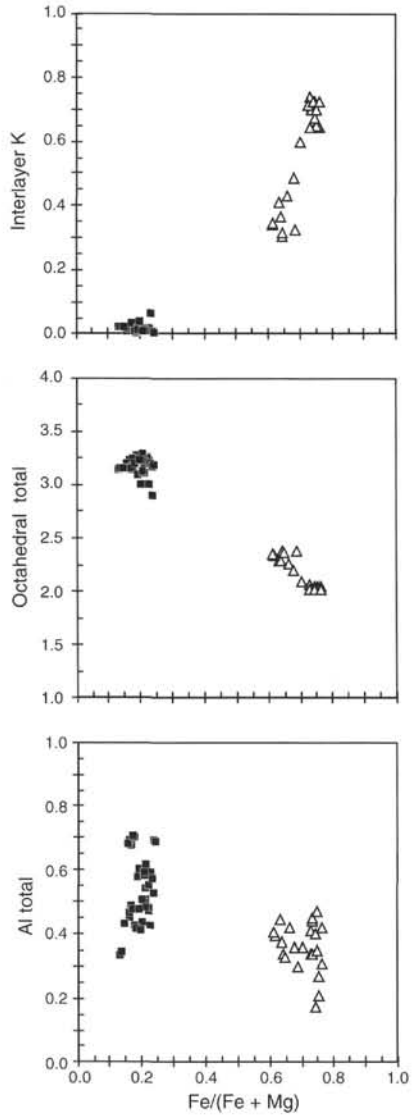

Figure 4. Compositions of secondary phyllosilicates from Hole 896A plotted vs. Fe/(Fe + Mg). Units are moles per $O_{10}(OH)_2$ of calculated structural formulas in Tables 1 and 2. Squares = saponite; triangles = celadonite. The saponite and celadonite have distinct Fe:Mg ratios, although celadonites delineate a trend towards saponite, which indicates the presence of saponite/celadonite mixtures. The total Al of saponite exhibits an elongate trend toward altered glass with high Al contents.

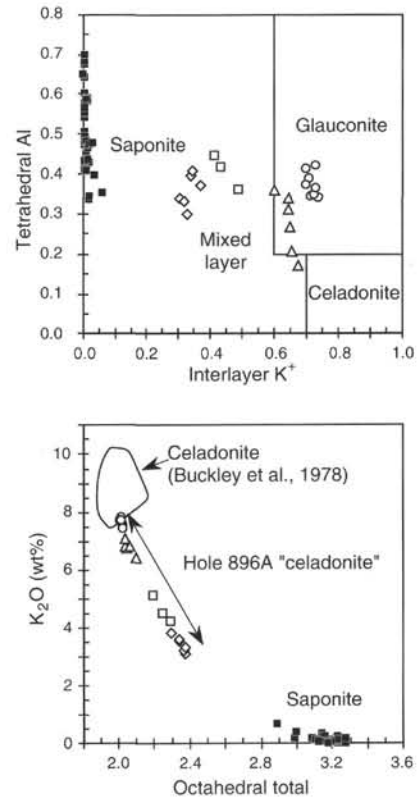

Figure 5. Upper plot shows tetrahedral Al vs. interlayer K^+ contents from structural formulas of secondary phyllosilicates (moles per $O_{10}[OH]_2$). Solid squares = saponite; open symbols = celadonite. Different symbols show range within a particular sample. Lower plot shows K_2O (wt%) vs. octahedral occupancy (same symbols). Celadonites from Hole 896A fall along a trend from pure celadonite (Buckley et al., 1978) to saponite, suggesting the presence of mixtures of celadonite and saponite.

several reasons: (1) to decipher magmatic processes obscured by alteration; (2) to constrain geochemical budgets associated with seafloor weathering and hydrothermal alteration; and (3) to assess the changes in weathering and alteration processes with the temporal and thermal evolution of the ocean basement.

Eighty-four whole-rock samples from Hole 896A have been analyzed for major oxide, trace-element and volatile contents (Table 3). Each of these samples have been classified into one of the alteration types previously described. These new data were combined with the shipboard XRF analyses, which were also classified by alteration type using the shipboard thin section descriptions (Alt, Kinoshita, Stokking, et al., 1993). There is generally good agreement between the shipboard whole-rock analyses (Nottingham) and the new data presented here. Slight systematic shifts to higher Zr and lower Y concentrations exist in the new data compared with the shipboard analyses, but these offsets are minor and have been ignored for the purposes of this paper (see Bach et al., this volume). Shipboard XRF analyses of Rb, Pb, Nb, and REE were not used in this paper because the reported concentrations are at or below the level of reliable quantification for this technique.

Basaltic Glass Compositions

In order to constrain absolute changes in chemical composition caused by alteration or mineralization processes, a detailed knowledge of the chemistry of the protolith is required. Obtaining this information is particularly difficult in magmatic complexes that show significant igneous differentiation as one must separate the combined effects of magmatic processes from alteration. Methods have been developed to assess the mass changes in altered igneous series (e.g., MacLean, 1990; Bednarz and Schmincke, 1989), however, a quantitative approach is beyond the scope of this paper and only a qualitative description of the changes associated with seafloor alteration in Hole 896A are presented.

An extensive database of microprobe analyses of fresh glass from Hole 896A has been compiled by Fisk et al. (this volume), and the data are plotted vs. depth as the shaded areas in Figure 6A. Glasses are present only in the pillow lavas and hence there is a paucity of data from some intervals in the core, particularly from 370 to 410 mbsf, where massive units are common. Glass analyses define a distinctive trend of igneous fractionation with depth, with increasing

Table 2. Representative electron microprobe analyses of celadonite from Hole 896A.

Core, section:	2R-1	2R-1	3R-1	3R-1	3R-1	17R-3	17R-3	17R-3	29R-1	29R-1	29R-1	29R-1	29R-1
Interval (cm):	101–108	101–108	135–139	135–139	135–139	45–47	45–47	45–47	10–14	10–14	10–14	10–14	10–14
Piece no.:	22	22	17	17	17	4	4	4	2	2	2	2	2
Spot:	4:1	4:2	1:3	2:1	2:3	1:2	1:3	2:1	1:1	2:1	2:2	2:3	3:3
Occurrence:	Vug	Vug	Vug	Vug	Vug, reddish	After olivine	After olivine	After olivine	Euhedral vug	Hexagonal vug	Hexagonal vug	Small vug	Euhedral vug
SiO_2	45.25	46.27	45.40	44.28	42.25	48.26	48.80	49.55	49.40	49.58	49.21	48.18	48.72
TiO_2	0.03	0.01	0.03	0.00	0.02	0.22	0.06	0.03	0.06	0.08	0.10	0.19	0.25
Al_2O_3	4.69	4.07	4.61	3.80	3.29	3.54	3.03	1.98	3.91	4.02	4.61	4.81	5.41
Fe_2O_3	28.05	28.25	27.53	29.94	33.25	28.72	28.49	29.27	26.61	27.00	26.27	27.34	26.34
MnO	0.09	0.08	0.16	0.15	0.17	0.02	0.02	0.02	0.04	0.04	0.02	0.04	0.05
MgO	7.23	6.74	8.75	8.40	7.70	4.52	4.72	5.09	4.91	4.66	4.64	4.35	4.45
CaO	1.17	1.15	1.20	1.02	1.02	0.63	0.61	0.50	0.50	0.53	0.54	0.66	0.64
Na_2O	0.15	0.13	0.15	0.06	0.12	0.15	0.12	0.11	0.10	0.10	0.09	0.13	0.10
K_2O	4.49	5.10	3.60	3.13	3.32	6.77	6.83	7.13	7.83	7.73	7.72	7.68	7.43
Total	91.14	91.81	91.42	90.78	91.15	92.83	92.68	93.67	93.35	93.72	93.19	93.38	93.39
Cations													
Tetrahedral													
Si^{4+}	3.419	3.477	3.398	3.362	3.253	3.601	3.642	3.671	3.651	3.650	3.636	3.574	3.589
Al^{3+} (IV)	0.417	0.361	0.406	0.340	0.299	0.311	0.267	0.172	0.340	0.349	0.364	0.421	0.411
Fe^{3+}	0.164	0.162	0.195	0.298	0.448	0.088	0.091	0.156	0.008	0.001		0.005	
Sum (IV)	4.000	4.000	4.000	4.000	4.000	4.000	4.000	4.000	4.000	4.000	4.000	4.000	4.000
Octahedral													
Ti^{4+}	0.002	0.001	0.002	0.000	0.001	0.012	0.004	0.002	0.003	0.004	0.005	0.011	0.014
Al^{3+} (VI)											0.037	0.059	
Fe^{3+}	1.430	1.436	1.355	1.413	1.479	1.525	1.509	1.475	1.472	1.494	1.460	1.521	1.461
Mn^{2+}	0.006	0.005	0.010	0.010	0.011	0.001	0.001	0.001	0.002	0.002	0.002	0.002	0.003
Mg^{2+}	0.814	0.755	0.977	0.950	0.884	0.503	0.525	0.562	0.541	0.511	0.511	0.481	0.489
Sum (VI)	2.252	2.197	2.343	2.373	2.376	2.041	2.039	2.040	2.019	2.012	2.015	2.016	2.025
Interlayer													
Ca^{2+}	0.095	0.092	0.096	0.083	0.084	0.051	0.049	0.040	0.040	0.042	0.043	0.053	0.051
Na^{+}	0.022	0.019	0.022	0.009	0.018	0.021	0.017	0.016	0.014	0.014	0.013	0.019	0.015
K^{+}	0.432	0.489	0.344	0.303	0.326	0.644	0.650	0.673	0.738	0.726	0.727	0.727	0.698
Interlayer total	0.549	0.600	0.461	0.396	0.428	0.716	0.716	0.729	0.792	0.781	0.783	0.799	0.763
$Fe^{3+}/(Fe^{3+} + Mg)$	0.662	0.679	0.614	0.643	0.686	0.762	0.753	0.744	0.732	0.745	0.741	0.760	0.749

Note: Structural formulas calculated on the basis of $O_{10}(OH)_2$. Iron assumed to be Fe^{3+} in all analyses.

SiO_2, TiO_2, FeO* (total iron as FeO) and Na_2O and decreasing Al_2O_3 and MgO to ≈420 mbsf (the base of massive Unit 36). A sharp step to lower and then higher TiO_2 concentrations near the bottom of the hole may indicate the beginning of another, deeper magma fractionation sequence.

Glass data are plotted vs. TiO_2 as a measure of igneous fractionation in Figure 7. Major element concentrations display magmatic differentiation trends typical of basaltic melts (i.e., increasing SiO_2, FeO*, and Na_2O and decreasing Mg# (= atomic ratio of 100 × Mg/[Mg + Fe*]), Al_2O_3, MgO, and CaO with increasing TiO_2).

Major Element Oxides

Major element oxide concentrations for whole-rock samples are plotted vs. depth in Figure 6A and vs. TiO_2 in Figure 7. These figures illustrate some significant differences between glass and whole-rock compositions. Analyses of glass record quenched liquid compositions, but the whole-rock samples include both the liquid and phenocryst phases accumulated in the magma. Basalts from Hole 896A contain an average of ≈10% phenocrysts: mostly 4%–12% plagioclase and <4% olivine, with <0.5% clinopyroxene phenocrysts present below 350 mbsf (Alt, Kinoshita, Stokking, et al., 1993). Preliminary modeling indicates that the major differences between glass and whole-rock compositions in Figures 6A and 7 are explained by the accumulation of plagioclase and olivine in the magmas. SiO_2, FeO*, TiO_2, and MgO contents of the glasses decrease and Al_2O_3 contents increase with phenocryst accumulation to coincide roughly with the whole-rock data. CaO contents of the glasses also increase slightly and Na_2O contents decrease slightly, but the glass and whole-rock data sets for these elements still overlap significantly. K_2O and P_2O_5 contents of the glasses decrease by insignificant amounts through accumulation of phenocrysts.

Loss on ignition (LOI) and Fe oxidation ratio ($Fe^{3+}/Fe^{(Total)}$) are plotted vs. depth on Figure 6A as convenient measures of alteration, and Mg# is plotted as an indicator of magmatic differentiation. Almost all samples are hydrated and oxidized relative to primary MORB magmas. LOIs range from 0% up to 3.45 wt% for the breccia Sample 148-896A-23R-1, 24–28 cm (Piece 3), values which are elevated significantly above the expected water contents of fresh MORB for these Mg# (0.1–0.2 wt%; Michael, 1988; Dixon et al., 1988). All samples are oxidized relative to MORB glass ($Fe^{3+}/Fe^{(Total)}$ ≈0.12; Puchelt and Emmermann, 1983), although there is not a clear distinction between the alteration types. Celadonite and $Fe(O,OH)_x$-bearing samples generally have higher $Fe^{3+}/Fe^{(Total)}$ ratios, but some Type 1 (saponite only) samples are also highly oxidized. There is a slight decrease in average $Fe^{3+}/Fe^{(Total)}$ ratio with depth, but a wide range of values exists to the bottom of the hole (Fig. 6A).

K_2O is clearly enriched in whole-rock samples, and the larger range of whole-rock concentrations for many elements relative to the glass data may be caused by alteration. P_2O_5 displays little systematic change with depth, though a couple of samples are strongly enriched in phosphorous, which is most likely the result of adsorption of phosphates onto Fe-oxyhydroxides (e.g., Mills et al., 1994).

Only one breccia was analyzed. Sample 148-896A-23R-1, 24–28 cm (Piece 3), comprises clasts of brecciated fine-grained, massive basalt altered to saponite, $Fe(O,OH)_x$, and minor K-feldspar in a matrix of saponite ± $Fe(O,OH)_x$. This sample is highly altered and the matrix makes up about 40% of the sample. This breccia displays profound geochemical changes in comparison to fresh glass. It is strongly enriched in Na_2O, K_2O, Al_2O_3, and MgO; depleted in SiO_2; and strongly depleted in CaO. Total Fe is unchanged and the MgO enrichment is reflected in a relatively high Mg#. The compositional changes to this breccia are much greater than other whole-rock samples, which suggests that analyses of further breccias are required for a comprehensive assessment of chemical change in the oceanic crust.

The compositional changes in the whole-rock samples are far greater that would be expected were they merely due to the hydration of basalt. In Figure 8A, major element oxides are plotted vs. LOI,

Table 3. Major, trace, and rare earth element analyses of whole-rock samples from Hole 896A.

Core, section:	1R-1	1R-1	2R-1	2R-1	3R-1	3R-1	3R-1	4R-1	4R-1
Interval (cm):	14–18	36–40	50–55	58–63	61–63	135–139	141–143	57–62	106–112
Piece no.:	4	8	11	13	8	17	17	9	17
Rock type:	P	P	P	P	P	P	P	P	P
Description:	Black halo + brown	Brown	Gray	Brown	Brown-gray	Red	Gray	Gray-brown	Brown
Alteration assemblage:	Cel + Sap + $Fe(O,OH)_x$	Cel + Sap + $Fe(O,OH)_x$	Sap	Sap + $Fe(O,OH)_x$ CO_3	Sap + $Fe(O,OH)_x$	Cel + Sap + $Fe(O,OH)_x$ CO_3	Sap + $Fe(O,OH)_x$ CO_3	Cel + Sap + $Fe(O,OH)_x$	Cel + Sap
Other secondary minerals:									
Alteration type:	3	3	1	2	2	3	2	3	4
Unit:	1	3	7	7	8	9	9	9	10
Depth (mbsf):	195.24	195.46	201.40	201.48	210.51	211.25	211.31	219.47	219.96
Major elements (wt%):									
SiO_2	48.66	49.85	49.05	47.98	49.42	48.19	49.39	48.97	47.45
TiO_2	0.75	0.76	0.76	0.78	0.73	0.70	0.70	0.75	0.75
Al_2O_3	17.95	18.23	18.51	19.09	18.01	16.99	16.97	17.73	17.43
Fe_2O_3*	9.05	8.06	7.91	10.23	8.42	9.75	9.36	8.82	10.92
Fe_2O_3	4.82	3.15	3.53	7.01	3.43	4.60	3.60	3.88	6.13
FeO	3.80	4.42	3.94	2.90	4.49	4.63	5.18	4.44	4.31
MnO	0.13	0.12	0.13	0.13	0.15	0.18	0.18	0.16	0.17
MgO	7.30	6.85	7.04	6.53	7.34	7.84	7.65	7.53	6.75
CaO	13.42	12.76	13.06	11.51	13.16	13.18	13.47	13.28	13.28
Na_2O	1.98	2.10	2.08	2.29	1.99	1.80	1.79	1.96	1.91
K_2O	0.10	0.32	0.07	0.24	0.08	0.07	0.02	0.07	0.15
P_2O_5	0.10	0.04	0.06	0.09	0.05	0.05	0.05	0.06	0.21
H_2O	1.35	1.14	1.36	2.29	1.33	1.49	1.26	1.28	1.75
CO_2	0.17			0.20		0.17	0.30		0.21
LOI	1.52	1.14	1.36	2.49	1.33	1.66	1.56	1.28	1.96
Total	100.93	100.22	100.00	101.34	100.68	100.40	101.13	100.58	100.96
Mg#	62	63	64	56	63	61	62	63	55
$Fe^{3+}/Fe^{(Total)}$	0.53	0.39	0.45	0.68	0.41	0.47	0.38	0.44	0.56
Trace elements (ppm):									
Li						10.23	5.74		
S						421	984		
Sc						42	43		
Cr	409	432	434	465	423	404	400	419	418
Ni	121	159	171	115	175	160	174	164	120
Cu	86	105	93	107	100	95	102	85	79
Zn	62	60	66	65	62	63	61	66	66
Ga	15	14	15	15	14	14	14	15	14
Rb	1.70	2	1	0	2	1.26	0.41	2	2
Sr	75	75	75	85	73	67	87	72	74
Y	27	20	23	28	20	23	24	22	21
Zr	39	38	37	41	36	37	37	37	39
Nb						0.21	0.21		
Cs						0.09	0.02		
La						0.75	0.79		
Ce						3.06	3.15		
Nd						3.83	3.93		
Sm						1.64	1.66		
Eu						0.68	0.61		
Gd						2.49	2.53		
Tb						0.49	0.51		
Dy						3.60	3.72		
Ho						0.77	0.80		
Er						2.45	2.54		
Tm						0.36	0.38		
Yb						2.52	2.61		
Lu						0.37	0.38		
Hf						1.07	1.04		
Tl						0.04	0.32		
Th						0.02	0.02		
U						0.04	0.01		

along with lines that represent the dilution effect of simple hydration of arbitrary starting concentrations (LOI ≈ 0.2 wt%) of particular oxides. A number of samples with low losses (or gains) on ignition may represent the least altered rocks from Hole 896A. These samples have anomalous physical and magnetic properties (see Alt, Kinoshita, Stokking, et al., 1993; H. Worm, pers. comm., 1994) including high sonic velocities and "fresh-basalt-like" magnetic behavior when heated.

Many elements exhibit enrichment or depletion trends with increasing LOI that deviate significantly from the dilution lines (see Fig. 8A). TiO_2 is generally considered to be an immobile element during low-temperature alteration processes (e.g., Pearce and Cann, 1973). TiO_2 concentrations fall into two groupings (Fig. 8A), following the igneous trends exhibited by glasses in Figure 7, with lower TiO_2 contents falling at higher losses on ignition. Trends of increasing SiO_2 and decreasing Al_2O_3 and CaO with decreasing LOI (and generally increasing TiO_2) in Figure 8A are consistent with the differentiation of liquids and lower proportions of accumulated plagioclase and olivine phenocrysts. These trends also indicate that rocks of more primitive compositions have higher LOI and are hence more altered than rocks with more evolved compositions. Similarly, MgO contents decrease with increasing LOI, which is consistent with the accumulation of plagioclase phenocrysts in the rocks and with more intense alteration of rocks of more primitive compositions. But some loss of Mg may have occurred during alteration of the rocks as well (Böhlke et al., 1981; Alt and Honnorez, 1984; Alt, in press). Other trends in Figure 8A confirm the K_2O and P_2O_5 gains apparent in Figure 6A, and suggest the addition of Na_2O to and the loss of MnO from these rocks.

Total iron (FeO*) exhibits increasing scatter with increasing LOI (Fig. 8A). Mg# does not display any consistent trend with LOI and most analyses fall within the range displayed by fresh glass (Fig. 8B). There is a strong trend of increasing $Fe^{3+}/Fe^{(Total)}$ with LOI, however, and ferrous and ferric iron display trends of decreasing and increasing concentrations, respectively, with LOI. These trends project back toward the expected primary concentrations (for $Fe^{3+}/Fe^{(Total)} \approx 0.12$)

Table 3 (continued).

Core, section:	5R-2	5R-2	5R-3	5R-3	6R-1	6R-1	6R-3	8R-1	8R-1	9R-1	9R-1
Interval (cm):	17–20	69–72	35–39	35–39	70–72	120–124	80–86	64–72	98–106	44–49	130–135
Piece no.:	1	2	5	5	8	13	14	14	20	7	25
Rock type:	P	P	M	M	P	P	P	P	P	P	P
Description:	Gray	Brown	Red	Gray	Gray	Gray	Gray	Brown	Brown	Brown	Brown
Alteration assemblage:	Sap	Cel + Sap + $Fe(O,OH)_x$	Sap + $Fe(O,OH)_x$	Sap	Sap	Cel + Sap + $Fe(O,OH)_x$	Sap + $Fe(O,OH)_x$	Cel + Sap + $Fe(O,OH)_x$	Cel + Sap + $Fe(O,OH)_x$	Sap + $Fe(O,OH)_x$	Sap + $Fe(O,OH)_x$
Other secondary minerals:			Chlorite			Phillipsite					
Alteration type:	1	3	2	1	1	3	2	3	3	2	2
Unit:	10	10	11	11	12	12	13	14	14	14	14
Depth (mbsf):	229.49	230.01	231.13	231.13	238.60	239.10	241.58	257.74	258.08	267.14	268.00
Major elements (wt%):											
SiO_2	48.93	48.43	48.93		48.59	48.59	48.63	47.46	48.42	48.64	48.73
TiO_2	0.76	0.74	0.75		0.74	0.75	0.78	0.78	0.77	0.75	0.76
Al_2O_3	17.36	17.22	16.96		17.04	17.00	16.69	18.06	17.62	17.42	16.57
$Fe_2O_3^*$	9.32	9.21	9.77		9.08	9.32	9.65	9.97	8.84	9.31	9.77
Fe_2O_3	3.67	3.59	4.20		2.10	3.87	3.83	5.91	3.97	3.98	4.26
FeO	5.08	5.06	5.01		6.28	4.90	5.23	3.65	4.38	4.79	4.96
MnO	0.18	0.17	0.16		0.16	0.18	0.17	0.13	0.15	0.15	0.16
MgO	7.41	7.80	7.88		8.74	8.90	7.56	7.32	8.25	6.99	8.33
CaO	13.44	13.14	13.24		12.17	12.47	13.28	12.20	12.46	13.38	12.16
Na_2O	1.87	1.86	1.89		1.80	1.82	1.87	2.05	1.93	1.92	1.94
K_2O	0.06	0.09	0.03		0.09	0.10	0.06	0.18	0.10	0.06	0.12
P_2O_5	0.05	0.06	0.05		0.05	0.07	0.05	0.20	0.06	0.05	0.07
H_2O	1.25	1.44	1.12	1.28	1.22	2.05	1.35	1.97	1.59	1.37	1.85
CO_2			0.16	0.22		0.20		0.29			0.17
LOI	1.25	1.44	1.28	1.50	1.22	2.25	1.35	2.26	1.59	1.37	2.02
Total	100.61	100.14	100.92		99.66	101.45	100.07	100.59	100.18	100.02	100.62
Mg#	61	63	62		66	65	61	59	65	60	63
$Fe^{3+}/Fe^{(Total)}$	0.39	0.39	0.43		0.23	0.42	0.40	0.59	0.45	0.43	0.44
Trace elements (ppm):											
Li			11.28								
S			136								
Sc			46								
Cr	412	407	378	392	400	385	417	412	403	401	403
Ni	153	160	143	172	157	145	147	89	137	148	127
Cu	96	96	91	102	98	74	102	74	96	94	97
Zn	66	65	62	62	64	61	68	64	65	67	65
Ga	15	14	14	15	14	14	15	14	15	15	14
Rb	2	4	0.64	0.22	2	2	2	2	3	2	2
Sr	67	68	65	63	72	69	66	50	82	73	79
Y	22	21	23	25	21	24	22	32	22	21	26
Zr	37	37	39	39	38	38	39	40	39	37	41
Nb			0.27								
Cs			0.04								
La			0.85								
Ce			3.40								
Nd			4.30								
Sm			1.81								
Eu			0.75								
Gd			2.80								
Tb			0.56								
Dy			3.94								
Ho			0.88								
Er			2.73								
Tm			0.42								
Yb			2.71								
Lu			0.42								
Hf			1.13								
Tl			0.10								
Th			0.03								
U			0.07								

(Fig. 8B). These data indicate that iron is oxidized in situ as opposed to the addition of oxidized iron from the alteration fluid. The four alteration types have overlapping ferric and ferrous iron contents, but there is a tendency for Type 1 (saponite only) alteration samples to have low $Fe^{3+}/Fe^{(Total)}$ for a particular LOI.

The diagnostic chemical characteristics of the three main alteration minerals, saponite (high MgO), celadonite (high K_2O and Fe_2O_3), and $Fe(O,OH)_x$ (high Fe_2O_3), suggests that a geochemical subdivision of the alteration assemblages based on these elements should be possible, but there is significant overlap in whole rock compositions of the different alteration types. This is caused by samples being mixtures of two or more alteration types with varying proportions of different secondary minerals, so that a continuum exists between the different groups. Also, many of the chemical trends are in the same direction for the different alteration types, with the main differences being the relative magnitudes of the changes (e.g., K_2O, LOI, $Fe^{3+}/Fe^{(Total)}$).

The magnitude of chemical changes also depends upon whether the samples are from massive flows or pillow lavas. In general, samples from massive units are less altered than rocks of the same alteration type from pillow lavas. In particular, samples of Type 1 alteration taken from massive flows have very low K_2O (≤0.02 wt%) contents and only slightly increased $Fe^{3+}/Fe^{(Total)}$ ratios. These rocks are probably the least altered of the whole-rock samples analyzed in this study.

Trace Elements

Trace-element data are presented in Table 3 and bulk-rock chemical changes are summarized in Table 4 for the different alteration types. A variety of trace elements are plotted vs. depth in Figure 6B and against LOI in Figure 9. Tie lines on some of these plots connect analyses of different alteration types from the same sample. Cr, Ni, Cu, and Sr contents vary with depth in a manner similar to that displayed by the Al_2O_3 and MgO contents of the fresh glasses and reflect igneous trends. Whole-rock concentrations of these trace elements decrease from the top of the hole down to ≈370 mbsf, then step to higher then lower contents at greater depths. V, Zn, Y, and Zr display

Table 3 (continued).

Core, section:	10R-1	10R-1	11R-1	11R-1	11R-1	11R-3	11R-3	12R-1	12R-1	12R-1
Interval (cm):	97–101	107–110	22–26	42–45	80–85	41–47	80–84	10–15	15–17	72–78
Piece no.:	9	9	3	3	8	7	14	1	1	10
Rock type:	P	P	P	P	P	P	P	P	P	P
Description:	Gray	Brown	Brown	Gray	Gray	Brown	Brown	Gray + red	Brown	Orange + brown
Alteration assemblage:	Sap	Cel + Sap + $Fe(O,OH)_x$ CO_3	Cel + Sap + $Fe(O,OH)_x$	Cel + Sap	Sap + $Fe(O,OH)_x$	Cel + Sap + $Fe(O,OH)_x$	Sap + $Fe(O,OH)_x$ CO_3, Phillipsite	Sap + $Fe(O,OH)_x$ CO_3	Sap + $Fe(O,OH)_x$	Cel + Sap + $Fe(O,OH)_x$
Other secondary minerals:										
Alteration type:	1	3	3	4	2	3	2	2	2	3
Unit:	14	14	14	14	14	16	16	16	16	16
Depth (mbsf):	277.37	277.47	286.22	286.42	286.80	289.33	289.72	295.70	295.80	296.32
Major elements (wt%):										
SiO_2	49.43	48.87	48.81	48.10	48.62	48.66	48.73	48.20	48.55	48.11
TiO_2	0.76	0.76	0.78	0.75	0.77	0.79	0.78	0.79	0.79	0.74
Al_2O_3	16.74	16.87	17.25	16.66	17.32	17.21	17.58	17.34	17.22	16.98
$Fe_2O_3^*$	9.43	9.91	9.75	9.51	9.21	9.71	9.35	9.59	8.66	9.68
Fe_2O_3	2.61	4.14	4.28	3.56	3.81	4.50	4.09	4.24	2.87	4.16
FeO	6.13	5.19	4.92	5.35	4.86	4.68	4.73	4.81	5.21	4.96
MnO	0.17	0.18	0.18	0.18	0.17	0.15	0.16	0.17	0.18	0.17
MgO	8.48	8.41	7.70	8.57	7.32	7.28	6.79	7.27	7.39	7.74
CaO	13.21	13.22	13.44	12.82	13.44	13.42	13.59	13.35	13.38	13.17
Na_2O	1.76	1.79	1.83	1.76	1.88	1.98	1.89	1.91	1.88	1.85
K_2O	0.02	0.13	0.07	0.10	0.07	0.07	0.05	0.11	0.02	0.09
P_2O_5	0.05	0.06	0.06	0.08	0.06	0.06	0.06	0.05	0.06	0.06
H_2O	0.85	1.41	1.29	1.71	1.30	1.29	1.26	1.19	1.00	1.30
CO_2		0.16	0.18	0.18		0.18		0.33	0.18	0.25
LOI	0.85	1.57	1.47	1.89	1.30	1.47	1.26	1.52	1.18	1.55
Total	100.88	101.77	101.32	100.40	100.14	100.79	100.22	100.29	99.30	100.11
Mg#	64	63	61	64	61	60	59	60	63	61
$Fe^{3+}/Fe^{(Total)}$	0.28	0.42	0.44	0.37	0.41	0.46	0.44	0.44	0.33	0.43
Trace elements (ppm):										
Li								6.15		
S								113		
Sc								40		
Cr	393	381	397	385	397	400	409	358	354	366
Ni	151	146	126	142	151	119	152	136	148	138
Cu	95	94	97	87	92	92	94	81	92	90
Zn	63	63	65	62	65	65	70	66	64	64
Ga	14	14	16	14	14	15	14	15	16	14
Rb	0.34	2.41	1.35	1.74	2	1	2	2.34	0.28	2
Sr	61	63	70	67	71	69	72	97	65	81
Y	21	25	25	24	22	26	21	26	26	25
Zr	37	40	41	39	38	41	39	42	42	40
Nb								0.27		
Cs								0.16		
La								0.89		
Ce								3.40		
Nd								4.06		
Sm								1.69		
Eu								0.70		
Gd								2.61		
Tb								0.58		
Dy								3.65		
Ho								0.79		
Er								2.42		
Tm								0.41		
Yb								2.41		
Lu								0.40		
Hf								1.13		
Tl								0.02		
Th								0.03		
U								0.04		

a pattern antithetic to Cr, similar to that yielded by SiO_2, TiO_2, FeO*, or Na_2O. There is a strong correlation in the behavior of the relatively immobile high-field-strength (HFS) elements TiO_2, Zr, and Y (+ Nb and Hf).

Concentrations of Li are generally similar to or higher than those proposed for fresh N-MORB (3–4 ppm; Ryan and Langmuir, 1987). Although the data are limited, enrichments in Li appear to be greater in the upper part of the core. $Fe(O,OH)_x$ ± celadonite-bearing assemblages are enriched relative to neighboring Type 1 basalts and there is a loose positive correlation between Li and LOI (Fig. 9). The breccia sample (148-896A-23R-1, 24–28 cm, Piece 3) has a very high Li content (11.9 ppm). Lithium generally behaves like the heavy alkali elements (e.g., K, Rb) during alteration or follows Mg^{2+}, which has a similar ionic radius, but there are no convincing correlations between Li and K_2O, Rb, or MgO contents.

Sulfur displays variable behavior with depth (Fig. 6B). Most Type 1 saponite-bearing basalts show little deviations from expected MORB compositions of 960 ± 60 ppm (Alt et al., 1989); however, some Type 1 samples from the main massive units intersected at ≈370 mbsf are strongly enriched in S. $Fe(O,OH)_x$- and celadonite-bearing samples are generally depleted, and some rocks have been quantitatively stripped of S. This agrees with the observation that Fe-oxyhydroxides replace sulfides in the red-colored rocks and the common occurrence of secondary sulfides in the adjacent dark gray saponite-bearing host rocks. When plotted vs. LOI, there is a general division between the gray saponitic basalts and the $Fe(O,OH)_x$-bearing assemblages at primary and depleted S concentrations, respectively (Fig. 9).

Vanadium follows a trend similar to fresh glass FeO* and TiO_2 contents in plots against depth, which reflects igneous processes (Fig. 6B). There appears to be a strong depletion of V with increasing LOI (Fig. 9), but this actually reflects the clustering of V contents into two igneous groups, as is also displayed by TiO_2 (Fig. 7).

The behavior of other trace elements is less evident. Cr and Ni define weak fractionation trends similar to MgO or Al2O3 in the glasses (Fig. 6B), and there are no clear trends of enrichments or depletions with LOI (Fig. 9). Cu and Zn define reciprocal trends with depth, mimicking MgO and FeO*, respectively (Fig. 6B). Neither element

Table 3 (continued).

Core, section:	12R-1	12R-2	12R-2	14R-1	14R-1	14R-2	14R-2	14R-3	15R-2	16R-1
Interval (cm):	90–95	12–16	30–34	45–49	134–136	55–62	137–141	28–32	0–4	59–65
Piece no.:	11	1	3	2	15	7	19	5	1	7
Rock type:	P	P	P	M	P	P	P	P	P	M
Description:	Brown	Gray, red-brown	Gray	Gray	Red-brown	Gray, clast in breccia	Gray, red-brown	Red	Red-brown	Red-brown
Alteration assemblage:	Sap + $Fe(O,OH)_x$	Cel + Sap + $Fe(O,OH)_x$	Cel + Sap	Sap	Sap + $Fe(O,OH)_x$	Sap	Cel + Sap + $Fe(O,OH)_x$	Sap + $Fe(O,OH)_x$	Sap + $Fe(O,OH)_x$	Cel + Sap + $Fe(O,OH)_x$
Other secondary minerals:			Chlorite				Phillipsite			
Alteration type:	2	3	4	1	2	1	3	2	2	3
Unit:	17	17	17	18	19	20	21	21	23	24
Depth (mbsf):	296.50	297.17	297.35	315.05	315.94	316.56	317.38	317.76	325.69	334.49
Major elements (wt%):										
SiO_2	48.39	50.31	48.07	48.04	48.96	48.77	48.18	48.28	48.68	48.96
TiO_2	0.77	0.76	0.73	0.79	0.83	0.91	0.75	0.75	0.80	0.86
Al_2O_3	17.12	17.37	17.09	17.30	17.76	16.90	17.00	17.21	17.37	16.89
$Fe_2O_3^*$	9.46	9.09	9.05	9.55	9.14	9.39	10.05	9.48	9.47	9.76
Fe_2O_3	3.78	2.93	3.77	3.89	4.14	4.05	4.41	3.98	3.38	3.69
FeO	5.11	5.54	4.75	5.09	4.50	4.80	5.07	4.95	5.48	5.46
MnO	0.18	0.17	0.17	0.18	0.15	0.16	0.18	0.18	0.16	0.17
MgO	7.51	7.81	7.97	7.20	6.77	7.38	7.65	7.82	7.79	7.63
CaO	13.32	13.44	13.00	13.32	13.41	13.09	13.18	13.15	12.64	12.95
Na_2O	1.86	1.88	1.81	1.87	2.01	2.01	1.89	1.89	1.88	1.94
K_2O	0.07	0.02	0.12	0.07	0.05	0.07	0.07	0.06	0.09	0.12
P_2O_5	0.07	0.05	0.05	0.07	0.05	0.06	0.06	0.06	0.06	0.07
H_2O	1.38	0.81	1.55	1.30	1.26	1.19	1.29	1.22	1.41	0.81
CO_2			0.25				0.16			
LOI	1.38	0.81	1.80	1.30	1.26	1.19	1.45	1.22	1.41	0.81
Total	100.11	101.68	99.85	99.66	100.38	99.92	100.44	100.08	100.34	100.15
Mg#	61	63	64	60	59	61	60	62	62	61
$Fe^{3+}/Fe^{(Total)}$	0.40	0.32	0.42	0.41	0.45	0.43	0.44	0.42	0.36	0.38
Trace elements (ppm):										
Li										
S										
Sc										
Cr	405	369	374	394	383	405	364	376	369	363
Ni	155	151	140	143	141	113	134	152	126	110
Cu	88	99	91	93	92	100	92	74	93	88
Zn	67	63	61	68	73	75	62	64	69	71
Ga	14	15	14	15	15	15	14	15	15	16
Rb	2	2	3	3	2	2	2	2	3	4
Sr	67	62	71	67	72	72	66	68	68	63
Y	22	21	25	22	23	24	25	22	22	24
Zr	38	37	39	40	42	45	40	38	40	43
Nb										
Cs										
La										
Ce										
Nd										
Sm										
Eu										
Gd										
Tb										
Dy										
Ho										
Er										
Tm										
Yb										
Lu										
Hf										
Tl										
U										

displays any particular behavior with respect to LOI, though Type 1 saponitic rocks generally have higher base metal contents than adjacent $Fe(O,OH)_x$-bearing samples. There is no significant correlation between Cu and Zn or between these elements and S (Fig. 10), except that the samples with very low S content tend to be depleted in Cu, reflecting oxidation and loss of primary Cu-sulfides from these samples. Doe (1994) has suggested that Zn is a mildly incompatible element in MORB and most likely incorporated into titanomagnetite. Data for fresh basalts from the East Pacific Rise indicate a strong correlation between Zn contents and the sum of $TiO_2 + Fe_2O_3$* (total iron as ferric iron oxide), but a relationship between $TiO_2 + Fe_2O_3$* and Cu is more equivocal (Doe, 1994). No such relationships are apparent for either Zn or Cu and $TiO_2 + Fe_2O_3$* for the Hole 896A data (Fig. 10). Zn concentrations for Hole 896A fresh glass compositions predicted from the Doe (1994) correlation are shown in Figure 10. Even if only gray Type 1 basalts, which are the least chemically altered rocks from Hole 896A, are considered there is still no good relationship between Zn and $TiO_2 + Fe_2O_3$*.

Rubidium has very low concentrations in the Type 1 saponite basalts, generally less than 0.5 ppm, which is close to primary igneous values. Although there is no well-developed trend of increasing Rb with LOI (Fig. 9), Rb is strongly enriched in alteration Types 2, 3, and 4 with greater than 7 ppm Rb in some samples. Rb correlates positively with K_2O (Fig. 11), and celadonite-bearing assemblages are the most strongly enriched. Strontium displays a good trend of increasing concentrations with LOI (Fig. 9), though there is considerable overlap between the different alteration assemblages. The immobile elements Y and Zr do not display any strong relationship in comparison to LOI (Fig. 9), though there is a hint of Zr depletion with increasing LOI.

The behavior of ultra-trace elements with LOI is addressed in Figure 12. Different alteration zones for adjacent samples are joined by tie-lines. The numerous subvertical tie-lines in Figures 9 and 12 illustrate that the formation of the different alteration types is generally not accompanied by an increase in volatile content. Nb, Hf, and Th do not display any consistent behavior. Cs is strongly enriched in all samples compared with pristine N-MORB (7 ppb; Sun and McDonough, 1989), and Cs enrichments generally correlate with K_2O and Rb enrichments. Type 1 basalts have a limited range of Cs contents (30–80 ppb) whereas the other alteration types are significantly more

Table 3 (continued).

Core, section:	16R-2	17R-1	17R-1	17R-2	17R-3	17R-4	18R-1	18R-2	20R-1	20R-1
Interval (cm):	86–90	30-36	130–135	72–76	45–47	59–62	73–79	37–41	80–83	128–131
Piece no.:	2	3	16	6	4	4	6	6	17	26
Rock type:	M	P	P	P	P	M	P	P	M	M
Description:	Orange-brown	Gray	Red, gray	Gray	Black halo + gray	Gray	Gray	Gray	Gray	Brown
Alteration assemblage:	Sap + $Fe(O,OH)_x$	Sap	Cel + Sap + $Fe(O,OH)_x$	Sap	Cel + Sap + $Fe(O,OH)_x$	Sap + Cel	Sap	Sap	Cel + Sap + $Fe(O,OH)_x$	Sap + $Fe(O,OH)_x$
Other secondary minerals:				Phillipsite						
Alteration type:	2	1	3	1	3	4	1	1	3	2
Unit:	24	25	27	27	27	28	29	30	31	31
Depth (mbsf):	336.11	343.80	344.80	345.72	346.89	348.49	353.83	354.92	364.30	364.78
Major elements (wt%):										
SiO_2	48.28	48.88	49.37	48.92	49.28	49.39	49.17	49.03	48.53	49.26
TiO_2	0.78	0.90	0.89	0.90	0.93	0.89	1.02	1.00	0.92	0.94
Al_2O_3	17.55	16.44	16.57	16.34	15.35	16.31	16.61	17.40	15.78	16.90
$Fe_2O_3^*$	9.33	10.02	9.89	9.64	11.11	9.69	9.63	8.64	10.53	9.50
Fe_2O_3	4.62	3.44	3.60	2.78	4.23	3.18	3.95	3.44	4.43	3.45
FeO	4.23	5.92	5.66	6.17	6.19	5.85	5.11	4.68	5.49	5.44
MnO	0.15	0.18	0.18	0.17	0.19	0.18	0.18	0.15	0.16	0.18
MgO	7.48	7.95	7.56	7.80	7.97	7.82	8.13	7.63	8.46	7.60
CaO	13.03	13.00	12.93	12.97	12.63	12.94	12.02	11.74	11.66	13.07
Na_2O	2.00	1.91	1.95	1.93	1.86	1.91	2.18	2.21	2.13	1.98
K_2O	0.05	0.07	0.20	0.04	0.29	0.15	0.07	0.09	0.24	0.06
P_2O_5	0.06	0.08	0.07	0.07	0.07	0.07	0.08	0.07	0.11	0.08
H_2O	1.41	0.77	0.76	0.85	0.78	0.61	1.10	1.12	1.61	0.87
CO_2	0.17			0.17	0.13				0.24	
LOI	1.58	0.77	0.76	1.02	0.91	0.61	1.10	1.12	1.85	0.87
Total	100.28	100.18	100.35	99.78	100.57	99.94	100.17	99.07	100.36	100.41
Mg#	61	61	60	62	59	62	63	64	61	61
$Fe^{3+}/Fe^{(Total)}$	0.50	0.34	0.36	0.29	0.38	0.33	0.41	0.40	0.42	0.36
Trace elements (ppm):										
Li							6.80	5.34		
S							691	865		
Sc							48	46		
Cr	370	337	337	333	350	331	383	382	334	373
Ni	112	88	89	99	90	122	98	114	78	98
Cu	80	72	76	84	86	87	85	83	63	80
Zn	67	72	73	74	73	73	86	81	73	77
Ga	15	16	17	14	14	16	17	16	15	16
Rb	1	3	5	0.40	6.83	3	1.12	0.40	5	3
Sr	70	63	61	63	58	61	63	69	64	62
Y	25	25	24	29	29	25	27	24	31	25
Zr	41	45	45	48	49	45	48	48	46	45
Nb							0.33	0.35		
Cs							0.03	0.08		
La							1.24	1.12		
Ce							4.53	4.06		
Nd							5.40	5.06		
Sm							2.20	2.11		
Eu							0.95	0.85		
Gd							3.46	3.05		
Tb							0.71	0.59		
Dy							4.45	4.08		
Ho							1.01	0.94		
Er							2.91	2.64		
Tm							0.48	0.42		
Yb							2.80	2.74		
Lu							0.48	0.41		
Hf							1.51	1.36		
Tl							0.04	0.05		
Th							0.02	0.03		
U							0.03	0.05		

enriched in Cs (up to 330 ppb), and the breccia (Sample 148-896A-23R-1, 24–28 cm, Piece 3) is very strongly enriched (512 ppb Cs).

Tl is one of the most sensitive indicators of low-temperature seawater-basalt interactions (McGoldrick et al., 1979). Tl shows contrasting behavior between the different alteration assemblages, though unlike most other mobile trace elements Tl is generally more strongly enriched in the gray Type 1 saponite basalts in Hole 896A. McGoldrick et al. (1979) reported Tl concentrations for fresh basalts of below 12 ppb, and analyses from the lower volcanic rocks in Hole 504B indicate an average Tl concentration of ≈3.4 ppb (Hubberten et al., 1983). Tl commonly behaves geochemically in a similar fashion to K (Hubberten et al., 1983), but Tl concentrations for Hole 896A differ inversely with respect to K_2O (Fig. 11), so the high Tl values from Hole 896A do not appear to be related to either the presence of celadonite or $Fe(O,OH)_x$. Tl contents are insensitive to variations in MgO, but are strongly influenced by the concentration of S (Fig. 13), suggesting that (secondary) pyrite is the host phase for the enriched Tl or that Tl is concentrated during alteration under more reducing conditions. Assuming that all S is present as pyrite and that all Tl is resident in pyrite, this would lead to Tl concentrations up to ≈200 ppm in the pyrite. Such high Tl concentrations are not unrealistic (e.g., DeAlbuquerque and Shaw, 1974). The behavior of Tl in Hole 896A contrasts to that described for Hole 504B where Tl enrichments are accompanied by low sulfur and high potassium contents and a high iron oxidation ratio, with the converse true for Tl-poor samples (Hubberten et al., 1983).

Uranium appears to behave similarly to P_2O_5 in Hole 896A basalts, with both elements exhibiting slight positive correlations with $Fe^{3+}/Fe^{(Total)}$ and rough negative trends with S contents (Fig. 14). For paired alteration zones, the celadonite- and $Fe(O,OH)_x$-bearing alteration types tend to be enriched in both U and P_2O_5 compared to adjacent Type 1 saponite zones. These data suggest that both U and P are adsorbed onto Fe-oxyhydroxides in the rocks. It may be possible that discrete secondary phosphate phases contain U (Mills et al., 1994), but there is no direct evidence for this. The increase in U in altered basalts is demonstrated in a plot of Th/U vs. U on which Th/U decreases from an original value of 2.5 (e.g., Sun and McDonough, 1989) with increasing U content.

Table 3 (continued).

Core, section:	21R-1	21R-2	21R-2	22R-1	22R-2	22R-2	22R-2	22R-4	23R-1	24R-1
Interval (cm):	79–84	60–63	63–66	5–10	97–102	97–102	121–123	26–31	24–28	19–21
Piece no.:	13	8	8	2	14	14	16	4	3	1
Rock type:	M	M	M	M	M	M	M	M	B	M
Description:	Brown	Red	Gray	Brown	Red	Gray	Gray, brown	Brown	Brown breccia	Gray
Alteration assemblage:	Cel + Sap + $Fe(O,OH)_x$	Sap + $Fe(O,OH)_x$ CO_3	Sap	Sap + $Fe(O,OH)_x$	Sap + $Fe(O,OH)_x$ CO_3	Sap	Sap + $Fe(O,OH)_x$	Cel + Sap + $Fe(O,OH)_x$	Sap + $Fe(O,OH)_x$	Sap
Other secondary minerals:										Chlorite
Alteration type:	3	2	1	2	2	1	2	3	2	1
Unit:	31	31	31	32	32	32	32	33	35	36
Depth (mbsf):	373.79	375.08	375.15	382.65	385.06	385.06	385.30	387.31	392.34	401.99
Major elements (wt%):										
SiO_2	49.03	48.34	48.20	49.49	49.04	50.27	49.19	49.07	48.01	48.50
TiO_2	0.92	0.90	0.89	0.90	0.89	0.91	0.89	0.91	0.80	0.84
Al_2O_3	18.94	17.27	16.89	16.41	16.04	16.35	16.65	16.97	16.67	16.35
$Fe_2O_3^*$	8.17	9.16	7.97	9.71	10.22	9.10	9.57	9.60	10.04	9.52
Fe_2O_3	4.31	3.52	3.14	3.55	4.00	2.81	3.30	3.68	6.76	2.15
FeO	3.47	5.07	4.34	5.54	5.59	5.66	5.64	5.33	2.95	6.63
MnO	0.12	0.18	0.16	0.19	0.19	0.17	0.15	0.15	0.12	0.16
MgO	6.61	7.62	7.74	7.59	7.85	7.89	7.75	7.96	10.29	9.39
CaO	11.97	12.51	13.59	13.15	13.08	13.16	12.39	12.33	7.97	12.28
Na_2O	2.52	2.28	2.26	1.89	1.85	1.91	1.95	2.05	2.41	1.99
K_2O	0.13	0.05	0.01	0.05	0.05	0.01	0.12	0.11	0.63	0.01
P_2O_5	0.09	0.06	0.05	0.06	0.07	0.06	0.06	0.09	0.07	0.05
H_2O	1.34	1.44	1.14	0.79	0.95	0.99	1.38	1.06	3.07	1.55
CO_2		0.23	1.34		0.18	0.16			0.38	0.19
LOI	1.34	1.67	2.48	0.79	1.13	1.15	1.38	1.06	3.45	1.74
Total	99.83	100.01	100.23	100.20	100.39	100.97	100.10	100.29	100.45	100.83
Mg#	62	62	66	61	60	63	62	62	67	66
$Fe^{3+}/Fe^{(Total)}$	0.53	0.38	0.39	0.37	0.39	0.31	0.35	0.38	0.67	0.23
Trace elements (ppm):										
Li		6.90	5.44		7.70	6.64			12.39	
S		148	1605		676	611			69	
Sc		41	38		42	42			39	
Cr	413	383	332	363	351	336	363	376	361	367
Ni	114	107	148	128	114	125	120	115	158	145
Cu	90	91	88	84	76	83	82	79	54	89
Zn	68	63	61	75	71	70	76	75	59	60
Ga	16	15	14	16	14	15	15	16	14	14
Rb	4	2.26	0.18	1	1.08	0.22	2	3	7.15	0.24
Sr	89	76	95	58	60	58	64	65	81	63
Y	22	26	24	24	27	28	23	26	21	25
Zr	47	47	46	44	45	46	44	44	41	44
Nb		0.24	0.28		0.24	0.31			0.24	
Cs		0.33	0.08		0.12	0.08			0.51	
La		0.87	0.93		0.92	0.97			0.75	
Ce		3.63	3.53		3.68	3.50			3.08	
Nd		4.60	4.50		4.44	4.50			4.04	
Sm		1.91	1.83		1.82	1.90			1.56	
Eu		0.83	0.80		0.75	0.77			0.71	
Gd		2.82	2.63		2.81	2.78			2.45	
Tb		0.61	0.51		0.60	0.55			0.47	
Dy		3.76	3.49		3.84	3.92			3.23	
Ho		0.80	0.78		0.84	0.88			0.70	
Er		2.41	2.26		2.54	2.57			2.04	
Tm		0.40	0.35		0.42	0.39			0.31	
Yb		2.31	2.33		2.53	2.64			2.04	
Lu		0.39	0.34		0.40	0.39			0.32	
Hf		1.18	1.27		1.24	1.26			1.16	
Tl		0.05	0.43		0.05	0.20			0.01	
Th		0.02	0.02		0.02	0.02			0.02	
U		0.02	0.02		0.03	0.02			0.05	

Studies of weathered basalts dredged from the ocean floor indicate strong enrichments in REE relative to fresh basalts (Ludden and Thompson, 1979), however, such strong enrichments are generally not observed in samples from drill cores (Staudigel and Hart, 1983) and this is the case for samples from Hole 896A. Chondrite-normalized REE plots for paired alteration zones from Hole 896A are shown in Figure 15, against a background that displays the full range of REE data from the core. There is remarkable consistency between the traces for the different alteration types, with each sample describing light REE-depleted patterns typical of fresh N-MORB, and with the heavy REE at concentrations approximately 10 times that of chondrite. Slight irregularities in the profiles are due to minor analytical noise.

OXYGEN, CARBON, AND STRONTIUM ISOTOPIC STUDIES OF HOLE 896A

Stable O, C, S, and H and strontium isotopes are useful tracers of fluid-rock interaction in oceanic systems because of the different, and known, isotopic signatures of seawater and fresh MORB, and the relatively similar abundance of these tracers in both the fluid and rock (cf., Pb, Nd). Isotopic analyses of rocks and minerals can be used to estimate the temperatures of interaction, fluid isotopic composition, and the fluid fluxes involved. A subset of the whole-rock samples characterized for their major and trace-element chemistry were analyzed for their oxygen and strontium isotopic compositions. In addition to these analyses, calcium carbonates, smectites, and zeolites present as vein and vug fillings and as breccia cements in the Hole 896A cores were investigated for their isotopic signatures.

Whole-rock Oxygen and Strontium Isotopic Characteristics

Oxygen and strontium isotopic analyses, as well as Sr and Rb contents measured by TIMS-ID, of 29 samples from Hole 896A are presented in Table 5, and are plotted in Figures 16 through 19. $^{87}Sr/^{86}Sr$ and $\delta^{18}O$ measurements are plotted vs. depth, with respect to their different alteration types, in Figure 16. All samples have $^{87}Sr/^{86}Sr$ ele-

Table 3 (continued).

Core, section:	24R-1	24R-1	24R-1	24R-5	25R-1	25R-2	26R-1	26R-3	26R-3	26R-3
Interval (cm):	43–49	43–49	105–109	12–16	120–123	122–125	0–4	15–19	30–34	31–34
Piece no.:	3	3	7	2	16	22	1	1	3	3
Rock type:	M	M	M	M	P	P	M	P	P	P
Description:	Red	Gray	Gray	Gray	Brown	Brown	Brown	Brown	Gray	Gray
Alteration assemblage:	Sap + $Fe(O,OH)_x$	Sap	Sap	Sap	Cel + Sap + $Fe(O,OH)_x$	Sap + $Fe(O,OH)_x$	Sap + $Fe(O,OH)_x$	Sap	Sap	Sap
Other secondary minerals:	Chlorite	Chlorite						Chlorite		
Alteration type:	2	1	1	1	3	2	2	1	1	1
Unit:	36	36	36	36	37	37	37	42	42	42
Depth (mbsf):	402.39	402.39	402.85	407.80	412.50	414.02	421.00	424.01	424.16	424.40
Major elements (wt%):										
SiO_2	48.35	48.40	48.44	49.27	48.34	48.25	48.82	47.95	48.59	48.71
TiO_2	0.86	0.80	0.81	0.85	0.88	0.87	0.84	0.86	0.88	0.85
Al_2O_3	17.10	17.20	16.66	16.88	17.66	17.87	17.16	16.94	17.68	17.25
$Fe_2O_3^*$	9.35	8.12	9.18	9.14	9.24	9.43	9.47	9.85	9.73	9.44
Fe_2O_3	4.52	1.33	1.94	3.00	4.27	4.61	3.54	5.50	4.06	4.11
FeO	4.34	4.72	6.51	5.52	4.47	4.33	5.33	3.91	5.10	4.79
MnO	0.18	0.16	0.15	0.15	0.14	0.15	0.18	0.14	0.18	0.18
MgO	7.57	7.71	9.41	8.27	6.46	6.36	8.99	7.82	6.95	7.68
CaO	12.86	13.34	12.23	12.69	13.13	13.26	12.57	12.51	13.08	12.54
Na_2O	2.21	2.10	2.00	2.16	2.26	2.25	2.06	2.23	2.19	2.23
K_2O	0.04	0.01	0.01	0.02	0.04	0.04	0.07	0.08	0.05	0.06
P_2O_5	0.06	0.05	0.05	0.05	0.05	0.05	0.05	0.07	0.04	0.04
H_2O	1.42	1.55	1.35	0.96	1.31	1.32	1.50	1.67	1.42	1.69
CO_2	0.50	0.95						0.25		0.29
LOI	1.92	2.50	1.35	0.96	1.31	1.32	1.50	1.92	1.42	1.98
Total	100.48	100.37	100.28	100.43	99.49	99.84	101.68	100.35	100.77	100.94
Mg#	62	65	67	64	58	57	65	61	59	62
$Fe^{3+}/Fe^{(Total)}$	0.48	0.16	0.21	0.33	0.46	0.49	0.37	0.56	0.42	0.44
Trace elements (ppm):										
Li	7.80	6.88								
S	207	1020								
Sc	38	39								
Cr	382	400	357	375	390	396	383	390	398	383
Ni	136	145	147	153	167	170	165	155	175	198
Cu	84	84	83	88	91	91	85	89	85	84
Zn	64	64	59	63	69	67	63	69	66	64
Ga	14	14	15	15	16	15	15	15	14	15
Rb	1.96	0.18	0.22	1	2	1	3	2.05	1.02	2
Sr	75	81	61	71	75	74	67	70	68	70
Y	26	19	21	21	22	22	21	26	21	24
Zr	45	36	41	42	44	44	42	45	44	43
Nb	0.28	0.26								
Cs	0.18	0.04								
La	0.78	0.80								
Ce	3.33	3.19								
Nd	4.57	4.22								
Sm	1.66	1.50								
Eu	0.73	0.69								
Gd	2.51	2.45								
Tb	0.51	0.51								
Dy	3.86	3.53								
Ho	0.77	0.71								
Er	2.32	2.21								
Tm	0.34	0.34								
Yb	2.30	2.38								
Lu	0.38	0.35								
Hf	1.17	1.21								
Tl	0.09	0.37								
Th	0.02	0.03								
U	0.05	0.03								

Notes: P = pillow lava, M = massive unit, B = breccia, Cel = celadonite, and Sap = saponite. LOI = loss on ignition, and BD = below detection limit. Alteration types as classified in text. Mg# = atomic $100 \times Mg^{2+}/(Mg^{2+} + Fe^*)$. $Fe_2O_3^*$ = total iron as Fe_2O_3.

vated above the expected range for fresh MORB (≈0.7025–0.7027), though significantly below values for present-day or 5.9-Ma seawater of 0.70917 and 0.70893, respectively (e.g., Hodell et al., 1991).

The enrichment in radiogenic ^{87}Sr and the range displayed by the different alteration types decreases with depth. Samples below 400 mbsf are slightly elevated ($^{87}Sr/^{86}Sr$ = 0.7027–0.7037) above the MORB baseline and there are only small variations between different alteration types (e.g., subsamples of Sample148-896A-29R-1, 10–21 cm, Piece 2; Table 5). Higher up in the core, juxtaposed subsamples of contrasting alteration assemblages have quite different strontium isotopic compositions (Fig. 16), though a consistent pattern of elevated $^{87}Sr/^{86}Sr$ and a particular type of alteration is not observed. Breccia Sample 148-896A-23R-1, 24–28 cm (Piece 3), yields a moderately elevated $^{87}Sr/^{86}Sr$ (≈0.7048), indicating substantial incorporation of seawater strontium (≈65% seawater Sr). The Sr isotopic profile for Hole 896A is similar to that of nearby Hole 504B (see Alt et al., this volume, and references therein) however, samples from this study are more enriched in radiogenic strontium than the Hole 504B analyses. This may reflect, to some extent, a sampling bias towards less altered material in the Hole 504B studies.

Fresh MORB has $\delta^{18}O = 5.9‰ \pm 0.3‰$ (Taylor, 1968). All samples from Hole 896A have oxygen isotopic compositions elevated with respect to pristine MORB, indicating isotopic exchange of oxygen between seawater and basalts at low temperatures (≤150°C). In contrast to the strontium isotopic profile, sample pairs from the upper portion of the hole display only slight differences between the alteration assemblages. There are however, significant isotopic differences between the Type 1 and 2 basalts from the massive units between 370 and 415 mbsf, with the gray saponite basalts yielding higher $\delta^{18}O$ than the neighboring $Fe(O,OH)_x$-bearing samples. Samples from the

Table 3 (continued).

Core, section:	27R-1	27R-1	28R-1	29R-1	29R-1	29R-1	29R-1	29R-1	30R-1	30R-2
Interval (cm):	124–130	137–141	0–5	10–14	10–14	14–21	35–41	109–112	65–70	5–10
Piece no.:	15	16	1	2	2	2	5	16	10	1
Rock type:	P	P	P	P	P	P	P	M	P	M
Description:	Gray	Gray	Brown	Light gray	Black	Red	Gray	Brown	Red-brown	Red, gray
Alteration assemblage:	Sap	Cel + Sap	Sap + $Fe(O,OH)_x$	Sap	Cel + Sap + $Fe(O,OH)_x$	Cel + Sap + $Fe(O,OH)_x$	Sap	Sap + $Fe(O,OH)_x$	Sap + $Fe(O,OH)_x$	Cel + Sap + $Fe(O,OH)_x$
Other secondary minerals:		Phillipsite								
Alteration type:	1	4	2	1	3	3	1	2	2	3
Unit:	44	44	47	48	48	48	48	49	50	51
Depth (mbsf):	431.74	431.87	440.00	449.80	449.80	449.80	450.05	450.79	459.95	460.84
Major elements (wt%):										
SiO_2	48.83	48.49	48.44	49.65	49.56	49.50	50.20	49.14	49.40	50.11
TiO_2	0.65	0.87	0.68	0.88	0.88	0.87	0.88	0.86	0.82	0.88
Al_2O_3	16.38	16.38	17.25	15.55	15.38	15.26	15.45	17.13	15.91	15.41
$Fe_2O_3^*$	9.68	9.56	9.98	9.17	9.53	10.68	9.93	9.33	9.17	10.37
Fe_2O_3	1.44	3.44	4.40	2.55	2.85	3.76	2.67	4.14	2.60	3.40
FeO	7.41	5.50	5.02	5.95	6.01	6.23	6.53	4.67	5.91	6.27
MnO	0.16	0.18	0.16	0.18	0.19	0.20	0.20	0.17	0.20	0.23
MgO	9.50	7.80	7.42	8.57	8.42	8.04	8.52	7.52	8.06	8.33
CaO	13.20	13.10	13.84	13.06	13.00	12.95	13.09	13.31	12.82	13.05
Na_2O	1.67	2.03	1.79	2.06	2.06	1.98	2.01	2.22	2.06	2.01
K_2O	0.03	0.10	0.04	0.08	0.12	0.28	0.10	0.03	0.05	0.17
P_2O_5	0.04	0.07	0.04	0.06	0.07	0.06	0.06	0.06	0.07	0.06
H_2O	0.53	0.79	1.46	0.61	0.72	0.66	0.40	0.83	0.58	0.48
CO_2				0.18	0.15	0.13		0.19		
LOI	0.53	0.79	1.46	0.79	0.87	0.79	0.40	1.02	0.58	0.48
Total	100.64	99.36	101.08	100.02	100.05	100.60	100.82	100.78	99.12	101.08
Mg#	66	62	60	65	64	60	63	61	64	61
$Fe^{3+}/Fe^{(Total)}$	0.15	0.36	0.44	0.28	0.30	0.35	0.27	0.44	0.28	0.33
Trace elements (ppm):										
Li	3.84		3.77	4.85	4.79	4.30				
S	656		520	241	281	258				
Sc	38		41	46	43	45				
Cr	410	433	420	380	401	411	393	357	418	399
Ni	155	143	157	134	131	103	124	124	133	108
Cu	84	77	83	95	107	101	106	94	91	101
Zn	63	67	65	76	77	71	72	60	69	72
Ga	13	15	15	14	15	14	14	15	15	15
Rb	0.48	3	0.73	0.91	2.04	7.02	1.26	2	2	5
Sr	70	70	70	58	58	56	58	69	63	58
Y	16	23	16	28	29	26	24	25	23	25
Zr	28	43	30	44	44	43	41	42	40	42
Nb	0.24		0.25	0.42	0.38	0.40				
Cs	0.02		0.03	0.03	0.08	0.21				
La	0.66		0.72	0.90	0.86	0.87				
Ce	2.66		2.79	3.52	3.45	3.29				
Nd	3.27		3.47	4.56	4.49	4.15				
Sm	1.33		1.39	1.99	1.81	1.75				
Eu	0.55		0.57	0.79	0.71	0.70				
Gd	1.83		2.13	2.73	2.73	2.70				
Tb	0.37		0.42	0.54	0.55	0.52				
Dy	2.58		2.73	4.06	4.16	3.81				
Ho	0.55		0.61	0.88	0.94	0.80				
Er	1.72		1.79	2.60	2.61	2.41				
Tm	0.26		0.28	0.38	0.39	0.36				
Yb	1.74		1.90	2.61	2.61	2.42				
Lu	0.27		0.29	0.38	0.38	0.33				
Hf	0.88		0.93	1.15	1.21	1.22				
Tl	BD		0.02	0.03	0.03	0.05				
Th	0.01		0.01	0.02	0.02	0.02				
U	0.02		0.02	0.04	0.05	0.03				

pillow lavas deeper than 415 mbsf have only slightly elevated $\delta^{18}O$, and analyses of the different alteration types cluster tightly, consistent with the Sr isotope analyses of these samples. The saponite + $Fe(O,OH)_x$ + carbonate-rich breccia (Sample 148-896A-23R-1, 24–28 cm, Piece 3) has a highly elevated $\delta^{18}O$ of 9.3‰.

$\delta^{18}O$ and $^{87}Sr/^{86}Sr$ are compared in Figure 17. Values for both parameters increase during low-temperature isotopic exchange with seawater. There are no consistent trends between the different alteration types and the isotopic measurements. A number of alteration sensitive parameters are plotted vs. $^{87}Sr/^{86}Sr$ in Figure 18 to ascertain the processes and phases most important in the incorporation of seawater Sr. There is little variation of whole-rock CaO with $^{87}Sr/^{86}Sr$, though the two samples with the least radiogenic isotopic ratios have relatively low CaO contents. There is no correlation between Na_2O and $^{87}Sr/^{86}Sr$. These parameters are important because plagioclase contains most of the Sr in fresh basalt, and the alteration of the primary plagioclase to albite or clay minerals should be accompanied by isotopic exchange of seawater strontium and elevated $^{87}Sr/^{86}Sr$ in the secondary mineral-bearing altered assemblages. The absence of a correlation between CaO and Na_2O and $^{87}Sr/^{86}Sr$ agrees with petrographic observations that the primary feldspars are little altered, and hence predominantly retain their primary isotopic characteristics. K_2O is enriched in most samples compared to fresh basaltic glass. This enrichment is accounted for by the presence of potassium-bearing celadonite (and, to a much lesser extent, saponite and rare K-feldspar) filling of pore space and replacing phenocrysts, particularly in the $Fe(O,OH)_x$-bearing basalts. The strong potassium enrichment in a number of samples with relatively low $^{87}Sr/^{86}Sr$ ratios, indicates that celadonite does not contain much strontium. Rb displays a similar pattern with $^{87}Sr/^{86}Sr$ as K_2O. Strontium contents and $^{87}Sr/^{86}Sr$ are presently not available for samples of celadonite from Hole 896A.

Strontium concentrations form two subparallel trends with increasing $^{87}Sr/^{86}Sr$, which indicates that elevated $^{87}Sr/^{86}Sr$ reflect both the exchange and addition of seawater strontium to the altered rocks. This agrees with the strong trend of increasing strontium contents with increasing LOI (Fig. 9). The reason for the two subparallel

trends is not apparent though this may reflect interaction with seawater-derived fluids with different strontium contents and isotopic characteristics.

$Fe^{3+}/Fe^{(Total)}$ shows a rough trend of increase with increasing $^{87}Sr/^{86}Sr$ (Fig. 18). The tie-lines between sample pairs of different alteration assemblages display a variety of attitudes emphasizing the irregular behavior of these parameters. $^{87}Sr/^{86}Sr$ is generally insensitive to LOI (Fig. 18), which includes both structurally bound water and other volatile components, of which CO_2 is generally the most important. CO_2 contents were analyzed for all the samples characterized for their isotopic compositions. The limit of reliable CO_2 analysis is probably 0.3 wt% (see Table 3). Most samples have low "background" CO_2 contents of less than 0.2 wt% and are essentially carbonate free. A number of samples have high CO_2 contents, including two samples of type 1 saponite basalt that have higher than expected $^{87}Sr/^{86}Sr$. $^{87}Sr/^{86}Sr$ is plotted vs. measured H_2O and CO_2 (Fig. 18). $^{87}Sr/^{86}Sr$ is essentially insensitive to these parameters, though samples with high CO_2 appear enriched in ^{87}Sr. In general, high $^{87}Sr/^{86}Sr$ are not the result of the simple addition of carbonate, though the $^{87}Sr/^{86}Sr$ of some samples may have been elevated somewhat by this process.

A number of Sr contents and strontium isotopic compositions of carbonate veins and cements from Hole 896A are available (see Table 6 and subsequent section). By identifying the carbonate mineral present in the contaminated whole-rock and its mode of formation (see subsequent section) "carbonate-free" $^{87}Sr/^{86}Sr$ and Sr contents were calculated (see Fig. 18). Calcium carbonate from Hole 896A displays only a limited range of strontium isotopic compositions ($^{87}Sr/^{86}Sr \approx 0.7079$–$0.7088$), but Sr contents are highly variable (35–3340 ppm, Table 6), which complicates these preliminary calculations. Further analyses of acid leachates and residues will have to be conducted to better constrain the effects of secondary carbonates on whole-rock Sr contents and isotopic compositions.

There are general trends of increasing whole-rock $\delta^{18}O$ with $Fe^{3+}/Fe^{(Total)}$ and LOI (Fig. 19), though carbonate-bearing type 1 basalts (Samples 148-896A-21R-2, 60–63 cm, Piece 8, and 24R-1, 43–49 cm, Piece 3) have higher $\delta^{18}O$ than might be expected given the trend from the majority of the samples toward the breccia sample (148-896A-23R-1, 24–28 cm, Piece 3). Carbonate-free whole-rock $\delta^{18}O$ values can be calculated for these samples in a fashion similar to that for the strontium isotopes, though with less uncertainty as the amount of oxygen in the carbonate is stoichiometrically fixed. The recalculated values are shown in the plot of H_2O vs. $\delta^{18}O$ on Figure 19. The $\delta^{18}O$ of the two outlier samples is significantly reduced, though not sufficiently so to group them with the main cluster of analyses.

A few samples fall close to the mixing trends between basalt and smectite formed at 0°–50°C (Muehlenbachs and Clayton, 1972; Böhlke et al., 1984), but most samples fall above these lines (Fig. 19). This is typical of many slightly altered basalts drilled from the oceanic crust and is most likely the result of several effects in the Hole 896A rocks, including the presence of high-H_2O, low-$\delta^{18}O$ Fe-oxyhydroxides, as well as higher alteration temperatures (Böhlke et al., 1984).

Isotopic Compositions and Trace-element Contents of Carbonates from Hole 896A

Calcium carbonate veins and breccia cements are present throughout the Hole 896A core. $\delta^{13}C$ in calcite, aragonite, and calcium carbonate mixtures range from –1.24‰ to 2.0‰ (Table 6; Fig. 20), which is consistent with the precipitation of carbonate from seawater. There are no systematic differences in the carbon isotopic compositions of the carbonate polymorphs (Figs. 20, 21), but there is a subtle trend of decreasing $\delta^{13}C$ with depth, though a range of compositions is present at any particular level. These analyses are consistent with the carbon isotopic measurements from the upper 400 m of basement in Hole 504B (Alt et al., 1986b).

Carbonate $\delta^{18}O$ values from Hole 896A have a bimodal distribution (Table 6; Fig. 20) with analyses falling in the ranges from 21.2‰ to 24.2‰ and from 26.1‰ to 28.1‰. Calcite and aragonite, in both blocky and fibrous habits are present in each group. $\delta^{18}O$ measurements of carbonates from Hole 504B range from 24‰ to 33‰, but display no bimodal distribution (Alt et al., 1986b).

The bimodal distribution of $\delta^{18}O$ values for Hole 896A carbonates suggests two different regimes of carbonate mineral formation. Assuming formation in equilibrium with normal seawater ($\delta^{18}O = 0‰$), the higher $\delta^{18}O$ carbonates precipitated at 26°–35°C and lower $\delta^{18}O$ carbonates formed at higher temperatures of 47°–67°C (Friedman and O'Neil, 1977; Fig 20). Alternatively, the bimodal distribution of $\delta^{18}O$ could have resulted from precipitation of carbonate from different composition fluids. Pore fluids in the sediments overlying Hole 504B have $\delta^{18}O$ as low as –3‰ to –4‰ as the result of low-temperature interaction of pore fluids with basaltic material in the sediment and basement (Mottl et al., 1983). If the low-$\delta^{18}O$ carbonates in Hole 896A formed from fluids having $\delta^{18}O = -4‰$, they would have formed at temperatures of 26°–42°C (Friedman and O'Neil, 1977). These temperatures overlap those for the high-$\delta^{18}O$ carbonates if the latter formed from unaltered seawater. Thus, the bimodal distribution of carbonate $\delta^{18}O$ values can be accounted for by either variations in temperature or fluid composition (or both); however, additional constraints provided by Sr isotopes and trace-element contents suggest that higher temperatures were the major difference causing the $\delta^{18}O$ variations of the carbonates.

All calcite, high-$\delta^{18}O$ aragonite, and mixed carbonate samples from Hole 896A have remarkably similar Sr isotopic compositions, which are apparently insensitive to depth of occurrence, carbonate mineralogy, and habit or oxygen isotopic composition ($^{87}Sr/^{86}Sr = 0.708775 \pm 0.000066$ [2σ], $N = 11$; Table 6; Figs. 20–22). Analyses of three splits of Sample 148-896A-14R-2, 55–62 cm (Piece 7), are almost within error of each other, with the clear, glassy separate slightly less radiogenic than the cloudy carbonate and the bulk mixture. Two samples of blocky and one of fibrous, low-$\delta^{18}O$ aragonite have somewhat lower $^{87}Sr/^{86}Sr$ than the range displayed by the other carbonates. Low-$\delta^{18}O$ aragonite is only a minor phase in Hole 896A and is generally present in uncommon fine veinlets. The $^{87}Sr/^{86}Sr$ of the fibrous, low-$\delta^{18}O$ aragonite (Sample 148-896A-22R-1, 53–54 cm, Piece 6) is just outside the 2σ range exhibited by the majority of carbonates and may not be anomalous. The saponite residue from this sample has a $^{87}Sr/^{86}Sr$ of 0.708571. The two low-$\delta^{18}O$ blocky aragonites are significantly less radiogenic ($^{87}Sr/^{86}Sr = 0.7079$–0.7084) than the other carbonates.

The strontium isotopic composition of seawater has increased monotonically for the last 45 Ma (Burke et al., 1982; Hodell et al., 1991) and present-day and 5.9-Ma seawater have $^{87}Sr/^{86}Sr$ ratios of 0.70919 and 0.70895, respectively (Hodell et al., 1991). All carbonate samples from Hole 896A (and Hole 504B; see Hart et al., 1994) have $^{87}Sr/^{86}Sr$ lower than that of 5.9-Ma seawater (Fig. 20), though significantly higher than fresh MORB or altered basalt ($^{87}Sr/^{86}Sr \approx 0.7027$–$0.7055$). Carbonate $^{87}Sr/^{86}Sr$ ratios lower than seawater values require the incorporation of basaltic strontium ($^{87}Sr/^{86}Sr = 0.7025$–0.7027) and preclude the use of the seawater strontium curve for constraining the time of deposition of these carbonates. Pore waters in the overlying sediments may have $^{87}Sr/^{86}Sr$ depleted with respect to modern seawater, but the lower value of this depletion is limited by the age of the oldest sediment (<5.9 Ma), and hence sediment pore waters cannot be the cause of the depleted radiogenic strontium ratios in the carbonate veins.

Depending on the time of carbonate precipitation (0–5.9 Ma) and the nature of the host rock with which basement fluids interacted ($^{87}Sr/^{86}Sr = 0.7027$–0.7055), approximately 2%–10% of the strontium in the carbonates must have been derived from the basalt. The limited range of $^{87}Sr/^{86}Sr$ ratios recorded from the majority of carbonates indicate that basement fluids, at the time of carbonate deposition, were buffered to this strontium isotopic composition by wall rock in-

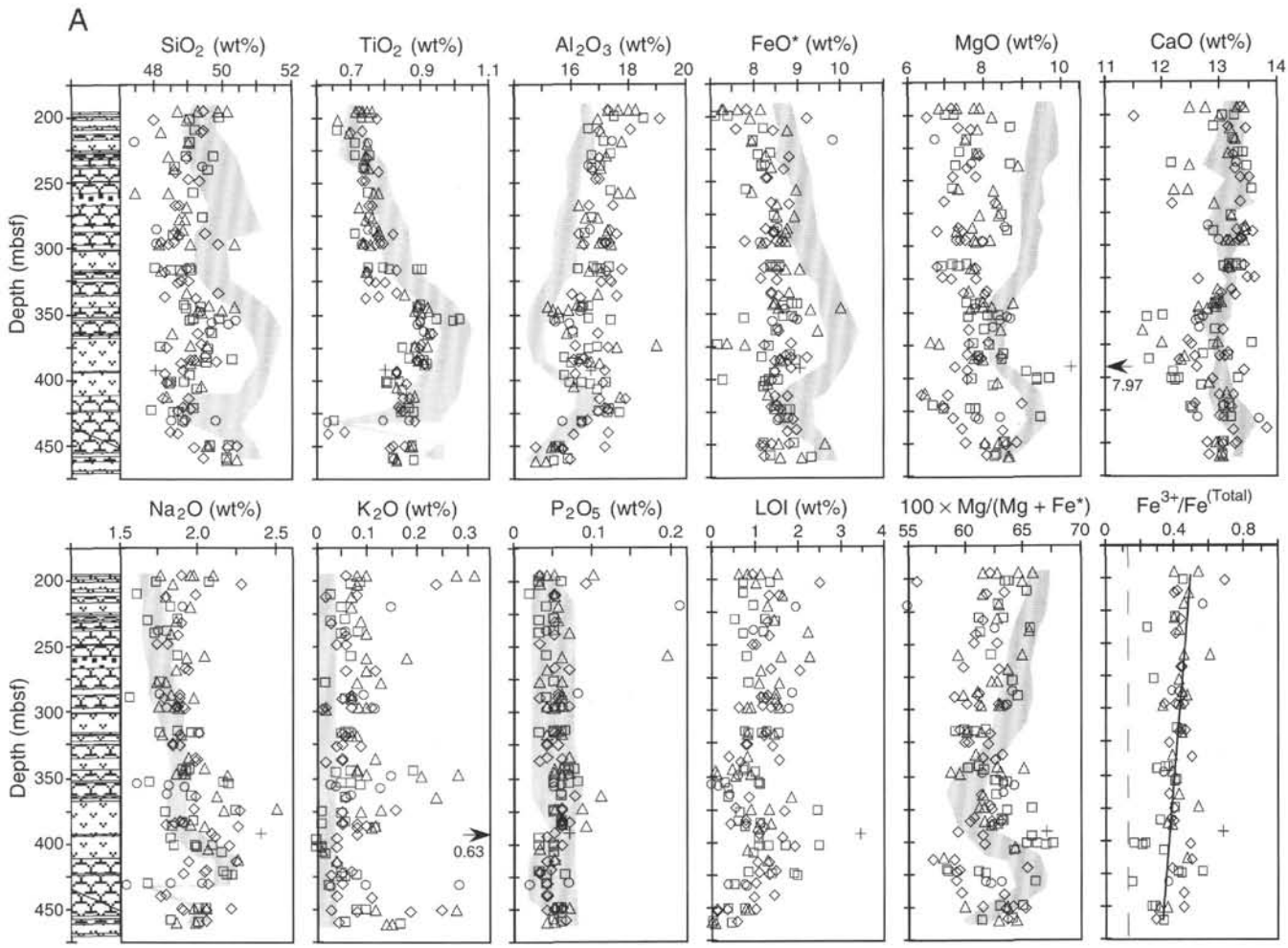

Figure 6. **A.** Shipboard and shore-based whole-rock major element contents plotted vs. depth for Hole 896A. Lithologic column provided for reference. Patterns as in Figure 3. Samples distinguished by secondary mineral assemblage: squares = Type 1 saponite; diamonds = Type 2 saponite + Fe(O,OH)$_x$; triangles = Type 3 celadonite + saponite + Fe(O,OH)$_x$; circles = Type 4 celadonite + saponite; (+) = breccia (Sample 148-896A-23R-1, 24–28 cm, Piece 3). Stippled area shows the range of fresh glass compositions (Fisk et al., this volume). Dashed line in $Fe^{3+}/Fe^{(Total)}$ panel indicates the primary N-MORB iron oxidation state of 0.12. Solid line is a regression line though the 25-m averages of measured $Fe^{3+}/Fe^{(Total)}$. **B.** Whole-rock trace-element contents of shipboard and new shore-based sample analyses from Hole 896A plotted vs. depth. Horizontal lines join subsamples with different alteration minerals in the Li panel. Subvertical solid and dashed lines shows the average primary S concentration of N-MORB (± 1 standard deviation; 960 ± 60 ppm; e.g., Alt et al., 1989).

teraction, at least in the upper few hundred meters of the ocean crust. There is no consistent difference between low- and high-$\delta^{18}O$ carbonates with respect to $^{87}Sr/^{86}Sr$ (Fig. 21) or proportion of basaltic Sr present (Fig. 22), which indicates no significant difference in amount of seawater-rock interaction before carbonate deposition. This supports the interpretation that there were no significant differences in the $\delta^{18}O$ of the fluids that formed the low- and high-$\delta^{18}O$ carbonates, and that the oxygen isotope variations of the carbonates reflect mainly differences in their temperatures of formation.

For the low-$\delta^{18}O$ aragonite with the lowest $^{87}Sr/^{86}Sr$ (≈0.7079), the proportion of rock-derived strontium is 15%–30%, approximately twice that in the other carbonates. This indicates that the fluid from which this carbonate precipitated contained a significantly greater basalt component, and suggests that the fluid could have been more depleted in ^{18}O. However, the trace-element composition of this sample is consistent with a higher temperature of formation than the high-$\delta^{18}O$ carbonates (see below).

The trace-element concentrations of carbonate minerals display contrasting behavior between the high- and low-$\delta^{18}O$ phases (Table 6; Fig. 23). The high-$\delta^{18}O$ calcites and aragonites have low Mg, Mn, and Fe (<100 ppm) but high Sr contents, whereas the low-$\delta^{18}O$ carbonates have variable but significantly higher Mg, Mn, and Fe and lower Sr (Fig. 23). The two low-$\delta^{18}O$ aragonite samples have extremely low Sr content (35 and 49 ppm) but incorporate the highest concentrations of Mg, Mn, and Fe (up to 1920, 5980, and 799 ppm, respectively). Mn and Fe concentrations increase linearly with increasing Mg content (Fig. 24) in most carbonate samples. Carbonate Sr concentrations decrease sharply with increasing Mg content. With the exception of the low-$\delta^{18}O$ aragonite, the strontium contents of the Hole 896A carbonates are similar to the limited data reported by Hart et al. (1994) for aragonite from the upper part of Hole 504B (1150–2300 ppm).

Low-Mg contents of the high-$\delta^{18}O$ carbonates indicate formation from fluids with Mg/Ca ratios lower than seawater (Baker et al., 1982; Delaney, 1989; Mucci and Morse, 1990), suggesting that the seawater-derived basement fluids had lost Mg and possibly gained Ca through prior reactions with basalt. If the low-$\delta^{18}O$ carbonates formed from more highly reacted, ^{18}O-depleted fluids, they would be

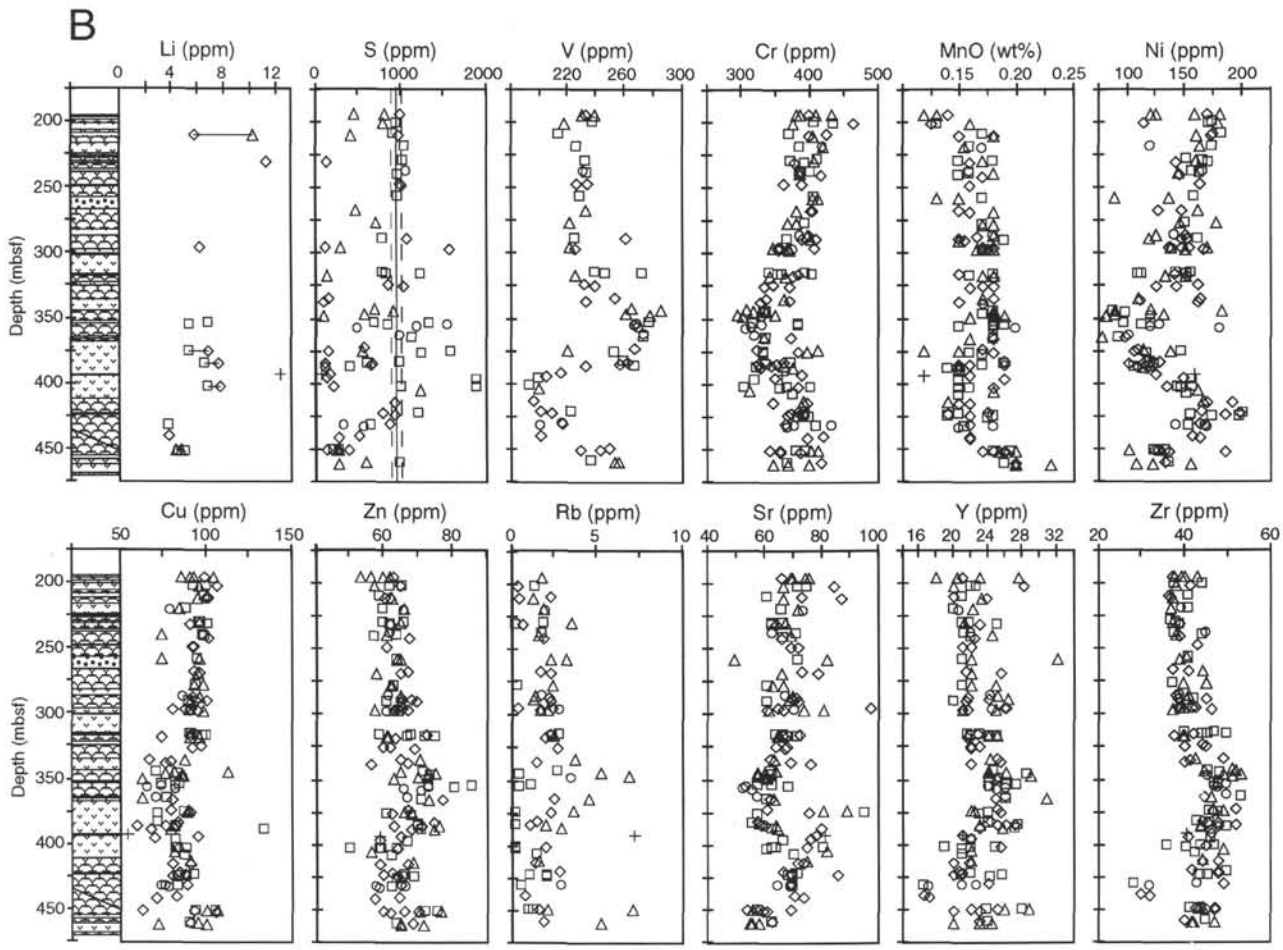

Figure 6 (continued).

expected to have similarly low, or even lower, Mg contents. On the contrary, the low-$\delta^{18}O$ carbonates have higher Mg contents. Mg is increasingly partitioned from solution into Ca-carbonates with increasing temperature (Mucci and Morse, 1990), so this supports the interpretation that the low $\delta^{18}O$-carbonates indeed formed at higher temperatures than the other carbonates, and that their low $\delta^{18}O$ values are not simply the result of formation from more highly-reacted fluids.

The distribution coefficient of Sr in calcite is only slightly affected by temperature (e.g., Katz et al., 1972) and hence the low Sr concentrations (35–1690 ppm; Fig. 23) of the low $\delta^{18}O$ carbonates suggest decreasing Sr/Ca of the fluids. Higher Mn and Fe concentrations in the low $\delta^{18}O$ carbonates reflect possible temperature effects similar to Mg or a greater mobilization of metals by more reducing conditions.

Strontium Isotopic Compositions of other Secondary Minerals from Hole 896A

Saponite is the most abundant secondary mineral in Hole 896A. Four of the five saponite samples from Hole 896A have measured $^{87}Sr/^{86}Sr$ from 0.70842 to 0.70904 (Table 7; Fig. 25). However, some of these saponite samples, have high Rb contents (>7 ppm) and high $^{87}Rb/^{86}Sr$ (≈10) for which a significant age correction may be necessary depending on the time of formation of the clay. Insufficient data are presently available to construct a rigorous isochron but lower limits on $^{87}Sr/^{86}Sr$ can be calculated as these clays can be no more than 5.9 Ma old. Applying this age correction these saponites could have $^{87}Sr/^{86}Sr$ initial ratios as low as 0.70825 (Table 7). One example of a fibrous saponite from a fine (≈1 mm) vein in pillow lavas from the upper part of the core (Sample 148-896A-6R-2, 66–72 cm, Piece 8) has a highly depleted strontium isotopic composition ($^{87}Sr/^{86}Sr$ = 0.7043 to 0.7044, for t = 5.9 to 0 Ma, respectively; Table 7), which is similar to the ratios in the host rocks.

Sample 148-896A-27R-3, 10–16 cm (Piece 2), contains a large (≈5 cm) vug filled with euhedral analcite and fibroradial natrolite that, from textural criteria, grew within a fluid-filled cavity within the pillow lavas. The natrolite sample has a $^{87}Sr/^{86}Sr$ measured ratio of 0.707440, intermediate between MORB and seawater, but the analcite ratio is extremely radiogenic ($^{87}Sr/^{86}Sr$ = 0.70914) close to the Sr isotopic composition of modern seawater (≈0.7092; Hodell et al., 1991). The natrolite sample has a low $^{87}Rb/^{86}Sr$ (≈0.02) and there is no significant age correction but the analcite has a moderately high $^{87}Rb/^{86}Sr$ (≈3.62) and could have an initial ratios as low as 0.7088 (for t = 5.9 Ma; see Fig. 25). These two minerals do not form a geologically sensible isochron (i.e., requires t >5.9 Ma) and the near seawater-like $^{87}Sr/^{86}Sr$ ratio of the analcite suggests that this mineral may have freely exchanged Sr with seawater up to the present day.

DISCUSSION

Timing of Alteration Effects in Hole 896A

The relative timing of different alteration processes and their effects in Hole 896A are directly constrained by the geometries of the alteration halos and the filling sequences of veins and vesicles in the

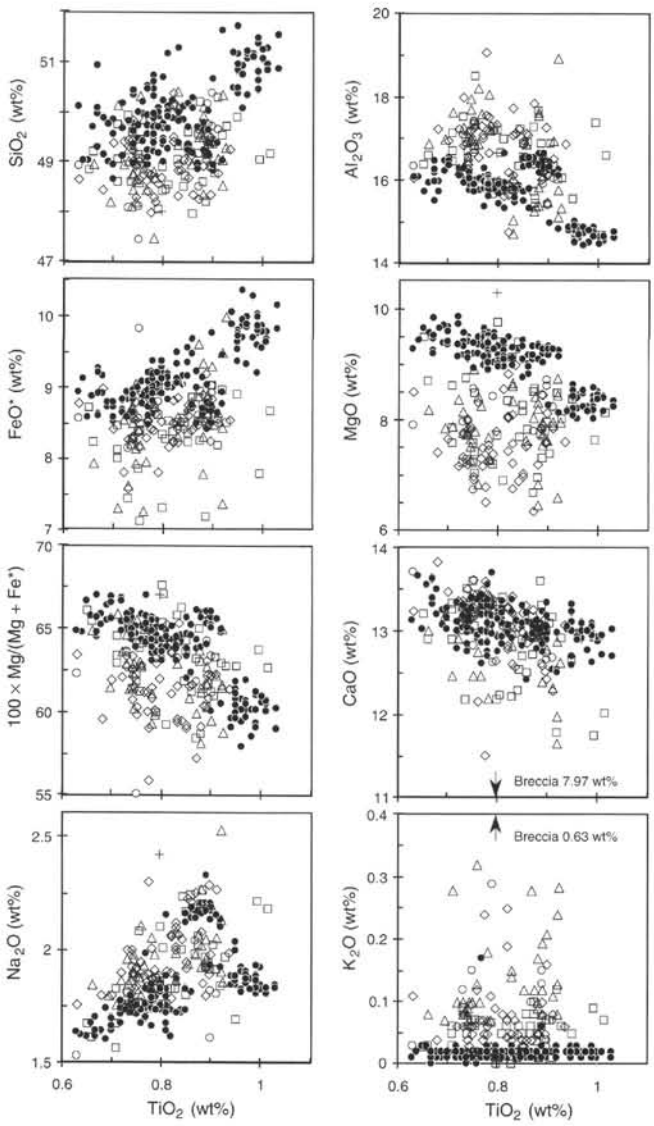

Figure 7. Whole-rock major element concentrations compared with TiO_2, an immobile incompatible element. Symbols as in Figure 6. Dots show the range of fresh glass compositions (see Fisk et al., this volume).

rocks. Comparison of the alteration assemblages in Hole 896A with other, particularly younger, rocks from the seafloor, in conjunction with the results from heat-flow and pore-water surveys of ridge flank environments provide further information on the timing and conditions of seawater-basalt interaction.

Occurrences of the four alteration types in Hole 896A provide important controls on the timing of different alteration processes:

1. Type 1 saponite-rich rocks occur pervasively throughout the core.

2. Type 2 saponite + $Fe(O,OH)_x$ assemblages occur in reddish alteration halos around fractures, with alteration clearly related to circulation of fluids in the fractures.

3. Celadonite is present locally in red alteration halos resulting in the Type 3 saponite + celadonite + $Fe(O,OH)_x$ assemblages, which occur (a) within the halos forming a band close to or immediately along fractures around which these halos are developed; (b) as patches or bands enclosed irregularly within the halos; and (c) rarely as a band at the outer edge of the red halo where it meets the dark gray, saponite-rich host rock.

4. Type 4 celadonite + saponite zones occur as darker alteration halos along fractures in otherwise gray rocks containing the Type 1 saponite assemblage.

Various geometrical relationships of the alteration assemblages suggest that three different processes, forming saponite, celadonite, and the $Fe(O,OH)_x$-rich halos, are superimposed in a variety of combinations. This suggestion is supported by secondary mineral paragenetic sequences in the rocks, and by analogy with other altered seafloor basalts.

The filling sequences of veins and vesicles provide some constraints on the relative timing of these processes. The generalized sequence in Hole 896A is as follows: (1A) celadonite ± $Fe(O,OH)_x$; (1B) $Fe(O,OH)_x$; (2) saponite ± carbonates; and (3) carbonates + zeolites. Some variations and complications of this sequence exist, however. One vein records a sequence from early saponite, to celadonite, and then saponite again. Minor chlorite is the earliest formed phase locally in the coarser grained portions of massive units. This chlorite most likely formed during initial cooling and penetration of seawater into the rocks. Carbonates commonly formed simultaneously with saponite in some veins, but carbonate also commonly postdates saponite, indicating continuing or multiple stages of carbonate formation. Carbonate veins postdate zeolites in some hyaloclastic breccias, but in most cases carbonates and zeolites do not occur together so their relative timing is unconstrained. Despite these variations, which document local differences or fluctuations in alteration conditions and their evolution, evidence for the generalized sequence is strong. The presence in breccias of rock fragments displaying red $Fe(O,OH)_x$-rich alteration halos, which are broken and cemented by saponite, provides good evidence that the formation of saponite in veins and breccias postdated (or at least continued to form later than) the oxidation and development of the red halos.

Altered oceanic volcanic rocks drilled from other localities are generally similar in mineralogy and sequence of alteration zonations to those sampled in Hole 896A (e.g., Andrews, 1977; Böhlke et al., 1981; Alt and Honnorez, 1984; Alt et al., 1986a; Alt, 1993). Basalts from oceanic crust younger than Hole 896A provide some constraints on the absolute timing of seafloor alteration. Celadonite is the only secondary mineral present in the very youngest basalts (<10 ka; Adamson and Richards, 1990), celadonite + Fe-oxyhydroxides are present in alteration halos in rocks less than 1 Ma, and saponite is present with the other minerals in rocks >2 Ma (Humphris et al., 1980; Laverne and Vivier, 1983). All of the mineral zones, including late zeolites and carbonates, are present in 3.2-m.y.-old rocks (Andrews, 1977), suggesting that most alteration of the crust may be complete by about 3 Ma, although carbonate veins may continue to form for several millions of years (e.g., Hart et al., 1994). Local and regional differences in structure (fracturing, faulting, and primary volcanic stratigraphy) and sedimentation rate most likely play important roles in controlling the evolution and duration of alteration, however.

Alteration Processes in the Ridge-Flank Hydrothermal Upflow Zone at Site 896

Alteration effects in the rocks recovered from Hole 896A are generally similar to those present in the uppermost volcanic rocks of Hole 504B (<600 mbsf) that have been affected by oxidizing alteration at low temperatures (0°–100°C) by the open circulation of seawater through the highly permeable upper extrusives (e.g., Alt et al., 1986a). The most striking differences between the Hole 896A and 504B cores include the greater abundance of carbonate, hyaloclastite and breccias and the development of thick (≈1 cm) saponite veins in the new hole.

Off-axis circulation and alteration of the volcanic section of ocean crust can be broadly divided into "open" and "restricted" circulation

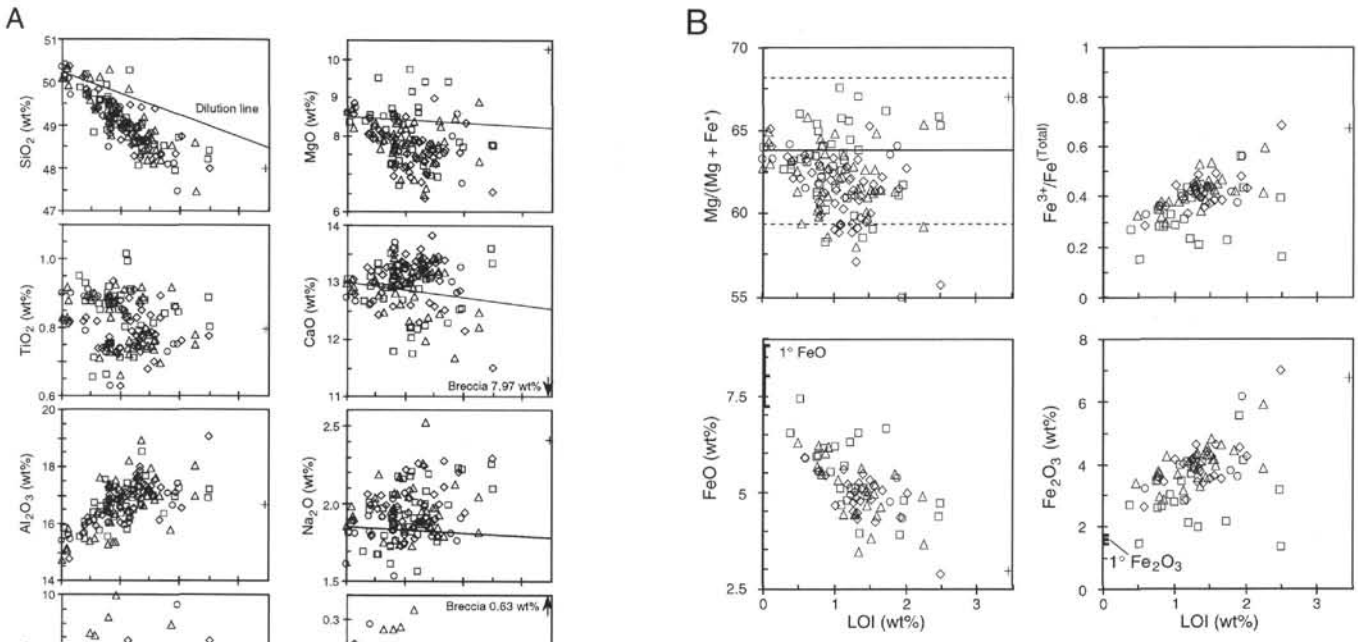

Figure 8. **A.** Whole-rock major element concentrations compared to loss on ignition (LOI). Symbols as in Figure 6. Solid lines show the trend from an arbitrary primary content (at LOI = 0 wt%), of simple dilution owing to hydration. **B.** Magnesium number (Mg# = atomic ratio of 100 × Mg/[Mg + Fe*]), iron oxidation ($Fe^{3+}/Fe^{(Total)}$), and measured ferrous and ferric iron contents vs. LOI. Solid and dashed horizontal lines show the average Mg number (± 2 standard deviations) for fresh glasses from Hole 896A (see Fisk et al., this volume). Ferrous and ferric iron contents trend towards the expected range of fresh glasses, assuming $Fe^{3+}/Fe^{(Total)}$ = 0.12 (e.g., Puchelt and Emmermann, 1983).

systems, in which open systems are colder and seawater dominated, and restricted circulation is warmer and the compositions of seawater fluids circulating in the basement are more altered (Alt and Honnorez, 1984; Alt et al., 1986a, 1992; Alt, 1993, in press; Mottl and Wheat, 1994). Early celadonite formation at Site 896 probably occurred during open circulation of seawater, but may also have been influenced by solutions derived from deeper in the crust. In very young rocks, where chemical changes can be determined unequivocally by comparison to adjacent fresh rock, such early celadonite alteration results in addition of alkalies and iron to the rocks. In addition, the rocks are oxidized and hydrated (Laverne and Vivier, 1983). Iron may be derived locally from the breakdown of igneous titanomagnetite or volcanic glass, but could also be derived from reactions deeper in the volcanics, where conditions are more reducing and iron more easily mobilized (Alt et al., 1986a; Alt, in press). Alternatively, the formation of celadonite could be related to low-temperature, distal upwelling hydrothermal fluids close to the spreading axis. There is no direct evidence for the temperature of formation of celadonite in Hole 896A, but celadonite in other seafloor basalts formed at temperatures up to 40°C (e.g., Seyfried et al., 1978; Stakes and O'Neil, 1982; Böhlke et al., 1984). Chemical changes in the rocks included increased alkali contents, hydration, and oxidation, and slight increases in $\delta^{18}O$ and $^{87}Sr/^{86}Sr$.

Open circulation of seawater through the upper crust occurs in ridge-flank circulation systems relatively near the spreading axis, where there is little sediment cover and common outcrops of basement allow direct access of large volumes of seawater into the permeable upper crust (e.g., Mottl and Wheat, 1994). The large flux of seawater into the crust results in low temperatures (<25°C) in the upper volcanic section (Mottl and Wheat, 1994; Wheat and Mottl, 1994) and the composition of basement fluids is little changed from bottom seawater and oxidized conditions are maintained. Similar conditions have been inferred on the basis of whole-rock chemical changes in basement rocks (e.g., Alt and Honnorez, 1984; Alt et al., 1986a, 1992; Alt, 1993, in press). The formation of the $Fe(O,OH)_x$-rich, red alteration halos in Hole 896A occurred during such open circulation of seawater. The main effect on the rocks was oxidation, but chemical changes included increased H_2O, alkali, U, and P contents, elevated $\delta^{18}O$ and $^{87}Sr/^{86}Sr$, as well as losses of S and possibly Tl, Mg, and Ca. The general decrease of $Fe^{3+}/Fe^{(Total)}$ with depth in Hole 896A (Fig. 6A) possibly suggests a decreasing effect of cold seawater circulation with depth in the crust; however, alteration throughout the crust is heterogeneous and local high-permeability zones that control fluid circulation in the basement may be present at greater depths in the volcanic section, so this depth trend in Hole 896A must be taken with caution.

Saponite contains ferrous iron and is commonly associated with secondary pyrite in Hole 896A and other altered seafloor basalts, indicating formation under reducing conditions and more restricted seawater circulation. This more restricted circulation in ridge-flank systems occurs farther off-axis, where sediment cover is thicker and basement outcrops are less common (Mottl and Wheat, 1994; Fisher et al., 1994). Basement temperatures are higher (>40°C) under such conditions, and fluids circulating in the basement are significantly

Table 4. Summary of secondary minerals and geochemical changes associated with the development of the different alteration assemblages.

Diagnostic secondary minerals:	Type 1 Saponite	Type 2 Saponite + $Fe(O,OH)_x$	Type 3 Celadonite + $Fe(O,OH)_x$ + saponite	Type 4 Celadonite + saponite	Breccia Saponite + celadonite + K-feldspar + $Fe(O,OH)_x$ + $CaCO_3$
Occurrence:	Pillows/ massive	Pillows/ massive	Pillows/ massive	Pillows	Pillows/ massive
Geochemical changes					
SiO_2					–
MgO					++
CaO					––
Na_2O					++
K_2O	+	+	++	++	+++
LOI	+	+	+	+	+++
$Fe^{3+}/Fe^{(Total)}$	+	++	++		
Li	+	+			
S		––	––	±	–––
Cu	±	±	±	±	–
Zn	±	±	±	±	
Rb (Cs)	+	++	+++	++	+++
Sr	(+)	(+)	(+)	(+)	(+)
Tl	++	+			
U		+	+	+	+

Note: Blank = no change; + = enriched; ++ = strongly enriched; +++ = very strongly enriched; – = depleted; –– = strongly depleted; ––– = very strongly depleted; ± = either enriched or depleted; (+) = slightly enriched with increasing hydration. Breccia: Sample 148-896A-23R-1, 24–28 cm, Piece 3.

depleted in Mg compared to seawater (Mottl and Wheat, 1994). Formation of saponite, removing Mg from solution into breccia cements and vein fillings, and postdating the oxidation halos in Hole 896A, is consistent with this type of circulation. The pervasive clogging of fractures and pore-space by saponite also further reduces basement permeability and leads to even more restricted seawater circulation. Temperatures of formation of saponite in other altered seafloor rocks, estimated from oxygen isotope ratios, range from 15° to 170°C (Stakes and O'Neil, 1982; Honnorez et al., 1983; Böhlke et al., 1984).

Sr isotope ratios of saponite veins from Hole 896A generally indicate that basement fluids have near-seawater $^{87}Sr/^{86}Sr$. One fibrous saponite vein has a Sr isotopic composition similar to the host rock ($^{87}Sr/^{86}Sr = 0.7043$; see Fig. 25), which suggests that fluids may react locally to rock-dominated compositions, perhaps in regions of much more restricted fluid access. Chemical changes in the rocks include increased hydration, $\delta^{18}O$, and $^{87}Sr/^{86}Sr$, very slight increases in alkali concentrations, and local increases in S and Tl contents. Although individual rocks may not show any significant gain of Mg, the abundance of saponite veins and the strong Mg-enrichment of the breccia indicate that the volcanic section as a whole has taken up Mg during saponite formation.

Carbonate is in some cases associated with the formation of saponite in veins of Hole 896A, but also postdates saponite in some veins. Formation of carbonates led to slight increases in CO_2 and further increases in $\delta^{18}O$ and $^{87}Sr/^{86}Sr$ in the host rocks. The carbonates formed under two differing temperature regimes, at 27°–35°C and at 47°–67°C. There is no direct constraint on relative or absolute timing of the carbonates formed at the different temperatures, but the general evolution of ridge-flank circulation from early low temperatures to later higher temperatures suggests that the lower-temperature vein carbonates formed before the higher temperature carbonates. Combination of the temperature at the basement/sediment interface in Hole 896A (≈50°C; Alt, Kinoshita, Stokking, et al., 1993) with the thermal gradient measured for the upper part of Hole 504B (116°C/km) provides an estimate of current temperatures in the crust at Site 896 (Fig. 20). Temperatures of formation estimated for the higher temperature carbonates in Hole 896A are similar to the present-day temperatures in the upper crust (Fig. 20). This suggests that these carbonates could have formed under the current thermal conditions, that result from the location of Site 896 in a zone of ridge-flank hydrothermal upwelling.

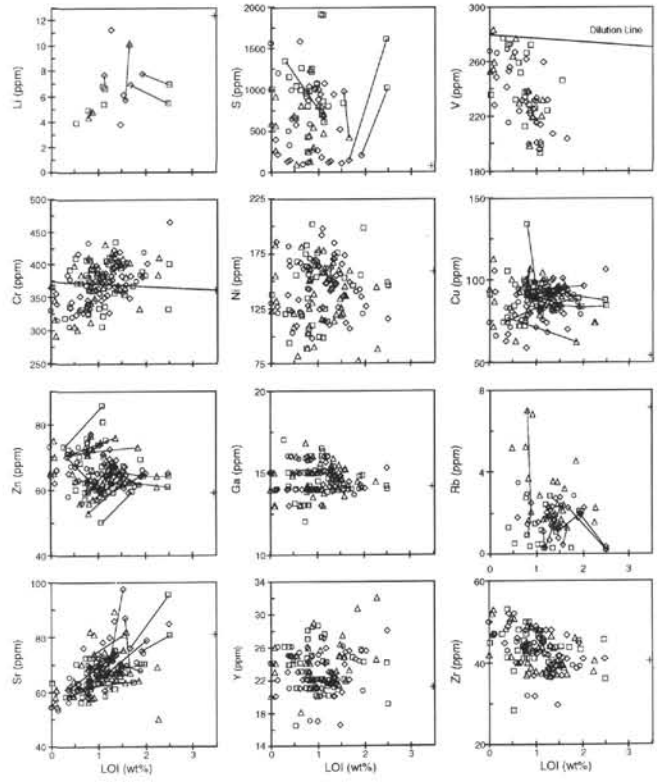

Figure 9. Whole-rock trace-element concentrations vs. LOI. Symbols as in Figure 6. Solid lines join adjacent subsamples with contrasting secondary mineral assemblages.

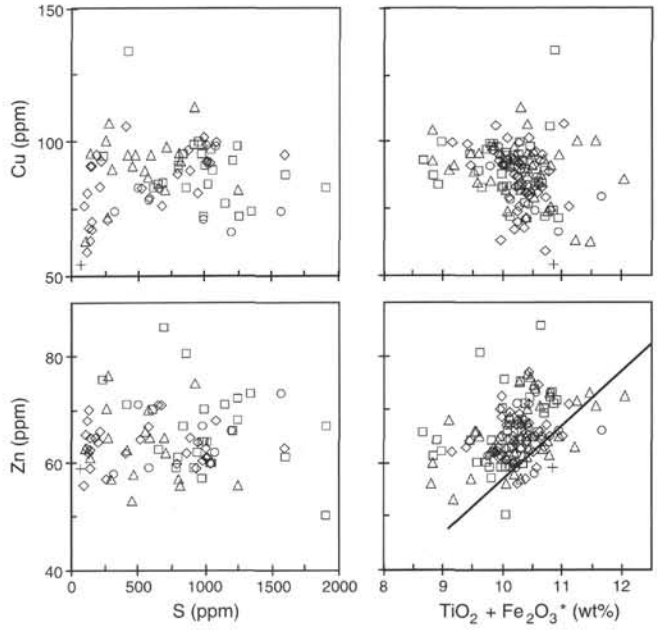

Figure 10. Variation of whole-rock copper and zinc contents with sulfur and $TiO_2 + Fe_2O_3^*$ (where $Fe_2O_3^*$ = total iron as ferric oxide). Symbols as in Figure 6. Heavy line in Zn vs. $TiO_2 + Fe_2O_3^*$ shows the predicted Zn contents for fresh glass compositions, based on the relationship derived by Doe (1994) for magmas from the East Pacific Rise.

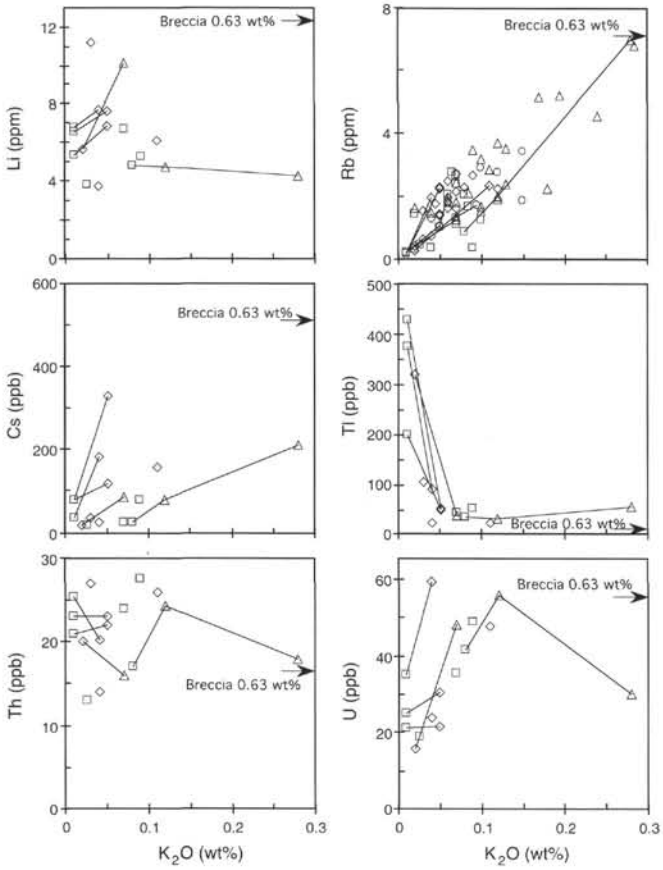

Figure 11. Variation of whole-rock trace-element contents vs. K_2O for elements commonly enriched by seafloor-alteration processes. Symbols as Figure 6. Tie lines join subsamples with different alteration assemblages.

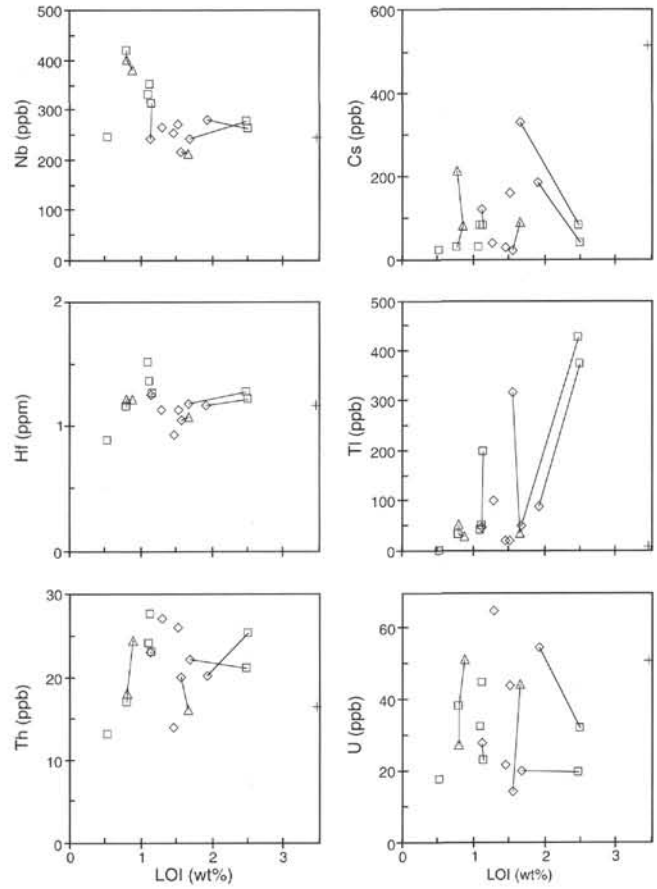

Figure 12. Whole-rock, low-abundance trace-element contents vs. LOI. Symbols as in Figure 6. Solid lines join adjacent subsamples with contrasting secondary mineral assemblages.

It was hoped that the trace-element contents of the carbonates might preserve a record of fluid compositions during the different ridge-flank circulation regimes, with the early, low-temperature carbonates forming from more unaltered seawater and the later, higher-temperature carbonates recording Mg-depleted seawater solutions. Two high-temperature aragonites suggest local fluid evolution to more rock-influenced compositions, but there is no evidence for systematic Mg depletion or increased $^{87}Sr/^{86}Sr$ ratios of basement fluids from the low- to high-temperature carbonates (from relatively open to more restricted seawater flow). The relatively high Fe and Mn contents of the high-temperature carbonates indicates that Fe and Mn were mobilized from basalt during this stage, and that conditions were sufficiently reducing to mobilize these elements. The association of pyrite with late calcite as well as the formation of late Mn calcite in other submarine basalts (e.g., Alt and Honnorez, 1984; Alt, 1993) suggest that this evolution of fluid chemistry is common in the upper ocean crust. The general similarity in $^{87}Sr/^{86}Sr$ of carbonate and most saponite veins suggests that the fluids forming these minerals in Hole 896A may have had similar Sr isotopic compositions, consistent with petrographic evidence that at least some carbonate and saponite formed simultaneously. It is possible that the oxygen isotopic compositions of saponites may record an increase in temperature, similar to the carbonates, and such analyses are ongoing in order to test this question.

Another question that remains is why the high-temperature carbonates are mostly restricted to the interval from 315–410 mbsf. It is possible that the massive units in this zone somehow acted as barriers or focused fluid flow (e.g., Pezard et al., 1993), but the presence of high-temperature carbonates in the overlying pillow basalts indicates that such fluids were present elsewhere as well. Most likely, the high-temperature carbonates simply provide some record of the permeability of the crust at the time of their formation: local high-permeability zones are important in focusing fluid flow in the volcanic section (Larson et al., 1993; Fisher et al., 1994). The permeability of the crust evolves with time, with some zones becoming sealed with secondary minerals and others opening up through fracturing and faulting. The fibrous texture commonly exhibited by both saponite and carbonate veins in Hole 896A provides further evidence for these processes (Alt, Kinoshita, Stokking, et al., 1993).

Analyses of aragonite from the upper volcanic section of Hole 504B (Staudigel and Hart, 1985; Hart et al., 1994) indicate a range of $^{87}Sr/^{86}Sr$ ratios similar to, though not as tightly clustered as the calcite and high-$\delta^{18}O$ aragonite in Hole 896A ($^{87}Sr/^{86}Sr = 0.70870 \pm 0.00015$ [2σ], $N = 6$). These data suggest that carbonates may form at a specific point during the evolution of fluid-rock interactions in the uppermost oceanic crust.

SUMMARY AND CONCLUSIONS

Hole 896A penetrates into the upper volcanic section of a ridge-flank hydrothermal upflow zone. Secondary mineralogy and chemistry, whole-rock geochemistry, and oxygen, carbon, and strontium

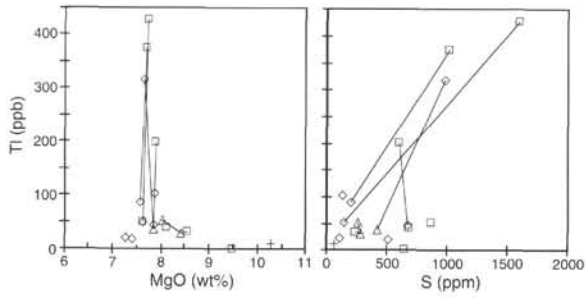

Figure 13. Whole-rock Tl concentrations compared with MgO and S. Tl contents appear independent of Mg but are strongly influenced by the presence of secondary pyrite. Symbols as in Figure 6.

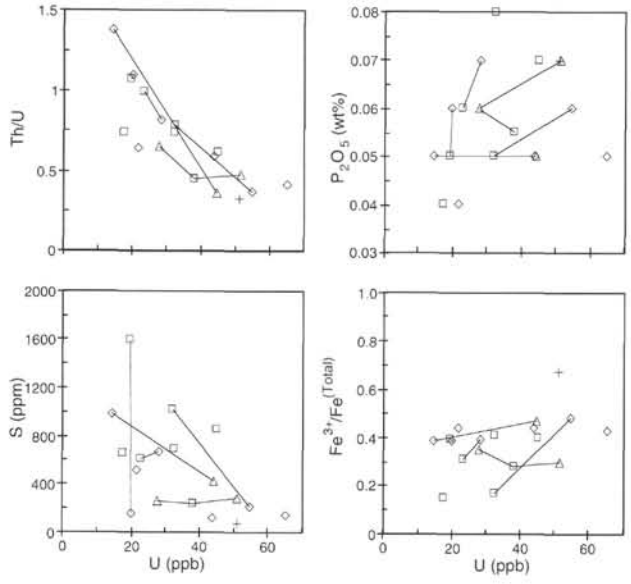

Figure 14. Whole-rock uranium concentrations vs. phosphorous and sulfur contents and $Fe^{3+}/Fe^{(Total)}$ and Th/U ratios. The decreasing Th/U ratio with increasing U content indicates that U is enriched, particularly in the $Fe(O,OH)_x$-bearing assemblages. In light of this relationship, the general trend of increasing P and U concentrations indicates that both of these elements may be adsorbed onto $Fe(O,OH)_x$. Symbols as in Figure 6.

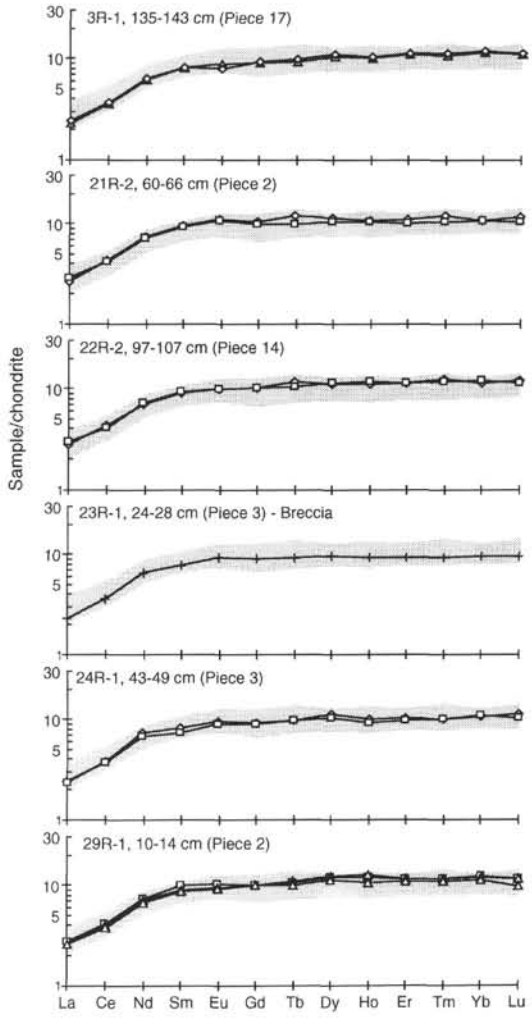

Figure 15. Chondrite-normalized rare earth element concentrations for juxtaposed rocks with contrasting secondary mineral assemblages. Stippled regions show the full range of REE contents of samples from Hole 896A (Table 3). REE contents of the upper few hundred meters of ocean basement appear unaffected by low-temperature alteration processes. Symbols as in Figure 6. Chondrite-normalization factors from Nakamura (1974).

isotope data provide constraints on the conditions and evolution of hydrothermal alteration and its effects on the upper crust at Site 896.

Fresh basaltic glass compositions exhibit trends against depth and on variation diagrams that record magmatic processes. Relative to these fresh glasses, the compositions of whole-rock samples reflect both the accumulation of phenocrysts in the rocks and the integrated effects of evolving conditions of alteration. Accumulation of plagioclase and minor olivine phenocrysts in the basalts led to higher Al and Ca and lower Fe, Mg, and Ti in the whole-rocks compared to the glasses. Alteration effects include increased H_2O, CO_2, $Fe^{3+}/Fe^{(Total)}$, K, Rb, Cs, U, P, $\delta^{18}O$, and $^{87}Sr/^{86}Sr$; local losses and gains of S and possibly Tl; and possible slight losses of Ca and Mg. Overall, the crust has gained Mg however, in the form of abundant millimeter- to centimeter-sized saponite veins and breccia cements.

Breccias are sites of intense geochemical changes, exhibiting extreme enrichments of Mg, alkalies and CO_2. Breccias comprise 5% of the core from Hole 896A, which was drilled with an average recovery of 27.7%. Logging by down-hole geophysical tools (FMS and GLT; see Brewer et al., 1994) suggests that the proportion of breccia in the upper oceanic crust at Site 896A may be considerably higher. In light of the significant changes in bulk rock chemistry exhibited by brecias (e.g., Sample 148-896A-23R-1, 24–28 cm, Piece 3), further characterization and quantification of breccias is important to understand alteration processes in the upper oceanic crust and for the estimation of chemical fluxes related to low-temperature, seawater-basalt interaction.

The alteration of the bulk rock can be classified into four alteration types, based on the presence of diagnostic secondary minerals: Type 1 saponite; Type 2 saponite + $Fe(O,OH)_x$; Type 3 celadonite + saponite + $Fe(O,OH)_x$; and Type 4 celadonite + saponite. The classification of rocks using simple geochemical parameters is not possible however, as a continuum of compositions exists between the different secondary mineral assemblages. Samples commonly record the integrated effects of superimposed alteration processes.

Alteration at Site 896 occurred in multiple stages that can be related to the evolution of hydrothermal circulation and the thermal history of the crust. Chlorite was the first secondary phase to form in minor amounts in the coarser grained portions of massive units, during initial cooling and penetration of seawater into the rocks.

Celadonite ± Fe-oxyhydroxides formed at an early stage, before the crust was 1 m.y. old, and perhaps younger than 10,000 yr. These minerals occur in patchy or bandlike alteration halos along fractures

Table 5. Oxygen and strontium isotopic compositions of whole-rock samples from Hole 896A.

Core, section, interval (cm), piece no.	Depth (mbsf)	Unit	Host	Description	Alteration type	$\delta^{18}O$ (‰)	$^{87}Sr/^{86}Sr$ (measured)	±2σ	Sr (ppm)	Rb (ppm)
148-896A-										
1R-1, 14–18 (Piece 4)	195.24	1	P	Black halo + brown	3	6.7	0.704177	±0.000014	75	1.70
3R-1, 135–139 (Piece 17)	211.25	9	P	Red	3	7.0	0.704037	±0.000014	67	1.26
3R-1, 141–143 (Piece 17)	211.31	9	P	Gray	2	6.4	0.705129	±0.000014	87	0.41
5R-3, 35–39 (Piece 5A)	231.13	11	M	Gray	1	7.1	0.703639	±0.000014	65	0.22
5R-3, 35–39 (Piece 5A)	231.13	11	M	Red	2	6.5	0.703734	±0.000014	63	0.64
10R-1, 97–101 (Piece 9A)	277.40	14	P	Gray	1	7.0	0.703455	±0.000014	61	0.34
10R-1, 107–110 (Piece 9B)	277.47	14	P	Brown	3	7.4	0.703987	±0.000013	63	2.41
11R-1, 22–26 (Piece 3C)	286.22	14	P	Brown	3	7.1	0.704201	±0.000013	70	1.35
11R-1, 42–45 (Piece 3E)	286.42	14	P	Gray	4	7.7	0.704435	±0.000013	67	1.74
12R-1, 10–15 (Piece 1A)	295.70	16	P	Gray + red	2	7.1	0.705550	±0.000014	97	2.34
12R-1, 15–17 (Piece 1B)	295.80	16	P	Brown	2	6.9	0.703721	±0.000018	65	0.28
17R-2, 72–76 (Piece 6)	345.72	27	P	Gray	1	6.4	0.703633	±0.000015	63	0.40
17R-3, 45–47 (Piece 4)	346.89	27	P	Black halo + gray	3	6.7	0.703412	±0.000014	58	6.83
18R-1, 73–79 (Piece 6)	353.83	29	P	Gray	1	7.3	0.704134	±0.000014	63	1.12
21R-2, 60–63 (Piece 8)	375.08	31	M	Red	2	6.6	0.703387	±0.000015	76	2.26
21R-2, 63–66 (Piece 8)	375.15	31	M	Gray	1	8.9	0.704468	±0.000015	95	0.18
22R-2, 97–102 (Piece 14)	385.06	32	M	Gray	1	6.7	0.703324	±0.000015	58	0.22
22R-2, 97–102 (Piece 14)	385.06	32	M	Red	2	6.9	0.703603	±0.000014	60	1.08
23R-1, 24–28 (Piece 3)	392.34	35	B	Brown breccia	2	9.3	0.704810	±0.000014	81	7.15
24R-1, 19–21 (Piece 1)	401.99	36	M	Gray	1	6.8	0.702776	±0.000015	63	0.24
24R-1, 43–49 (Piece 3)	402.39	36	M	Gray	1	10.4	0.703715	±0.000015	81	0.18
24R-1, 43–49 (Piece 3)	402.39	36	M	Red	2	7.0	0.703343	±0.000013	75	1.96
24R-1, 105–109 (Piece 7)	402.85	36	M	Gray	1		0.702756	±0.000015	61	0.22
26R-3, 15–19 (Piece 1C)	424.01	42	P	Brown	3	7.0	0.703090	±0.000014	70	2.05
26R-3, 30–34 (Piece 3)	424.40	42	P	Gray	1	7.5	0.703233	±0.000020	68	1.02
29R-1, 10–14 (Piece 2)	449.80	48	P	Light gray	1	6.5	0.703120	±0.000014	58	0.91
29R-1, 10–14 (Piece 2)	449.80	48	P	Black halo	3	6.4	0.703051	±0.000013	58	2.04
29R-1, 14–21 (Piece 2)	449.80	48	P	Red	3	6.5	0.702973	±0.000015	56	7.02
29R-1, 35–41 (Piece 5)	450.05	48	P	Gray	1	6.4	0.703033	±0.000027	58	1.26

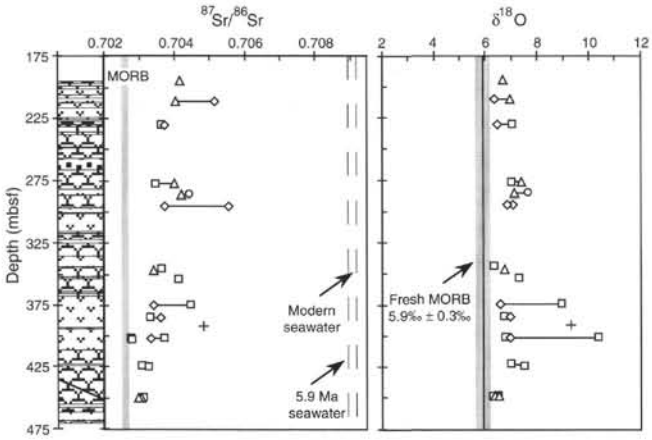

Figure 16. Whole-rock strontium ($^{87}Sr/^{86}Sr$) and oxygen ($\delta^{18}O$, ‰) isotopic compositions vs. depth in Hole 896A. Symbols as in Figure 6.

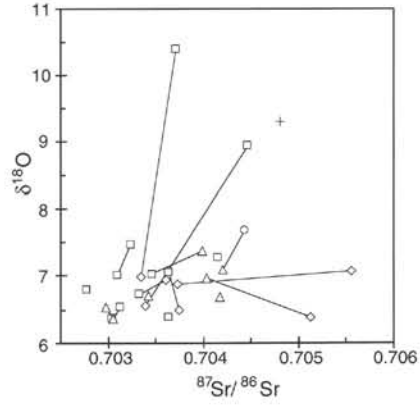

Figure 17. Whole-rock $^{87}Sr/^{86}Sr$ vs. $\delta^{18}O$ (‰). Symbols as in Figure 6.

in the rocks. Temperatures were probably less than 50°C (e.g., Böhlke et al., 1984), and the crust was open to free circulation of oxidizing seawater. Solutions derived from deeper in the volcanic section, or distal, low-temperature hydrothermal fluids may have provided some of the Fe, Si, and alkalies for celadonite formation. Whole-rock chemical changes involved increased alkalies, and slight increases in H_2O, $Fe^{3+}/Fe^{(Total)}$, $\delta^{18}O$, and $^{87}Sr/^{86}Sr$.

Subsequently, Fe-oxyhydroxides formed reddish alteration halos in the rocks, which are particularly well developed along fractures in the massive units. This alteration occurred in relatively young crust, where little sediment cover and abundant exposed basement outcrops allowed open circulation of seawater, which maintained oxidizing conditions and low temperatures. Whole-rock chemical changes are characterized mainly by oxidation, but include increased H_2O, alkalies, U, P, $\delta^{18}O$, and $^{87}Sr/^{86}Sr$; local losses of S and possibly Tl; and possible slight losses of Ca and Mg.

The next alteration stage was characterized by the pervasive formation of saponite replacing olivine, partly replacing plagioclase and glass, and filling fractures and cementing breccias. This alteration occurred in slightly older crust, with thicker sediment cover and fewer basement outcrops, that combined with the clogging of pore space and fractures by saponite precipitation, resulted in a more restricted circulation of seawater. Conditions were more reducing and temperatures were probably greater than 40°C (See Fig. 19; Mottl and Wheat, 1994), perhaps as high as 100°–150°C. Whole-rock chemical changes include increased Mg, H_2O, $\delta^{18}O$, and $^{87}Sr/^{86}Sr$; slight alkali increases; and local gains of S and Tl. Although individual whole-rock samples may not have gained Mg, the abundance of saponite filling fractures and cementing breccias records significant uptake of Mg by the upper crust as a whole. Four saponites have $^{87}Sr/^{86}Sr$ = 0.70842–0.70875 indicating that fluids were partly evolved seawater. One fibrous saponite vein has $^{87}Sr/^{86}Sr$ = 0.704363, suggesting that fluids may evolve to rock-dominated compositions in localized zones of more restricted fluid access.

Calcium carbonates (both aragonite and calcite) formed in veins and breccias, in some cases simultaneously with saponite, but in others postdating saponite formation. From $\delta^{18}O$ measurements two generations of carbonate were identified: (1) an early, low-temperature (26°–35°C) generation, with low Mg, Fe, and Mn concentrations and

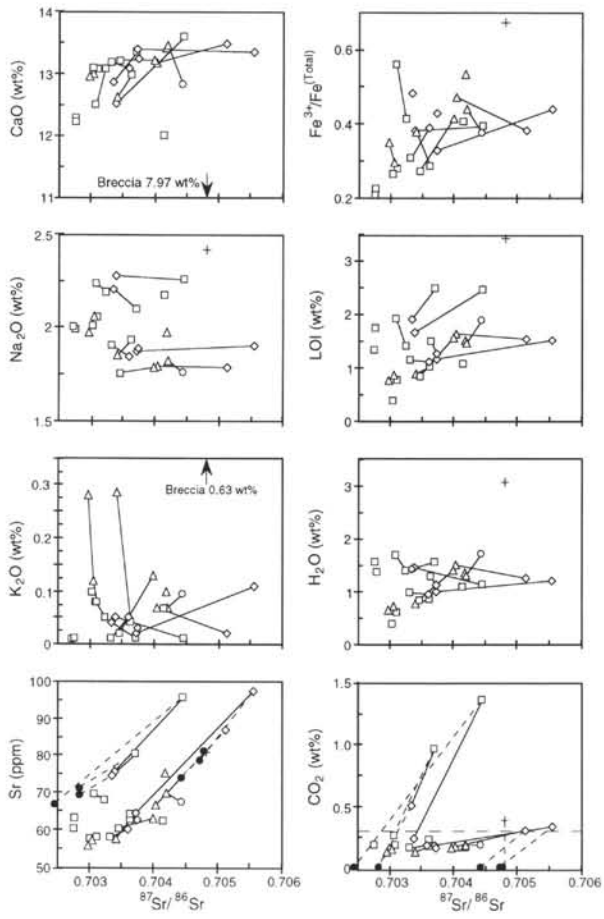

Figure 18. Whole-rock $^{87}Sr/^{86}Sr$ vs. alteration-sensitive geochemical parameters. Sr contents and $^{87}Sr/^{86}Sr$ ratios, recalculated "carbonate-free" (dots) are plotted on the CO_2 and Sr vs. $^{87}Sr/^{86}Sr$ panels, with dashed tie-lines joining the measured and calculated values. The difficulty of estimating the Sr content of the carbonate is highlighted by Sample 148-896A-21R-2, 63–66 cm (Piece 8), a Type 1 basalt from a massive flow that contains 1.34 wt% CO_2. Analysis reveals that the carbonate vein in this sample comprises fibrous aragonite formed at ≈50°C (see text and Table 6). Sr content is not available for this carbonate vein however, an analysis of a similar fibrous aragonite vein from Sample148-896A-22R-1, 53–54 cm (Piece 6), suggests Sr concentrations of ≈1010 ppm. Recalculation of the $^{87}Sr/^{86}Sr$ ratio of Sample 148-896A-21R-2, 63–66 cm (Piece 8), using Sr content of the carbonate of 1010 ppm, yields a bulk rock strontium isotopic ratio of $^{87}Sr/^{86}Sr \approx 0.70246$ and a bulk-rock Sr content of 67 ppm (cf., 0.70447, 95 ppm measured). Although the Sr content is reasonable, the $^{87}Sr/^{86}Sr$ ratio is much lower than all others measured from Hole 896A. A lower Sr content of the carbonate would increase both the bulk-rock Sr content and the $^{87}Sr/^{86}Sr$ ratio (e.g., if $Sr_{aragonite} = 925$ ppm, then $Sr_{whole\text{-}rock} = 69$ ppm and $^{87}Sr/^{86}Sr_{whole\text{-}rock} = 0.7027$). Similarly, the Sr content of the carbonate present in the Type 1 and 2 subsamples of Sample 148-896A-24R-1, 43–49 cm (Piece 3), will determine which alteration assemblage has the higher $^{87}Sr/^{86}Sr$ ratio (for $Sr_{calcite} > 550$ ppm, $^{87}Sr/^{86}Sr_{type\ 2} > {}^{87}Sr/^{86}Sr_{type\ 1}$). The $^{87}Sr/^{86}Sr$ ratios of three other samples, including the breccia sample (148-896A-23R-1, 24–28 cm, Piece 3), have been adjusted for carbonate contents just above background levels ($CO_2 < 0.3$ wt%). Note that the carbonate in the breccia sample is probably a high-temperature (≈66°C) blocky aragonite (see Table 6) with a very low Sr content (49 ppm), lower than typical bulk-rock values (≥60 ppm). This results in a very slight decrease in the bulk-rock $^{87}Sr/^{86}Sr$ ratio, but an increase in Sr content as recalculated carbonate-free. The recalculation of carbonate-free, whole-rock Sr contents and $^{87}Sr/^{86}Sr$ ratios disrupts the two subparallel groups of samples; when Sr and $^{87}Sr/^{86}Sr$ are compared, however, two separate trends remain.

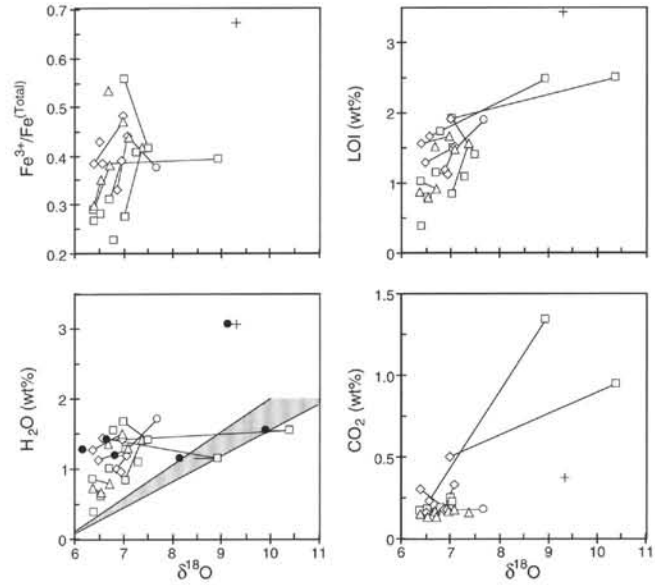

Figure 19. Whole-rock $\delta^{18}O$ vs. $Fe^{3+}/Fe^{(Total)}$ and volatile content. Dots show the $\delta^{18}O$ of samples with significant carbonate, for measured values recalculated carbonate-free. Stippled region on the H_2O vs. $\delta^{18}O$ plot shows the limits of the smectite-basalt mixing line for temperatures of 0°–50°C (Muehlenbachs and Clayton, 1972; Böhlke et al., 1984).

high Sr contents, that formed from partly reacted seawater with a decreased Mg/Ca ratio and contained 2.5%–10% basaltic Sr (carbonate $^{87}Sr/^{86}Sr = 0.708775 \pm 0.000066$ [2σ], $N = 11$); and (2) a later generation of carbonates with higher Mg, Fe, and Mn concentrations and lower Sr contents formed at higher temperatures (47°–67°C). These later generation carbonates may reflect more restricted circulation of seawater, and higher basement temperatures (e.g., Mottl and Wheat, 1994), and could be related to the current thermal regime at Site 896; a ridge-flank hydrothermal upflow zone with basement temperatures greater than 50°C. Sr isotope compositions of the late carbonates are indistinguishable from the earlier lower temperature generation though rare, high-temperature (55°–66°C) aragonites formed from circulating seawater-derived solutions that were locally more evolved, containing up to 15%–30% basaltic Sr ($^{87}Sr/^{86}Sr = 0.7079$–0.7084).

Zeolites are relatively late, in some cases preceding carbonate precipitation, but of uncertain timing elsewhere. The low $^{87}Sr/^{86}Sr$ of natrolite (0.7074) suggests possible later formation, from more reacted basement fluids than most of the carbonates or saponites. A coexisting analcite has a high $^{87}Sr/^{86}Sr$ (0.70914) very near the Sr isotopic composition of present-day seawater suggesting that this mineral may have continued to freely exchange Sr with seawater.

Alteration effects in the rocks recovered from Hole 896A are generally similar to those present in the uppermost volcanic rocks of Hole 504B (<300 m sub-basement) that have been affected by oxidizing alteration at low temperatures (0°–100°C) by the open circulation of seawater through the highly permeable upper extrusives (e.g., Alt et al., 1986a). The most striking differences between the Hole 896A and the Hole 504B cores include the greater abundance of carbonate, hyaloclastite and fragmentation breccias, and the development of thick (≈1 cm) saponite veins in the new hole.

ACKNOWLEDGMENTS

This research was supported by grants from JOI/USSAC (USSSP 148-20731b and USSSP 148-20738b), the National Science Foundation (OCE-9314218), and the Deutsche Forschungsgemeinschaft

Table 6. Carbon, oxygen, and strontium isotopic compositions and cation concentrations of calcium carbonate from veins and breccia cements in Hole 896A.

Core, section, interval (cm), piece no.	Depth (mbsf)	Unit	Host rock	Sample description	Mineralogy	Texture	$\delta^{13}C$ (‰PDB)	$\delta^{18}O$ (‰PDB)	$\delta^{18}O$ (‰SMOW)	T (°C) (fluid = 0‰)	$^{87}Sr/^{86}Sr$ (measured)	±2σ	Ca (wt%)	Mg (ppm)	Sr (ppm)	Fe (ppm)	Mn (ppm)
148-896A-																	
1R-1, 59–63 (Piece 12)	195.58	3	P	Dark gray	C	F	0.7	–8.3	21.8	62							
3R-1, 135–139 (Piece 17)	211.06	9	P	Brown, Sap + Cel	A	F	0.6	–2.8	27.5	29							
4R-1, 23–30 (Piece 5)	219.09	9	V	Dark gray, thick Sap + CO_3	A	B	2.0	–3.2	27.1	32							
5R-2, 20–23 (Piece 1)	229.17	10	P	Dark gray, 3 mm Sap + CO_3	A + C	B	1.4	–2.7	27.6	29	0.708807	±0.000021	39.9	26	2220	17	13
6R-3, 16–17 (Piece 2)	240.29	12	P		A	B	1.6	–2.9	27.4	30							
7R-1, 65–67 (Piece 10)	247.81	13	V,B	Dark gray, nontronite + phillisite + CO_3 + Sap	A	B	1.0	–2.5	27.8	28							
8R-1, 45–48 (Piece 9)	257.35	14	P	Calcite vein	C	?	1.2	–9.0	21.2	67	0.708719	±0.000018	40.0	232	177	61	1360
9R-1, 78–81 (Piece 13)	267.37	14	B,G	Calcite	C	?	1.7	–3.2	27.1	32	0.708812	±0.000020	39.9	36	1850	15	29
10R-1, 24–27 (Piece 4)	276.61	14	G		A	?	1.7	–2.8	27.5	30							
11R-1, 42–45 (Piece 3)	286.06	14	P	Dark gray, trace Cel, $Fe(O,OH)_x$	A	B	–0.2	–3.3	26.9	32							
11R-2, 7–10 (Piece 1)	287.29	14	P,V		A + C	B	0.7	–3.5	26.8	33	0.708780	±0.000021	39.9	41	2020	17	120
12R-1, 0–8 (Piece 1)	295.60	16	B,V		C	B	0.7	–2.2	28.1	27	0.708781	±0.000020	39.9	68	2590	39	55
12R-1, 63–71 (Piece 5)	295.83	16	B,V	Pillow-rim breccia	A + C	B	0.9	–3.1	27.2	31							
13R-1, 2–5 (Piece 1)	305.10	17	V,P	Dark gray	A	B	0.6	–2.2	28.1	27							
14R-2, 55–62 (Piece 7)	316.33	20	P	Dark gray, Sap + Cel	C	G/B	1.1	–7.7	22.4	58	0.708788	±0.000021	39.9	164	1120	69	632
14R-2, 55–62 (Piece 7)	316.33	20	P	Glassy calcite separate	C	G					0.708727	±0.000026	39.9	208	1690	106	534
14R-2, 55–62 (Piece 7)	316.33	20	P	Cloudy calcite separate	C	B					0.708803	±0.000020	39.9	119	1260	50	443
15R-1, 23–28 (Piece 4)	324.48	22	V		A + C	?	–1.2	–6.6	23.6	51	0.708732	±0.000023	40.0	271	359	141	1760
16R-2, 43–47 (Piece 1)	335.08	24	M	Brown + gray, Sap	C	G	0.8	–6.4	23.8	50							
17R-2, 72–76 (Piece 6)	345.51	27	P,G	Dark gray	A	B	0.7	–6.4	23.7	50							
21R-2, 63–66 (Piece 8)	374.76	31	M,V	Dark gray	A	F	–0.5	–7.1	23.1	54							
22R-1, 53–54 (Piece 6)	382.80	32	P	Dark gray, fibrous CO_3 + Sap	A	F	–0.4	–6.0	24.2	47	0.708690	±0.000021	39.8	1160	1010	388	28
22R-1, 53–54 (Piece 6)	382.80	32	P	Intergrown saponite residue	Residue	F					0.708571	±0.000018					
23R-1, 31–36 (Piece 5)	392.37	36	V		A	?	0.2	–8.8	21.3	66	0.708452	±0.000026	39.9	734	49	294	3850
24R-1, 43–49 (Piece 3)	402.20	36	M	Dark gray	C	F	–0.6	–6.8	23.4	52							
24R-1, 80–84 (Piece 5)	402.41	36	V		A	?	0.4	–7.2	22.9	55	0.707911	±0.000029	39.8	1920	35	799	5980
25R-1, 20–27 (Piece 4)	411.46	37	P,G	Dark gray	C	B	0.8	–2.8	27.5	30	0.708776	±0.000023	39.8	97	3340	57	49
27R-1, 25–30 (Piece 2)	430.74	42	P	Brown, Sap, thick CO_3 vein	A	B	1.2	–4.1	26.1	36	0.708797	±0.000018	39.9	21	2560	10	23
30R-1, 27–33 (Piece 5)	459.54	50	P,B	Breccia: Sap + blocky CO_3	A?	B	0.3	–3.8	26.5	35							

Note: Host: P = pillow lava, M = massive unit, B = breccia, G = glass, V = vein, Sap = saponite, Cel = celadonite, $Fe(O,OH)_x$ = Fe-oxyhydroxide, and CO_3 = calcium carbonate. Mineralogy: C = calcite, and A = aragonite. Texture: F = fibrous, B = blocky, and G = glassy.

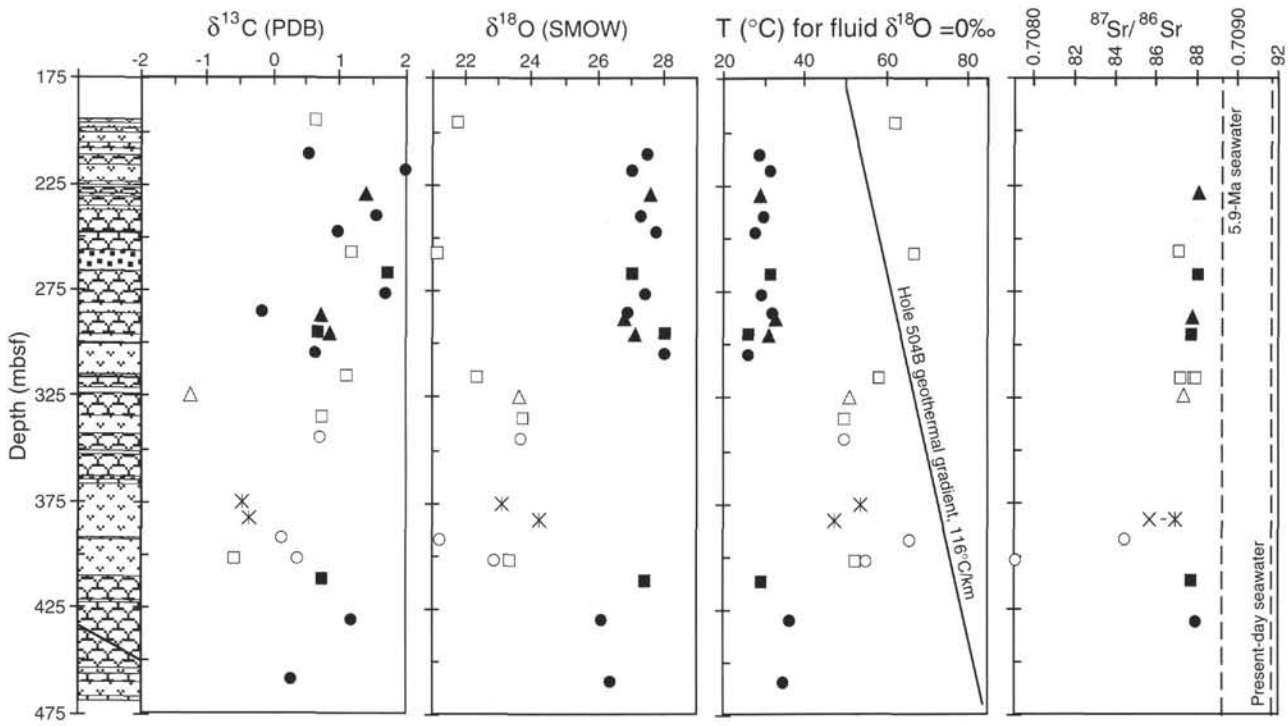

Figure 20. Carbon ($\delta^{13}C$, ‰), oxygen ($\delta^{18}O$, ‰) and strontium ($^{87}Sr/^{86}Sr$) isotopic compositions of calcium carbonate minerals vs. depth in Hole 896A. Squares = calcite; circles = aragonite; triangles = calcite-aragonite mixtures; crosses with vertical bars = low $\delta^{18}O$, fibrous aragonite; simple cross = leached residue (fibrous saponite) in Sample 148-896A-22R-1, 53–54 cm (Piece 6). Solid and open symbols denote high- and low- $\delta^{18}O$ carbonate, respectively. Temperature of formation of carbonates calculated asuming a fluid $\delta^{18}O = 0‰$ using the carbonate-water fractionation relationship of Friedman and O'Neil (1977). A geogherm for Hole 896A was calculated from the equilibrium thermal gradient at Hole 504B (Alt, Kinoshita, Stokking, et al., 1993), anchored to the measured basement/sediment interface temperature of ≈50°C in Hole 896A. Calcium carbonates from Hole 896A show a limited range of $^{87}Sr/^{86}Sr$ ratios, slightly lower than either the $^{87}Sr/^{86}Sr$ of modern or 5.9-Ma seawater, requiring the exchange of basaltic Sr with the basement fluids before the precipitation of carbonate.

(DFG-Er 123/7-1). The authors would like to thank J.R. O'Neil for the use of the stable isotope facilities and K.C. Lohmann ($\delta^{13}C$, $\delta^{18}O$) and Ted Huston (ICP-AES) for carbonate analyses. We thank R. Zier and H. Rothe for the ICP-MS analyses and M. Grünhäuser for the XRF analyses. This manuscript benefited greatly from reviews by Kathy Gillis and Lori Bettison-Varga and an anonymous reviewer.

REFERENCES

Adamson, A.C., and Richards, H.G., 1990. Low-temperature alteration of very young basalts from ODP Hole 648B: Serocki volcano, Mid-Atlantic Ridge. *In* Detrick, R., Honnorez, J., Bryan, W.B., Juteau, T., et al. *Proc. ODP, Sci. Results,* 106/109: College Station, TX (Ocean Drilling Program), 181–194.

Alt, J.C., 1993. Low-temperature alteration of basalts from the Hawaiian Arch, Leg 136. *In* Wilkens, R.H., Firth, J., Bender, J., et al., *Proc. ODP, Sci. Results,* 136: College Station, TX (Ocean Drilling Program), 133–146.

———, in press. Subseafloor processes in mid-ocean ridge hydrothermal systems. *In* Lupton, J., Mullineaux, L., and Zierenberg, R. (Eds.), *RIDGE Theoretical Institute: Physical Chemical and Biological Interactions Within Submarine Hydrothermal Systems.* Geophys. Monogr., Am. Geophys. Union.

Alt, J.C., Anderson, T.F., and Bonnell, L., 1989. The geochemistry of sulfur in a 1.3 km section of hydrothermally altered oceanic crust, DSDP Hole 504B. *Geochim. Cosmochim. Acta,* 53:1011–1023.

Alt, J.C., France-Lanord, C., Floyd, P.A., Castillo, P., and Galy, A., 1992. Low-temperature hydrothermal alteration of Jurassic ocean crust, Site 801. *In* Larson, R.L., Lancelot, Y., et al., *Proc. ODP, Sci. Results,* 129: College Station, TX (Ocean Drilling Program), 415–427.

Alt, J.C., and Honnorez, J., 1984. Alteration of the upper oceanic crust, DSDP Site 417: mineralogy and chemistry. *Contrib. Mineral. Petrol.,* 87:149–169.

Alt, J.C., Honnorez, J., Laverne, C., and Emmermann, R., 1986a. Hydrothermal alteration of a 1 km section through the upper oceanic crust, Deep Sea Drilling Project Hole 504B: mineralogy, chemistry, and evolution of seawater-basalt interactions. *J. Geophys. Res.,* 91:10309–10335.

Alt, J.C., Kinoshita, H., Stokking, L.B., et al., 1993. *Proc. ODP, Init. Repts.,* 148: College Station, TX (Ocean Drilling Program).

Alt, J.C., Muehlenbachs, K., and Honnorez, J., 1986b. An oxygen isotopic profile through the upper kilometer of the oceanic crust, DSDP Hole 504B. *Earth Planet. Sci. Lett.,* 80:217–229.

Andrews, A.J., 1977. Low-temperature fluid alteration of oceanic layer 2 basalts, DSDP Leg 37. *Can. J. Earth Sci.,* 14:911–926.

Autio, L.K., and Rhodes, J.M., 1983. Costa Rica Rift Zone basalts: geochemical and experimental data from a possible example of multistage melting. *In* Cann, J.R., Langseth, M.G., Honnorez, J., Von Herzen, R.P., White, S.M., et al., *Init. Repts. DSDP,* 69: Washington (U.S. Govt. Printing Office), 729–745.

Autio, L.K., Sparks, J.W., and Rhodes, J.M., 1989. Geochemistry of Leg 111 basalts: intrusive feeders for highly depleted pillows and flows. *In* Becker, K., Sakai, H., et al., *Proc. ODP, Sci. Results,* 111: College Station, TX (Ocean Drilling Program), 3–16.

Baker, P.A., Gieskes, J.M., and Elderfield, H., 1982. Diagenesis of carbonates in deep-sea sediments: evidence from Sr^{2+}/Ca^{2+} ratios and interstitial dissolved Sr^{2+} data. *J. Sediment. Petrol.,* 52:71–82.

Becker, K., Sakai, H., et al., 1988. *Proc. ODP, Init. Repts.,* 111: College Station, TX (Ocean Drilling Program).

Bednarz, U., and Schmincke, H.-U., 1989. Mass transfer during subseafloor alteration of the upper Troodos crust (Cyprus). *Contrib. Mineral. Petrol.,* 102:93–101.

Böhlke, J.K., Alt, J.C., and Muehlenbachs, K., 1984. Oxygen isotope-water relations in altered deep-sea basalts: low temperature mineralogical controls. *Can. J. Earth Sci.,* 21:67–77.

Böhlke, J.K., Honnorez, J., Honnorez-Guerstein, B.M., Muehlenbachs, K., and Petersen, N., 1981. Heterogeneous alteration of the upper oceanic crust: correlation of rock chemistry, magnetic properties, and O isotope

ratios with alteration patterns in basalts from Site 396B, DSDP. *J. Geophys. Res.*, 86:7935–7950.

Brewer, T.S., Harvey, P.K., and Lovell, M.A., 1994. Core-log integration from ODP Hole 896A: reinterpretation of the volcanic stratigraphy. *Eos*, 75:315.

Buckley, H.A., Bevan, J.C., Brown, K.M., Johnson, L.R., and Farmer, V.C., 1978. Glauconite and celadonite: two separate mineral species. *Mineral. Mag.*, 42:372–382.

Burke, W.H., Denison, R.E., Hetherington, E.A., Koepnick, R.B., Nelson, H.F., and Otto, J.B., 1982. Variation of seawater $^{87}Sr/^{86}Sr$ throughout Phanerozoic time. *Geology*, 10:516–519.

Carpenter, S.J., Lohmann, K.C., Holden, P., Walter, L.M., Huston, T.J., and Halliday, A.N., 1991. $\delta^{18}O$ values, $^{87}Sr/^{86}Sr$ and Sr/Mg ratios of Late Devonian abiotic marine calcite: implications for the composition of ancient seawater. *Geochim. Cosmochim. Acta*, 55:1991–2010

Clayton, R.N., and Mayeda, T.K., 1963. The use of bromine pentafluoride in the extraction of oxygen from oxides and silicates for isotopic analysis. *Geochim. Cosmochim. Acta*, 27:43–52.

Craig, H., 1961. Standard for reporting concentrations of deuterium and oxygen-18 in natural waters. *Science*, 133:1833–1834.

DeAlbuquerque, C.A.R., and Shaw, D.M., 1984. Thallium. *In* Wedepohl, K.H. (Ed.), *Handbook of Geochemistry:* Berlin (Springer), 81:F1–F8.

Delaney, M.L., 1989. Temporal changes in interstitial water chemistry and calcite recrystallization in marine sediments. *Earth Planet. Sci. Lett.*, 95:23–37.

Dixon, J.E., Stolper, E., and Delaney, J.R., 1988. Infrared spectroscopic measurements of CO_2 and H_2O in Juan de Fuca Ridge basaltic glasses. *Earth Planet. Sci. Lett.*, 90:87–104.

Doe, B.R., 1994. Zinc, copper and lead in mid-ocean ridge basalts and the source rock control on Zn/Pb in ocean ridge hydrothermal deposits. *Geochim. Cosmochim. Acta*, 58:1125–2224.

Emmermann, R., 1985. Basement geochemistry, Hole 504B. *In* Anderson, R.N., Honnorez, J., Becker, K., et al., *Init. Repts. DSDP*, 83: Washington (U.S. Govt. Printing Office), 183–199.

Fisher, A.T., Becker, K., and Narasimhan, T.N., 1994. Off-axis hydrothermal circulation: parametric tests of a refined model of processes at DSDP/ODP Site 504. *J. Geophys. Res.*, 99:3097–3123.

Fisher, A.T., Becker, K., Narasimhan, T.N., Langseth, M.G., and Mottl, M.J., 1990. Passive, off-axis convection through the southern flank of the Costa Rica rift. *J. Geophys. Res.*, 95:9343–9370.

Friedman, I., and O'Neil, J.R., 1977. Compilation of stable isotope fractionation factors of geochemical interest. *In* Fleischer, M. (Ed.), *Data of Geochemistry* (6th ed.). Geol. Surv. Prof. Pap. U.S., 440-KK:1–12.

Garbe-Schoenberg, C.-D., 1993. Simultaneous determination of thirty-seven trace elements in twenty-eight international rock standards by ICP-MS. *Geostand. Newsl.*,17:81–97.

Hart, S.R., Blusztajn, J., Dick, H.J.B., and Lawrence, J.R., 1994. Fluid circulation in the oceanic crust: contrast between volcanic and plutonic regimes. *J. Geophys. Res.*, 99:3163–3174.

Hobart, M.A., Langseth, M.G., and Anderson, R.N., 1985. A geothermal and geophysical survey on the south flank of the Costa Rica Rift: Sites 504 and 505. *In* Anderson, R.N., Honnorez, J., Becker, K., et al., *Init. Repts. DSDP*, 83: Washington (U.S. Govt. Printing Office), 379–404.

Hodell, D.A., Mueller, P.A., and Garrido, J.R., 1991. Variations in the strontium isotopic composition of seawater during the Neogene. *Geology*, 19:24–27.

Honnorez, J., Laverne, C., Hubberten, H.-W., Emmermann, R., and Muehlenbachs, K., 1983. Alteration processes in Layer 2 basalts from Deep Sea Drilling Project Hole 504B, Costa Rica Rift. *In* Cann, J.R., Langseth, M.G., Honnorez, J., Von Herzen, R.P., White, S.M., et al., *Init. Repts. DSDP*, 69: Washington (U.S. Govt. Printing Office), 509–546.

Hubberten, H.-W., Emmermann, R., and Puchelt, H., 1983. Geochemistry of basalts from Costa Rica Rift Sites 504 and 505 (Deep Sea Drilling Project Legs 69 and 70). *In* Cann, J.R., Langseth, M.G., Honnorez, J., Von Herzen, R.P., White, S.M., et al., *Init. Repts. DSDP*, 69: Washington (U.S. Govt. Printing Office), 791–803.

Humphris, S.E., Melson, W.G., and Thompson, R.N., 1980. Basalt weathering on the East Pacific Rise and Galapagos Spreading Center, DSDP Leg 54. *In* Rosendahl, B.R., Hekinian, R., et al., *Init. Repts. DSDP*, 54: Washington (U.S. Govt. Printing Office), 773–787.

Katz, A., Sass, E., Starinsky, A., and Holland, H.D., 1972. Strontium behavior in the aragonite-calcite transformation: an experimental study at 40°–98°. *Geochim. Cosmochim. Acta*, 36:481–496.

Kempton, P.D., Autio, L.K., Rhodes, J.M., Holdaway, M.J., Dungan, M.A., and Johnson, P., 1985. Petrology of basalts from Hole 504B, Deep Sea Drilling Project, Leg 83. *In* Anderson, R.N., Honnorez, J., Becker, K., et al., *Init. Repts. DSDP*, 83: Washington (U.S. Govt. Printing Office), 129–164.

Langseth, M.G., Mottl, M.J., Hobart, M.A., and Fisher, A., 1988. The distribution of geothermal and geochemical gradients near Site 501/504: implications for hydrothermal circulation in the oceanic crust. *In* Becker, K., Sakai, H., et al., *Proc. ODP, Init. Repts.*, 111: College Station, TX (Ocean Drilling Program), 23–32.

Larson, R.L., Fisher, A.T., Jarrard, R.D., Becker, K., and Ocean Drilling Program Leg 144 Shipboard Scientific Party, 1993. Highly permeable and layered Jurassic oceanic crust in the western Pacific. *Earth Planet. Sci. Lett.*, 119:71–83.

Laverne, C., and Vivier, G., 1983. Petrographical and chemical study of basement from the Galapagos Spreading Center, Leg 70. *In* Honnorez, J., Von Herzen, R.P., et al., *Init. Repts. DSDP*, 70: Washington (U.S. Govt. Printing Office), 375–390.

Ludden, J., and Thompson, G., 1979. An evaluation of the behavior of rare-earth elements during the weathering of sea-floor basalts. *Earth Planet. Sci. Lett.*, 43:85–92.

MacLean, W.H., 1990. Mass change calculations in altered rock series. *Mineral. Depos.*, 25:44–49.

McGoldrick, P.J., Keays, R.R., and Scott, B.B., 1979. Thallium: a sensitive indicator of rock/seawater interaction and of sulfur saturation of silicate melts. *Geochim. Cosmochim. Acta*, 43:1303–1311.

Michael, P.J., 1988. The concentration, behavior, and storage of H_2O in the suboceanic upper mantle: implications for mantle metasomatism. *Geochim. Cosmochim. Acta*, 52:555–566.

Mills, R.A., Thomson, J., Elderfield, H., Hinton, R.W., and Hyslop, E., 1994. Uranium enrichment in metalliferous sediments from the Mid-Atlantic Ridge. *Earth Planet. Sci. Lett.*, 124:35–47.

Mottl, M.J., 1989. Hydrothermal convection, reaction, and diffusion in sediments on the Costa Rica Rift flank: pore-water evidence from ODP Sites 677 and 678. *In* Becker, K., Sakai, H., et al., *Proc. ODP, Sci. Results*, 111: College Station, TX (Ocean Drilling Program), 195–213.

Mottl, M.J., Lawrence, J.R., and Keigwin, L.D., 1983. Elemental and stable-isotope composition of pore waters and carbonate sediments from Deep Sea Drilling Project Sites 501/504 and 505. *In* Cann, J.R., Langseth, M.G., Honnorez, J., Von Herzen, R.P., White, S.M., et al., *Init. Repts. DSDP*, 69: Washington (U.S. Govt. Printing Office), 461–473.

Mottl, M.J., and Wheat, C.G., 1994. Hydrothermal circulation through mid-ocean ridge flanks: fluxes of heat and magnesium. *Geochim. Cosmochim. Acta*, 58:2225–2238.

Mucci, A., and Morse, J.W., 1990. Chemistry of low-temperature abiotic calcites: experimental studies on coprecipitation, stability, and fractionation. *Aquat. Sci.*, 3:217–254.

Muehlenbachs, K., and Clayton, R.N., 1972. Oxygen isotope studies of fresh and weathered submarine basalts. *Can. J. Earth Sci.*, 9:172–184.

Nakamura, N., 1974. Determination of REE, Ba, Fe, Mg, Na, and K in carbonaceous and ordinary chondrites. *Geochim. Cosmochim. Acta*, 38:757–776.

Natland, J.H., Adamson, A.C., Laverne, C., Melson, W.G., and O'Hearn, T., 1983. A compositionally nearly steady-state magma chamber at the Costa Rica Rift: evidence from basalt glass and mineral data, Deep Sea Drilling Project Sites 501, 504, and 505. *In* Cann, J.R., Langseth, M.G., Honnorez, J., Von Herzen, R.P., White, S.M., et al., *Init. Repts. DSDP*, 69: Washington (U.S. Govt. Printing Office), 811–858.

Pearce, J.A., and Cann, J.R., 1973. Tectonic setting of basic volcanic rocks determined using trace element analyses. *Earth Planet. Sci. Lett.*, 19:290–300.

Pezard, P., Anderson, R.N., Ryan, W.B.F., Becker, K., Alt, J.C., and Gente, P., 1993. Accretion, structure and hydrology of intermediate spreading-rate oceanic crust from drillhole experiments and seafloor observations. *Mar. Geophys. Res.*, 14:93–123.

Puchelt, H., and Emmermann, R., 1983. Petrogenetic implications of tholeiitic basalt glasses from the East Pacific Rise and the Galapagos Spreading Center. *Chem. Geol.*, 38:39–56.

Ryan, J.G., and Langmuir, C.H., 1987. The systematics of lithium abundances in young volcanic rocks. *Geochim. Cosmochim. Acta*, 51:1727–1741.

Seyfried, W.E., Jr., Shanks, W.C., III, and Dibble, W.E., Jr., 1978. Clay mineral formation in DSDP Leg 34 basalt. *Earth Planet. Sci. Lett.*, 41:265–276.

Stakes, D.S., and O'Neill, J.R., 1982. Mineralogy and stable isotope geochemistry of hydrothermally altered oceanic rocks. *Earth Planet. Sci. Lett.*, 57:285–304.

Staudigel, H., and Hart, S.R., 1983. Alteration of basaltic glass: mechanisms and significance for the oceanic crust-seawater budget. *Geochim. Cosmochim. Acta,* 47:337–350.

————, 1985. Dating of ocean crust hydrothermal alteration: strontium isotope ratios from Hole 504B carbonates and a reinterpretation of Sr isotope data from Deep Sea Drilling Project Sites 105, 332, 417, and 418. *In* Anderson, R.N., Honnorez, J., Becker, K., et al., *Init. Repts. DSDP,* 83: Washington (U.S. Govt. Printing Office), 297–303.

Sun, S.-S., and McDonough, W.F., 1989. Chemical and isotopic systematics of oceanic basalts: implications for mantle composition and processes. *In* Saunders, A.D., and Norry, M.J. (Eds.), *Magmatism in the Ocean Basins.* Geol. Soc. Spec. Publ. London, 42:313–345.

Taylor, H.P., 1968. The oxygen isotope geochemistry of igneous rocks. *Contrib. Mineral. Petrol.,* 19:1–71.

Wheat, C.G., and Mottl, M.G., 1994. Hydrothermal circulation, Juan de Fuca Ridge eastern flank: factors controlling basement water composition. *J. Geophys. Res.,* 99:3067–3080.

Date of initial receipt: 16 August 1994
Date of acceptance: 5 February 1995
Ms 148SR-113

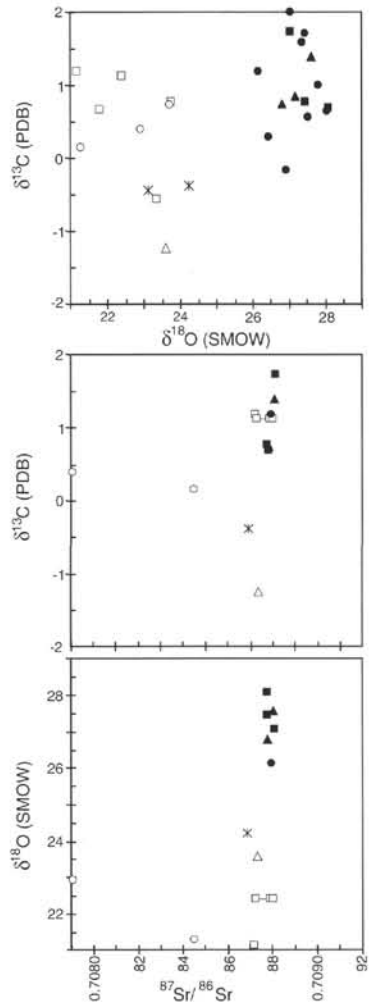

Figure 21. Comparison of oxygen ($\delta^{18}O$), carbon ($\delta^{13}C$), and strontium ($^{87}Sr/^{86}Sr$) isotopic compositions of vein carbonates. Symbols as in Figure 20.

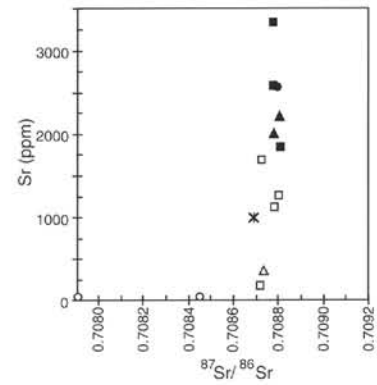

Figure 22. $^{87}Sr/^{86}Sr$ vs. Sr content of calcium carbonates from Hole 896A. Sr contents vary by a factor of ≈100 with no effect on $^{87}Sr/^{86}Sr$. High-temperature aragonite samples have lower $^{87}Sr/^{86}Sr$ and extremely low Sr contents. Symbols as in Figure 20.

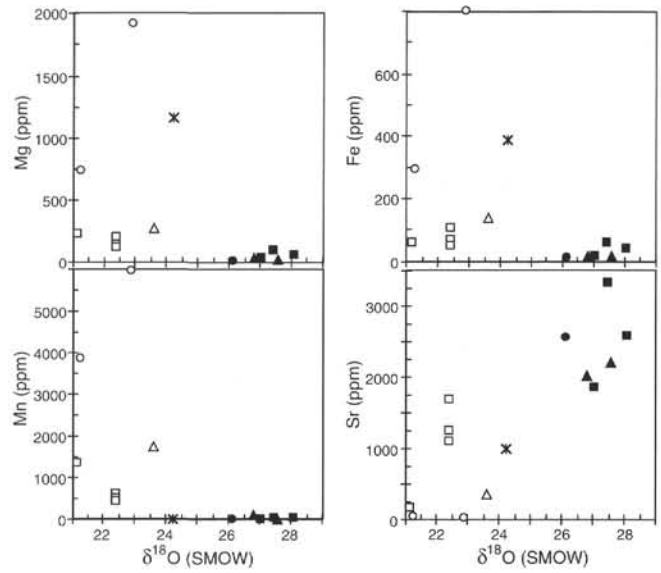

Figure 23. Carbonate trace-element concentrations vs. $\delta^{18}O$. Sr contents increase with increasing $\delta^{18}O$. High-$\delta^{18}O$ carbonates have low Mg, Mn, and Fe contents, whereas low-$\delta^{18}O$ carbonates show a significant range in trace-element contents. Symbols as in Figure 20.

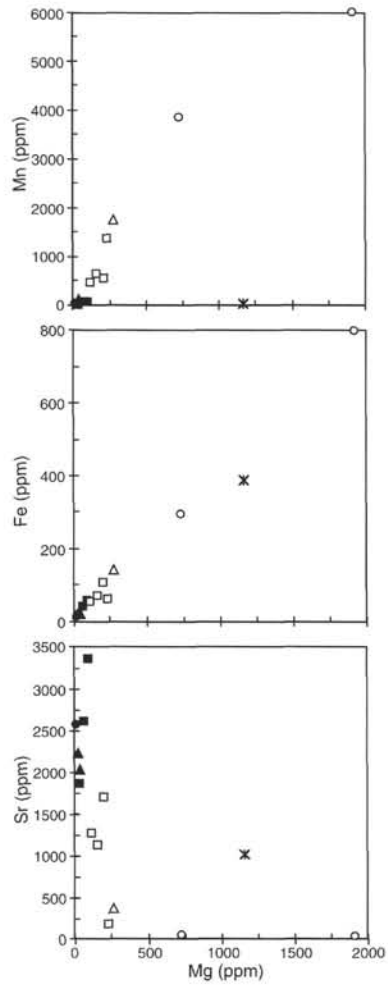

Figure 24. Carbonate trace-element contents vs. Mg concentration. Mn and Fe increase linearly with Mg. Sr shows an inverse relationship with increasing Mg. Symbols as in Figure 20.

Table 7. Strontium isotopic compositions of saponite and zeolites from Hole 896A.

Core, section, interval (cm), piece no.	Depth (mbsf)	Unit	Host rock	Sample description	$^{87}Sr/^{86}Sr$ (measured)	±2σ	Sr (ppm)	Rb (ppm)	$^{87}Rb/^{86}Sr$	$^{87}Sr/^{86}Sr$ (t = 5.9 Ma)
Saponite:										
4R-1, 5–8 (Piece 1)	218.90	9	P	Coarse saponite vein	0.708750	±0.000018	3.05	0.09	0.081	0.708743
6R-2, 66–72 (Piece 8)	239.59	12	P	Fibrous saponite	0.704363	±0.000031	1.69	0.76	1.303	0.704254
9R-1, 78–81 (Piece 13)	267.37	14	B	Coarse saponite in hyaloclastic breccia	0.708752	±0.000028	0.85	0.26	0.877	0.708679
16R-1, 85–88 (Piece 9A)	334.53	24	M	Reddish saponite	0.708424	±0.000023	1.79	1.06	1.719	0.708280
23R-2, 57–61 (Piece 4B)	393.75	36	M	Brownish saponite in coarse vein	0.709094	±0.000018	2.09	7.30	10.096	0.708248
Zeolites:										
27R-3, 10–16 (Piece 2)	433.18	46	P	Analcite as coarse-grained vug filling	0.709137	±0.000028	1.76	2.21	3.621	0.708834
27R-3, 10–16 (Piece 2)	433.18	46	P	Natrolite, fibrous	0.707440	±0.000020	7.14	0.23	0.024	0.707438

Note: Minimum $^{87}Sr/^{86}Sr$ calculated from the measured Rb and Sr concentrations of these secondary minerals and calculated using the maximum age of formation possible (i.e., t = 5.9 Ma). Host rock: P = pillow lava, M = massive unit, and B = breccia. Rb and Sr concentrations determined by TIMS-ID.

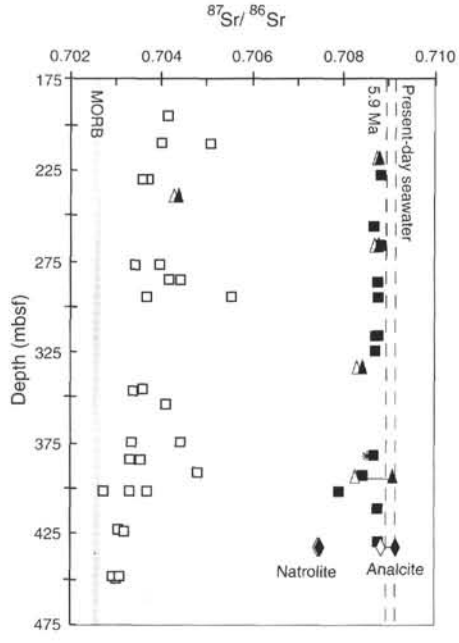

Figure 25. Compilation of whole-rock, carbonate, and secondary mineral $^{87}Sr/^{86}Sr$ ratios for Hole 896A. Open squares = whole rock; solid squares = calcium carbonate; cross = fibrous saponite residue from Sample 148-896A-22R-1, 53–54 cm (Piece 6); solid triangles = measured $^{87}Sr/^{86}Sr$ for saponite; solid diamonds = measured $^{87}Sr/^{86}Sr$ for zeolites from open-space-filled vug (Sample 148-896A-27R-3, 10–16 cm, Piece 2); open triangles and diamonds = age-corrected $^{87}Sr/^{86}Sr$ for saponite and zeolite samples, respectively (recalculated for 5.9 Ma using measured Rb and Sr concentrations). Stippled region shows composition of fresh MORB.